



# System design assessment for innovative support structures

Agreement n.:	308974
Duration	November 2012 – October 2017
Co-ordinator:	DTU Wind



The research leading to these results has received funding from the European Community's Seventh Framework Programme FP7-ENERGY-2012-1-2STAGE under grant agreement No. 308974 (INNWIND.EU).

---

#### PROPRIETARY RIGHTS STATEMENT

This document contains information, which is proprietary to the "INNWIND.EU" Consortium. Neither this document nor the information contained herein shall be used, duplicated or communicated by any means to any third party, in whole or in parts, except with prior written consent of the "INNWIND.EU" consortium.

---

## Document information

Document Name:	System design assessment for innovative support structures
Document Number:	Deliverable D1.35
Author:	Frederik Berger (OLD) John Dalsgaard Sørensen (AAU), Tomas Gintautas (AAU), Martin Kühn (OLD), Martin Kraft (OLD)
Document Type	Report
Dissemination level	PU
Review:	Bernard Bulder (ECN)
Date:	19. January 2015
WP:	1
Task:	1.3
Approval:	Approved by WP Leader

## TABLE OF CONTENTS

OVERALL INTRODUCTION.....	5
PART A - SYSTEM INTEGRATION OF RNA AND SUPPORT STRUCTURE (OLD).....	6
1 INTRODUCTION – DESIGN DRIVERS AND TRENDS FOR DESIGN OF RNA AND SUPPORT STRUCTURES .....	6
2 ANALYSIS OF INTERACTING DESIGN PARAMETERS AND DESIGN CHOICES .....	9
2.1 Hub height and design frequency for fundamental support structure mode .....	9
2.2 Aerodynamic rotor design and operational speed range .....	15
2.3 Blade – tower interaction.....	21
2.4 Effect of tower top mass and electro-mechanical drivetrain .....	22
2.5 Effect of first eigenfrequency of the support structure – RNA system.....	25
3 COST-EFFECTIVE DESIGN METHODOLOGIES .....	28
4 CONCLUSIONS.....	32
BIBLIOGRAPHY.....	34
PART B - O&M FOR INNOVATIVE SUPPORT STRUCTURES (AAU).....	35
1 INTRODUCTION.....	35
2 RELIABILITY AND RISK-BASED PLANNING FOR O&M FOR OFFSHORE WIND TURBINE SUPPORT STRUCTURES .....	37
2.1 Acceptance criteria for individual joints .....	38
2.2 Optimal reliability-based inspection planning.....	41
2.3 Reliability-based inspection planning.....	46
2.4 Probabilistic modelling of inspections.....	47
2.5 Reliability modelling of fatigue.....	47
2.6 System effects .....	57
3 METHODOLOGY FOR COST-OPTIMAL PLANNING OF O&M FOR INNOVATIVE SUPPORT STRUCTURES .....	66

4	ILLUSTRATION OF METHODOLOGY .....	67
5	SUMMARY AND CONCLUSIONS.....	84
	APPENDIX A. ILLUSTRATION OF RELIABILITY-BASED PLANNING OF INSPECTION FOR CALIBRATION OF SAFETY FACTORS FOR FATIGUE.....	85
	APPENDIX B. RESULTS OF INSPECTION PLANNING FOR ALL THE ANALYZED JOINTS .....	92
	BIBLIOGRAPHY.....	106

## OVERALL INTRODUCTION

The present report deals with the system level integration of the innovations of the different work packages (WPS) of the InnWind.eu project with respect to support structure design assessment. Emphasis is put on the following two crucial aspects:

- System integration of rotor-nacelle-assembly (RNA) and support structure
- WT integration and reliability- and risk-based planning of operation and maintenance (O&M) for innovative support structures in order to minimize total lifetime costs

These two aspects contributed by ForWind – University of Oldenburg (OLD) and Aalborg University (AAU) respectively are presented in separated sections of the report denoted as Part A and Part B. The specific targets of Part A include:

- Challenges in design integration for very large wind turbines and the interaction of RNA and a bottom-mounted support structure are described in terms of frequency design window, operational range and optimization of energy yield.
- Recommendation shall be given on design choices for rotor orientation, blade planform and stiffness, tower clearance and tower diameter with respect to blade-tower interaction.
- The overall effect of tower top mass as well as drivetrain and generator configurations shall be investigated.
- Cost-effective design methodologies shall be assessed.

While Part B aims at:

- The report shall describe the state of the art of reliability and risk-based planning of O&M for offshore wind turbine support structures.
- Development of a methodology for cost-optimal, reliability and risk-based planning of O&M incl. inspections for innovative support structures.
- Illustration in numerical examples of methodology developed in cooperation with WP4.

The two above-mentioned methodologies are used as part of the assessment of the innovative designs which are developed in WP 2-4. Success will be measured by the completeness of the methodology in addressing the specific targets of the deliverable and its applicability in assessing application of system integration design and O&M incl. inspections in design and operation of innovative support structures.

## PART A - SYSTEM INTEGRATION OF RNA AND SUPPORT STRUCTURE (OLD)

### 1 INTRODUCTION – DESIGN DRIVERS AND TRENDS FOR DESIGN OF RNA AND SUPPORT STRUCTURES

Beside the requirements with respect to ultimate and fatigue limit state the lower eigenfrequencies of a wind turbine support structure are an important design consideration. The lower eigenfrequencies of the entire system of support structure and rotor-nacelle-assembly (RNA) are mainly driven by the stiffness of the support structure including its foundation and the mass of the RNA. A proper design has to prevent significant resonances between such eigenfrequencies and excitations from the waves or the rotor frequency and its higher harmonics. In this chapter it will be elaborated that for large offshore wind turbines in or beyond the 8 MW class the combination of a relatively stiff jacket support structure and the RNA can result in severe dynamic problems

At an early design stage the dynamics of wind turbines can be estimated by the Campbell diagram. For this purpose the excitation frequencies 1P, 2P, 3P, etc., i.e. multiple of the rotational speed, as well as the eigenfrequencies of the whole wind turbine system are plotted over the rotor speed. This way potential resonances are graphically indicated if an intersection of an excitation ray with an eigenfrequency takes place within the operational rotor speed range.

The Campbell diagram of the INNWIND reference turbine with the reference jacket is shown in Figure 1-1. At a rotor speed of 6 rpm a resonance between the blade passing frequency and the 1<sup>st</sup> combined eigenfrequency occurs. In order to reduce the dynamic excitation a rotor speed exclusion window between 5.5 and 6.8 rpm is considered.

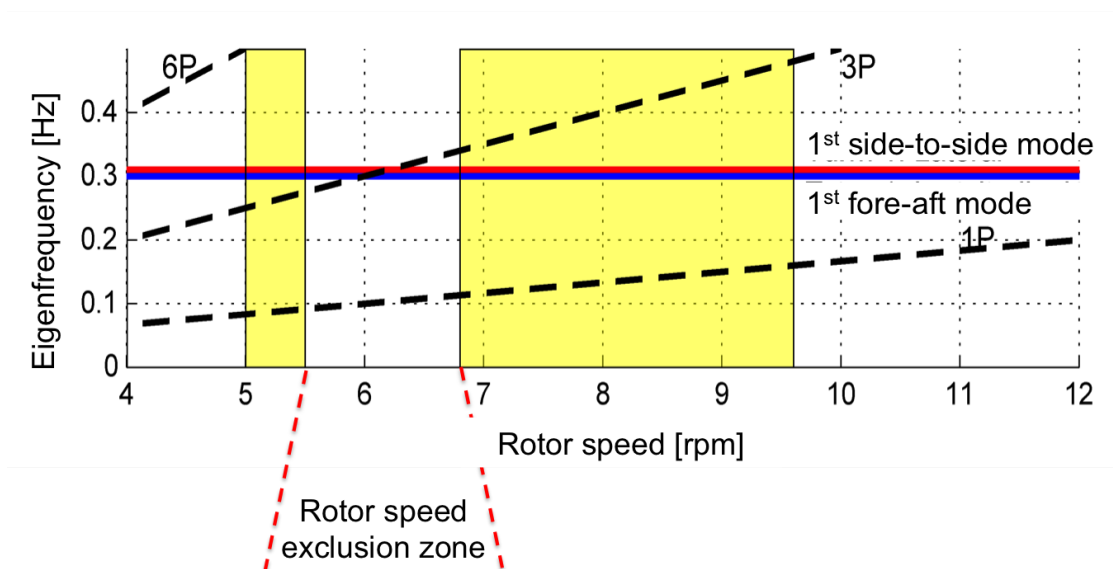


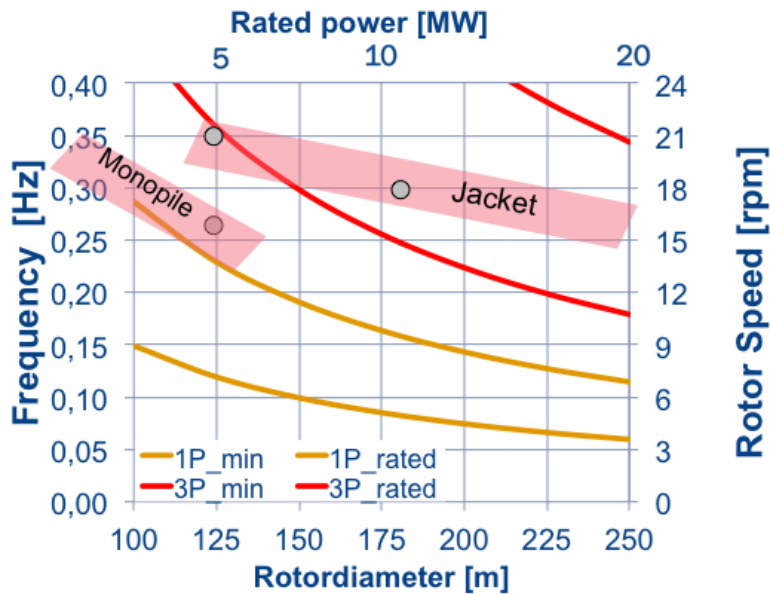
Figure 1-1: Campbell diagram of reference turbine with focus on RNA eigenfrequency

This resonance problem of the INNWIND reference turbine is considered to be the consequence of a direct up-scaling of both the support structure concept and the rotor design from the 5 MW class to larger turbines. In order to elaborate this Figure 1-2 illustrates two trends in the design of large turbines with rotor diameter between 100 and 250 m, i.e. the rotor rotational frequency and the first eigenfrequency of the entire support structure-RNA system.

Firstly, when the design tip speed of the rotor is maintained, the rated rotor speed decreases inversely proportional to the rotor diameter. In the diagram two excitation bands are related to the rotor speed, the operational range of the rotor speed and the corresponding range of the blade passing frequency with a three times larger magnitude of the frequencies at a three-bladed rotor. The lower frequency of these two ranges is given by the cut-in rotor speed which depends on the used generator-converter concept. A typical ratio between rated rotor speed and cut-in rotor speed is 1.6 and 2 for double fed-induction generator (DFIG) and full power converter with synchronous generator respectively. In the diagram the parameters of the INNWIND reference turbines with a design tip speed of 90 m/s, which is a quite typical value for offshore wind turbines above 3 MW, and a frequency ration of 1.92 is assumed.

Secondly, the increase of the overall height and tower top mass for growing rotor size results in a decrease of the first eigenfrequency of the entire support structure-RNA system. Even with the recently developed extra large (XXL) monopiles their applicability is limited up to the 6-8 MW class and by water depth as well. Typically the first eigenfrequency of these monopile structures ranges between 0.3 and 0.26 Hz as indicated by a transparent red band in Figure 1-2. This band has a negative slope with respect to the turbine diameter and is located close above the rated rotor speed range separated by an at least 10 % safety margin. For some monopile designs this lower limit of the design eigenfrequency rather than the fatigue strength is the design driver.

For large turbine size and deep water locations jacket type structures are considered the only economic alternative at present since floating structures are regarded not mature and competitive, yet. These jackets are providing inherently considerably higher stiffness even if combined with a slender tubular tower. Typical values for the first eigenfrequency range between 0.35 Hz for the 5MW class and 0.3 Hz for the 10 MW class. As a matter of fact the first eigenfrequency of the currently considered design concepts decreases only rather small when the size of the turbines increases. The reason for this trend is the reinforcement of the structural stiffness due to the larger footprint and member size required to provide sufficient strength against the ultimate limit state loads. Apparently the rather low slope of the band of the first eigenfrequency is penetrating more and more into the blade passing frequency range when the turbine size and diameter are rising. In the transparent red band entitled “jacket” in the diagram two dots are indicating the value of the first eigenfrequency of a typical 5 MW and the INNWIND reference turbine respectively. When the resonance frequency moves further towards the rated rotational frequency the resonating rotor speed is associated with a higher mean wind speed. This implies higher excitation energy as well as larger number of operational hours at this wind speed at exposed offshore sites. In order to limit the amplification of the fatigue loads a rather wide rotor speed exclusion zone (wider than  $\pm 10\%$ ) would be required if such a mitigation attempt will be effective at all.



$V_{tip} = 90 \text{ m/s}$   
 $1P_{rated} / 1P_{min} = 1.92$

Design trend for 1st eigenfreq.

Figure 1-2: Design trends on first design eigenfrequency and the rotor and blade resonance ranges for three-bladed offshore turbines in the 5 to 20 MW class

In summary, a strong and severe 3P (blade passing) resonance is expected for very large offshore turbines with jacket structures. Therefore the next two chapters shall highlight and assess challenges and opportunities for an integrated design approach for RNA and support structure on the basis of the 10 MW INNWIND reference turbine.

## 2 ANALYSIS OF INTERACTING DESIGN PARAMETERS AND DESIGN CHOICES

In order to investigate the interrelation of important design parameters of the support structure and the RNA the focus in this chapter is on loads that cause fatigue at the jacket structure. Therefore loads at the tower base node, which connects the tower to the jacket, are considered. The emphasis is on the fore-aft and side to side direction, as illustrated in Figure 2-1 and 2-2. Table 2-1 provides the associated frequencies of these first two combined RNA and support structure eigenfrequencies, as determined with the aeroelastic code HAWC2.

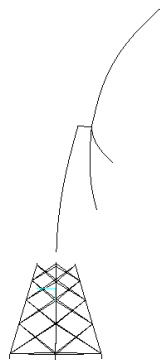


Figure 2-1: 1<sup>st</sup> Combined RNA and support structure mode (fore-aft)

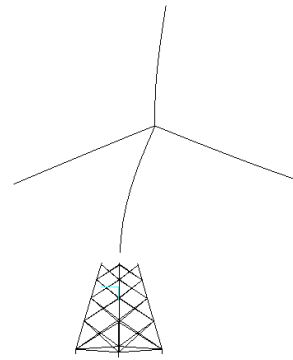


Figure 2-2: 2<sup>nd</sup> Combined RNA and support structure mode (side to side)

Table 2-1: Modes 1 and 2 of RNA in combination with support structure, obtained by HAWC2

Eigenmode	Frequency [Hz]
Combined mode 1 fore-aft	0.30
Combined mode 2 side to side	0.31

### 2.1 Hub height and design frequency for fundamental support structure mode

The first set of interacting design parameter to be investigated is the hub height and the first eigenfrequency of the support structure. Obviously a taller structure with larger hub height has significant influence among others on:

1. The systems dynamics through lower stiffness of the structure, i.e. lower eigenfrequencies and larger displacements of the tower top. This effects the aeroelastic loads of the rotor as well as the hydrodynamic excitation of the substructure, aerodynamic damping, and potential interaction of vibration modes of the rotor and support structure.

2. Higher loads at the substructure and foundation for the same tower top loads due to the longer lever arm.
3. the wind conditions at the rotor, affecting the annual energy production (higher annual average wind speed at hub height) and the aerodynamic loads (lower wind shear, lower turbulence, less sea spray and possibly more directional shear)
4. The investment cost of the support structure and possibly the installation cost of both the support structure and the rotor nacelle assembly.

In this section we are focusing on the influence of the fundamental eigenfrequency of the structure and on the annual energy yield

In several deliverables of WP4 (D4.1.2, D4.3.2) the dependency of the fatigue loads of the support structure to the first natural frequency of the structure has been analysed because the 10 MW reference design with its rather stiff jacket structure is sensitive to a resonance between the blade passing frequency and the first natural frequency of the structure. Kuhnle (Kuhnle-2015b) discussed the effect on the damage equivalent fatigue loads in both fore-aft and sideways direction. The results showed that the selected rotational speed characteristics of the reference design caused unfavourable excitations in partial load which causes supplement fatigue damage.

One option to influence the first eigenfrequency of the structure is to vary the hub height of the overall system. In this case the tower has been stretched in order to increase the hub height moderately by 6 % to 9 %. Hence the first eigenfrequency of the structure is lowered by 4 % to 8 % (Table 2-2). The moderate increase of the hub height results only in a small improvement of the wind conditions at hub height. Assuming a Rayleigh distribution with  $v_{ave} = 10$  m/s at 119 m height the extra energy yield is only 0.6 to 0.8 %

The length of the different tower sections has been linearly extrapolated and the mass has been adjusted accordingly. With this setting different aeroelastic simulations over the whole operational range from 4 to 24 m/s with turbulent wind field and wave excitation have been performed. The wind speed bins of 1 m/s have been chosen below till rated for a more detailed look on the behaviour around the resonance zone of the structure with the blade passing frequency (3P). Above rated the wind speed is varied by 2 m/s steps.

**Table 2-2: Variation of hub height and first eigenfrequency of the structure**

Hub height [m] and relative change in %		Eigenfrequency [Hz] and relative change in %		Relative change in annual energy production (AEP)
119		0.30		
126.05	5.9 %	0.2875	-4.2 %	0.58 %
129.25	8.6 %	0.275	-8.3 %	0.83 %

For comparison purposes the reference design with the speed exclusion zone has been compared with the reference design and the two taller variants without a speed exclusion zone in order to highlight the influence of the change of the eigenfrequency in the different wind speed regions.

Next aeroelastic simulations with wind and wave conditions according to the specification of the reference jacket deliverable (D4.3.1) are performed with the HAWC2 code. The parameters are listed in Table 2-3. Missing values in the partial load range (5, 7, 9, 11 m/s) have been interpolated linearly.

**Table 2-3: Wind and wave conditions for the aeroelastic simulations (D4.31)**

Mean wind speed [m/s]	Longitudinal turbulence intensity [%]	Significant wave height [m]	Peak spectral period [s]	Occurance [hours/year]
4	20.4	1.1	5.88	874.7
6	17.5	1.18	5.76	992.8
8	16	1.31	5.67	1181.8
10	15.2	1.48	5.74	1076.3
12	14.6	1.7	5.88	1137.2
14	14.2	1.91	6.07	875.6
16	13.9	2.19	6.37	764.7
18	13.6	2.47	6.71	501.3
20	13.4	2.76	6.99	336.0
22	13.3	3.09	7.4	289.4
24	13.1	3.42	7.8	130.4

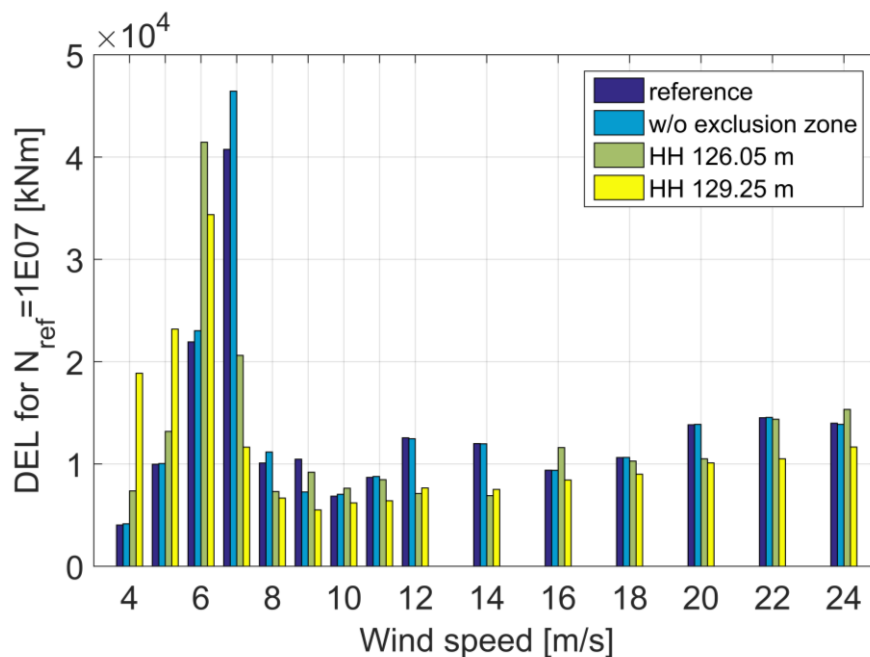


**Figure 2-3: DEL of tower base fore-aft moments for a hub height of 119 m, 126.05 m and 129.25 m respectively**

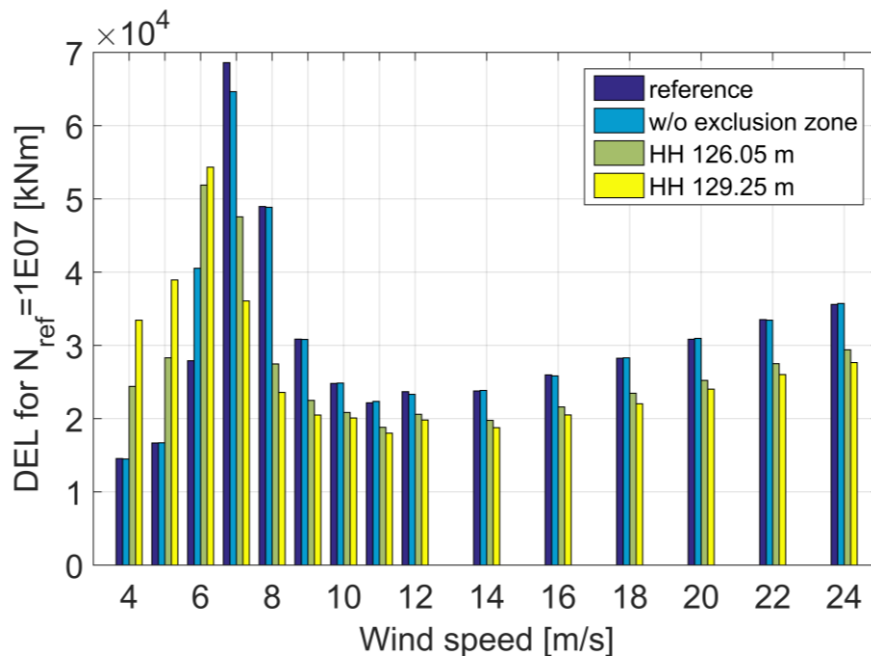


Figure 2-4: DEL of tower base sideways moment for a hub height of 119 m, 126.05 m and 129.25 m respectively

Figures 2-3 and 2-4 demonstrate that higher hub heights result in higher 1 Hz fatigue damage equivalent loads (DEL) for the fore-aft direction at the region where the 3P frequency matches the first eigenfrequency. This can be seen at wind speeds from 4 to 6 m/s. Wind speeds from 7 m/s to 24 m/s are experiencing a lower DEL. This is consistent with the findings of (Kuhnle 2015b), where it has been emphasized that a lower first eigenfrequency reduces the fatigue damage for wind speeds above the intersection between 3P and the first eigenfrequency. It is also visible that the highest hub height of 129.5 m gives only small advantages above this intersection region but higher DELs in fore-aft direction below this region.

In Figure 2-5 the lifetime weighted equivalent loads of the tower base moments are based the probability distribution on reference turbine. They are normalized to the fore-aft DEL of the reference turbine. It can be seen, that higher hub heights reduce the DELs more than the speed exclusion zone. The highest reductions can be seen in the fore-aft moments for 126.05 m with -11 % and 129.25 m with -13 %, in sideways direction -7.2 % and -14 % respectively.

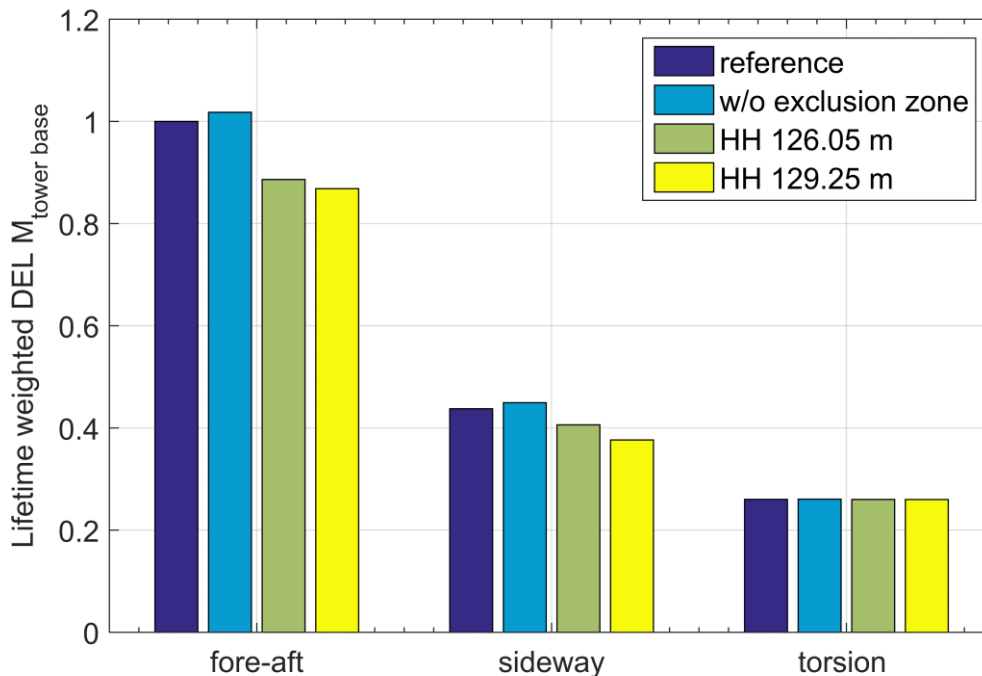


Figure 2-5: Lifetime weighted equivalent loads of tower base sideways moment for a hub height of 119 m, 126.05 m and 129.25 m normalized to fore-aft Moment of the reference design

The changes of the systems dynamics of the wind turbine lead to a change of the power characteristic as well. The electrical power output is analysed in comparison to the mean wind speed in turbulent wind conditions. Figure 2-6 plots the power curves of the different designs while Figure 2-7 shows the deviation of the mean electrical power with respect to the reference design with speed exclusion zone. So the effect of the reference design as well as the designs with 126.05 m hub height and 129.25 m hub height respectively each without speed exclusion zone can be compared. It can be seen that in partial load the power output slightly increases with hub height above 5 m/s.

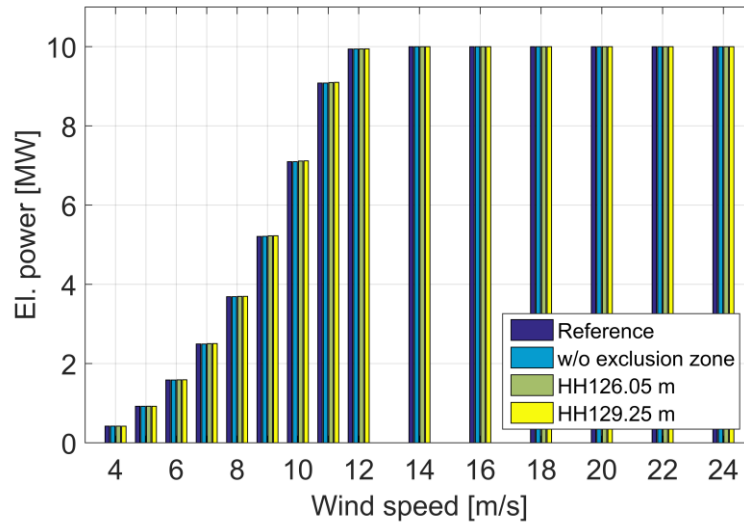


Figure 2-6: Electrical power output in turbulent wind field

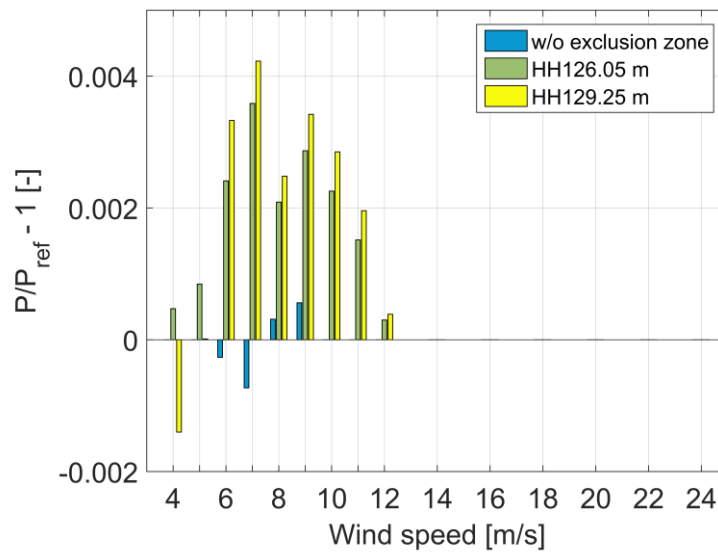


Figure 2-7: Difference of mean electrical power in turbulent wind compares to reference design with speed exclusion zone

## 2.2 Aerodynamic rotor design and operational speed range

In this section a further approach for a possible fatigue load alleviation for the support structure is investigated. Recently it has been shown for a generic 5MW turbine that a more slender blade design with an increased design tip speed ratio can lead to substantial fatigue load alleviations at the tower base in the fore-aft direction, especially in the partial load range (Berger 2015). Simulations in this section are performed within (Schwabe 2016).

For the INNWIND.eu reference turbine the fatigue loads at the tower base in fore-aft and side to side direction in the partial load range are of special interest, due to high fatigue load levels that originate from resonance effects (D4.1.2). With a higher design tip speed ratio this resonance effect is shifted to lower wind velocities. There are two effects that are anticipated to lower the fatigue loads due to this resonance operational point. Firstly the lower wind velocities have slightly less occurrence hours per year. Secondly with a shift to lower wind velocities the excitation energy due to the turbulent wind is reduced.

Based on the reference rotor two variants with a higher design tip speed ratio are redesigned. Firstly the operational speed range of the rotor is adapted to a higher tip speed ratio in the partial load range, including modifications to the speed exclusion zone. In a second step a simple scaling of the aerodynamic shape of the rotor blade is performed, based on the tip speed ratio increase. The two designs have a design tip speed ratio (TSR<sub>D</sub>) of 9.6 and 10.5 respectively.

The operational tip speed ratio in the partial load range is moved to higher values, so that the resonating blade passing frequency is reached at a lower wind speed. The recently updated controller of the reference design is equipped with a speed exclusion zone to minimize the influence of the driving frequency of about 0.3 Hz. This speed exclusion zone is adjusted, so that still the rotational frequencies between 0.275 and 0.325 Hz are avoided. The reference speed curve as well as the two adjusted speed curves for a design tip speed ratio of 9.6 and 10.5 are plotted in Figure 2-8. The curves have been obtained by a HAWC2 simulation with a firstly increasing and then decreasing wind ramp in the partial load range.

A hysteresis loop due to the speed exclusion zone is included. For increasing wind velocities the rotational speed is maintained at the lower level in this zone up to a defined generator torque and then quickly passes the hazardous frequency range. For decreasing wind velocities the rotational speed stays at the higher level and drops at a defined generator torque to the lower level. As mentioned above this exclusion zone is shifted to lower wind velocities for higher design tip speed ratios.

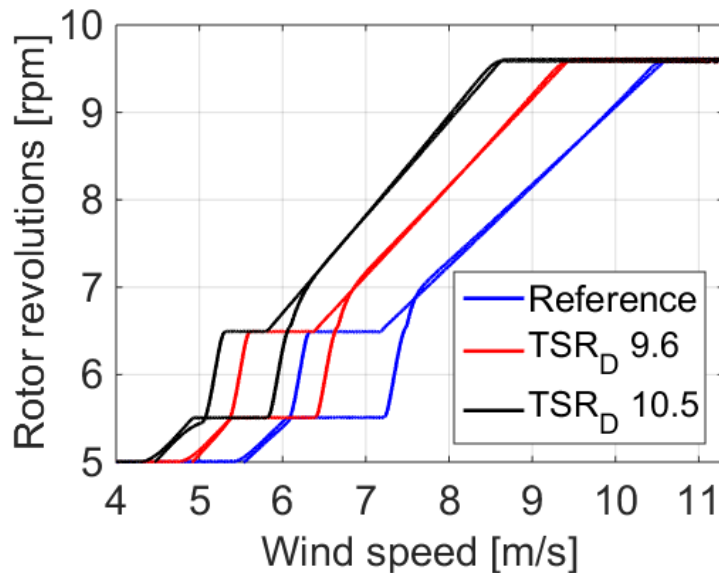


Figure 2-8: Rotational speed curve for wind velocities below rated operation with hysteresis loop due to speed exclusion zone for different design tip speed ratios

The slope of the speed curve of the reference rotor in Figure 2-8 corresponds to an operational tip speed ratio of 8.6, which is taken as the reference design tip speed ratio, although the rotor design is originally based on a lower design tip speed ratio (D2.1.1). For the purposes of this study the redesign of the blade is limited to the planform of the blades. The airfoils used at certain radii and the outer rotor radius are left unchanged. Therefore the reduction of chord leads to thinner blade cross sections in absolute terms. As a consequence the blade structure would have to be reinforced in order to maintain blade stiffness and strength. However at present the original distribution of geometrical moment of inertia and mass distribution is not altered. This crude assumption is considered as acceptable in this context where the focus is placed on the loading at the tower base. In this respect any change in the tower fatigue load levels can directly be attributed to the modifications in aerodynamic shape and operational speed.

The aerodynamic redesign of the blades is based on a change of the chord length by a tip speed ratio scaling (2-1), which is viable for high tip speed ratios (Gasch 2012).

$$f_{\text{chord}} = \left( \frac{\lambda_{D,\text{Ref}}}{\lambda_{D,\text{New}}} \right)^2 \quad (2-1)$$

For a design tip speed ratio of 9.6 the chord scaling factor  $f_{\text{chord}}$  accounts for 0.80 and for a tip speed ratio of 10.5 it accounts for 0.67, respectively. This chord scaling factor is applied to the blades from radii 0.43 R to the tip. The root region up to 0.22 R is left unchanged. Between 0.24 R and 0.41 R a linear transition is applied. The different blade planforms are illustrated in Figure 2-9.

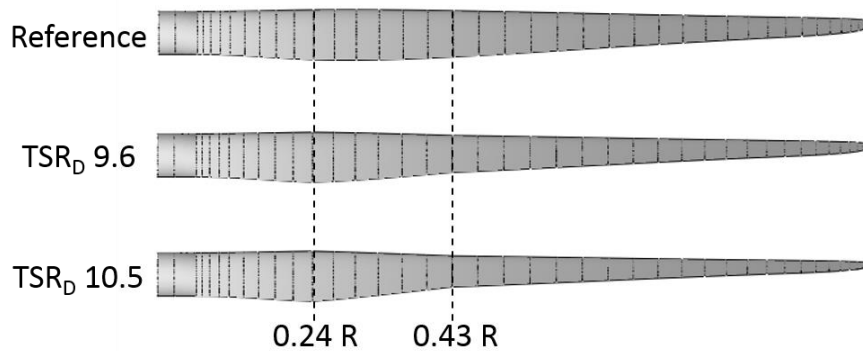


**Figure 2-9: Planform of the redesigned blades with increased design TSR (The operational TSR of the reference design equals 8.6.) (Schwabe 2016)**

The twist angle is adjusted by a constant value for radii up to 0.43 R and linearly interpolated between 0.43 R and the blade tip. For the design tip speed ratio of 9.6 the twist is reduced by 1° up to 0.43 R and by 0.5° at the tip. For the design tip speed ratio of 10.5 the pitch is diminished by 2° inboard and 1° at the tip. These values were obtained by basic Schmitz theory assumptions and validated by analysing the curves of power coefficient and thrust coefficient over tip speed ratio in a simple BEM code.

Simulations are performed with the aeroelastic code HAWC2. The wind and wave parameters are chosen according to the definition in Deliverable 4.3.1 (D4.3.1) as stated in Table 2-3. To get a higher resolution in the partial load range the wind speed bins have been refined in the region 4 - 12 m/s to 1 m/s steps by linear interpolation of the given values. For wind velocities 12 - 24 m/s the bin size is 2 m/s. For each wind velocity six ten minutes wind seeds are considered. This accounts to a total number of 270 ten minutes simulations for the three investigated designs.

The fatigue loads are given as 1 Hz damage equivalent loads and the median value of the six seeds for each design and wind velocity bin is shown. The results for the tower base in the fore-aft and the side to side direction are plotted for the three designs in Figure 2-10 and Figure 2-11, respectively.

It can be seen, that the highest load levels are obtained in the partial load range, especially in the range 6 - 8 m/s. This is where the triple rotational speed (3P) has the same value as the first combined eigenfrequency of the system. This resonance effect is already minimized by the adaption of a speed exclusion zone, as already was illustrated in Figure 2-8. With the reference rotational speed curve the highest fatigue load levels are obtained at 7 m/s in the fore-aft direction as well as in the side to side direction. The fatigue load in both directions are of the same magnitude. For the rotors with higher design tip speed ratio this passing through the avoided frequency range takes place at a lower wind speed. The fatigue loads in fore-aft direction for the TSR 9.6 and 10.5 reach their maximum level at 6 m/s and are also at a lower value than the maximum of the reference case. For the side to side fatigue loads the same trend is seen but the loads are significantly lower, than the maximum loads of the reference case.

For operation in the full load region from 12 m/s the fatigue load levels follow a linearly increasing trend with increasing wind velocity, whereas the reference rotor is suffering the highest fatigue loads and the most slender rotor, which has the highest design tip speed ratio is subject to the lowest fatigue load level. The plotted results indicate, that a shift of the speed exclusion zone to lower wind velocities through a higher tip speed ratio in the partial load range leads to a decrease of the maximum fatigue loads. This reduction takes place for both, the fatigue loads in fore-aft direction and in side to side direction, whereas the reductions is more pronounced for the side to side loads.

For the levelised cost of energy (LCOE) the investment in production, installation and operation of the wind turbine system stands against the revenues from the energy production. Therefore in addition to the load reduction potential the influence of the changes on the annual energy production (AEP) is assessed as well.

In Figure 2-12 the energy production of the two designs with increased design tip speed ratio is normalised to the energy production of the reference design. The electrical energy production of all six seeds, which are the same for the different designs, is taken.

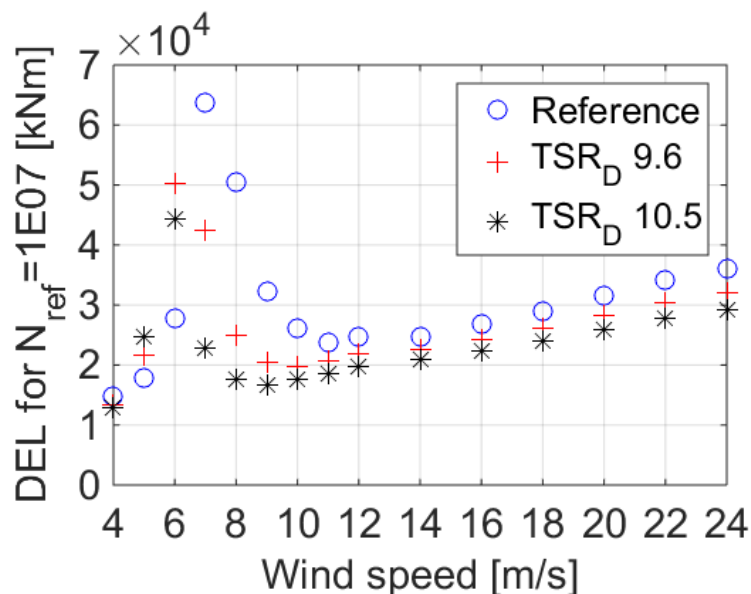


Figure 2-10: Median value of the fore-aft tower base DEL for different design tip speed ratios

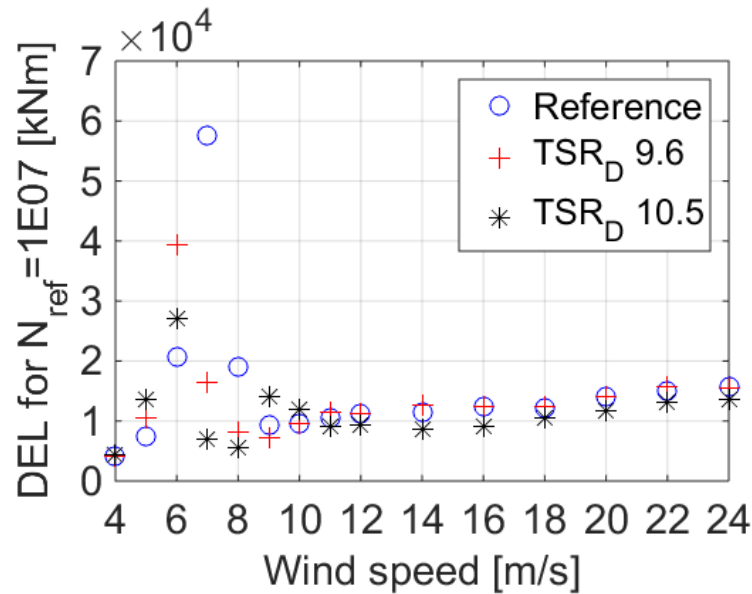


Figure 2-11: Median value of the side-side tower base DEL for different design tip speed ratios

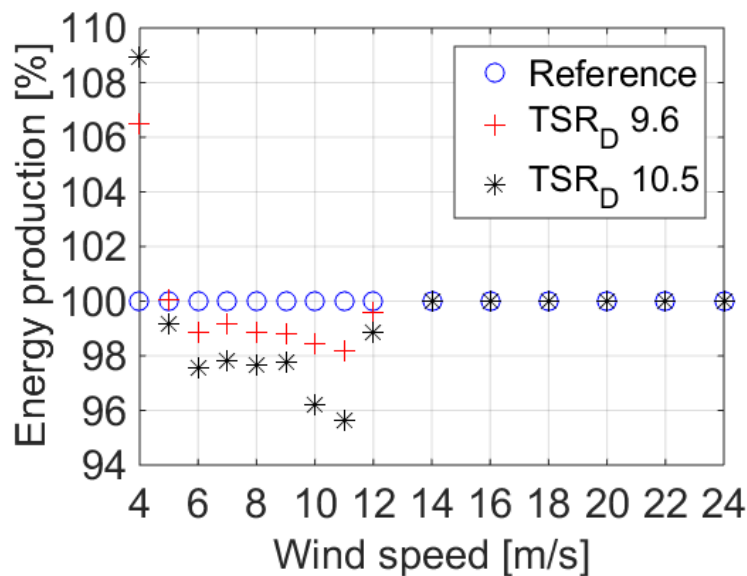


Figure 2-12: Energy production of the different design tip speed ratios at different wind speeds, normalized to the reference rotor

At the cut-in wind speed of 4 m/s the  $TSR_D 10.5$  design shows the highest energy production and also the  $TSR_D 9.6$  rotor is still in favour of the reference design. This is obvious, as all designs operate at a tip speed ratio above 11 at this point due to the minimum rotational speed, which benefits the higher  $TSR$  designs. For the wind speed region of 5 – 12 m/s the new designs suffer a slight drawback in terms of energy production. For the region 5 – 9 m/s these are thought to be

avoidable with a more thorough design approach. For the region 9 – 12 m/s another factor becomes important. As the designs with higher design tip speed ratio already operate at rated revolutions, the operational tip speed ratio is below the design tip speed ratio and the aerodynamic efficiency reduces.

In a last step the fatigue loads at the tower base and the energy production are compared on the basis of the given occurrence hours in Table 2-3, interpolated for the partial load range to a bin width of 1 m/s as before.

The life time equivalent loads (LTEL) are calculated based on (2-2), with  $m$  being the inverse slope of the SN curve,  $\omega$  a weighting factor based on the occurrence hours and  $k$  the maximum seed number per wind bin.

$$LTEL = \sqrt[m]{\sum_{i=1}^k [w_i * DEL(i)^m]} \quad (2-2)$$

The annual energy production is also calculated based on the given occurrence hours. The results are compared in Table 2-3.

**Table 2-3: Change is in lifetime weighted tower base fatigue loads (LTEL) and Annual Energy Production (AEP) for the high design tip speed rotors with respect to the reference design**

Rotor design	LTEL Tower bottom Mx (fore-aft)	LTEL Tower bottom My (side-to-side)	AEP
Reference TSR 8.6	-	-	-
TSR <sub>D</sub> 9.6	-19.3 %	-31.9 %	-0.22 %
TSR <sub>D</sub> 10.5	-32.3 %	-51.1 %	-0.90 %

A significant reduction in LTEL is found for the designs with higher design tip speed ratio, whereas the large TSR<sub>D</sub> yields most load mitigation. The load reductions for the side to side response are higher than in fore – aft direction. The reduction in AEP for the TSR<sub>D</sub> 9.6 is lower than for the TSR<sub>D</sub> 10.5, which still is less than 1 %.

Three main parameters have been identified, that lead to the substantial fatigue load reductions at the tower base. Firstly, as stated before, the occurrence of the critical rotor speed setting is reduced, as it is shifted to lower and scarcer wind speeds. Secondly with a shift to lower wind velocities the excitation energy due to the turbulent wind is reduced. The third reason is the reduced variance of the lift force along the blade span. Due to the turbulent nature of the wind there are frequent changes in the angle of attack at the blade. Considering one blade segment with the width  $b$  the lift force  $F_L$  (2-3) is dependent on two variables that alter due to the turbulent wind. These are firstly the relative wind velocity  $w$ , which is mainly dependent on the revolutions that change inertly. And secondly the lift coefficient  $C_L$ , that changes due to the variation of angle of attack, originating from the turbulent inflow. This parameter fluctuates strongly. The chord length  $c$  and the density  $\rho$  are constant factors. The mean lift force at a specific radius and a given wind condition at design operating conditions in the partial load range are the same for the three blade designs, as the

reduced chord is counteracted by the higher relative wind speed, for the high design tip speed ratios. Considering a simple velocity triangle with increasing tip speed ratio the rotational component gets more pronounced in relation to the wind component. Wind fluctuations therefore cause less variance in the angle of attack and thus the lift coefficient. Subsequently the lift variance on a blade station is reduced by the approach of higher design tip speed ratios.

$$F_L = C_L \frac{1}{2} \rho w^2 (bc) \quad (2-3)$$

In summary, based on a simple aerodynamic design exercise it has been demonstrated that an increase of the design tip speed ratio can benefit the fatigue loads at the tower base and thus jacket structure by a significant amount. The drawbacks in energy yield (AEP) remain reasonably small. It therefore is strongly advised to look further in this direction of slender high tip speed ratio blades for large offshore turbines, especially when there is a problem of 3P resonances in the operational range. However in reality these adaptations bring further challenges with it, which probably include use of very thick profiles to provide the needed blade stiffness, edgewise reinforcements and aerodynamic designs that work well over a range of tip speed ratios in the partial load range, due to tip speed constraints.

### 2.3 Blade – tower interaction

For both the common upwind as well as for downwind rotor orientation an aerodynamic interaction takes place between the blades and the tower. When a blade passes the tower the apparent wind speed and the inflow angle are changing suddenly due to the tower shadow effect. Apart from instationary aerodynamic effects the thrust loading is altered periodically during every blade passage. This periodic load is transformed in the frequency domain to harmonic load components which order number depend on the location in the turbine. The blades are experiencing multiples of the rotational (1P) frequency, i.e. 1P, 2P, 3P, 4P, etc. while the non-rotating nacelle and tower system is excited by multiples of the blade passing frequency, i.e. 3P, 6P, 9P, etc. Also the main shaft is suffering harmonic load components. Especially the 3P component of the longitudinal and lateral thrust is critical for the relatively stiff jacket type support structures required for very large 10-20 MW bottom-fixed offshore wind turbines. Generally the tower shadow effect for a downwind rotor will be more pronounced. Hence a truss type tower with semi-transparent aerodynamic shape will be beneficial for downwind rotors of large wind turbines. In the year 2015 a 6 MW prototype of a two-bladed downwind turbine has been installed onshore on a lattice type structure.

For long and slender blades the blade stiffness and the tower clearance at extreme load situations is one design driver. Commonly design choices to increase the tower clearance of the undeflected blades are the increase of the rotor tilt angle, a rotor cone angle or pre-bend blades. Increasing the blades stiffness without additional blade weight is another attempt which requires the usage of more expensive materials, like carbon fibre reinforced plastics. Each of these measures has collateral effects on the blade and drive train loads and/or on the blades structure. Nonetheless almost all large multi-megawatt turbines employ at least one or even a combination of these choices.

From a strength point of view an increase of the tower diameter or of the effective diameter of the cross section of the tower truss is beneficial. However tubular towers with large D over t ratio, i.e.

diameter to wall thickness ratio, are limited by shell buckling. Shell stiffener commonly used in aerospace engineering are not yet employed in wind engineering due to high manufacturing costs. If the tower is built from a truss its diameter will be governed by the above-mentioned blade clearance which in effect reduces the structural efficiency of such a tower design. In addition, a large stiffness of the tower is incompatible with a rather stiff jacket substructure since such an unfavourable combination yields a high fundamental eigenfrequency of the system which can again cause a 3P resonance in the partial load range as experienced with the reference design.

This qualitative discussion points out that there are several interactions between on the one hand blade and rotor design and on the other hand tower and support structure design which might become more critical for 10-20 MW turbines. Further systematic studies are recommended in order to develop more integrated and cost-effective design solutions.

## 2.4 Effect of tower top mass and electro-mechanical drivetrain

Obviously the mass of the rotor-nacelle-assembly (RNA) is one main cost driver for the investment cost of the machinery of wind turbines. The reduction of tower top mass by innovative rotor and drive train designs has been one quite effective mean to improve the cost-efficiency of modern wind turbines in the last two decades.

The first eigenfrequency is proportional to the square root of the ratio between horizontal tower top stiffness and effective tower top mass. Consequently for the commodity offshore wind turbines founded on monopiles a lower top mass is fully effective since it avoids that the fundamental eigenfrequency is getting in resonance with the rotor frequency and is lowered to far down into the energy rich wave excitation range. Furthermore a lower tower top mass stretches the applicability of cost-effective monopile design towards exposed locations with water depth in excess of 30 m.

A distinct influence is observed for large offshore turbines on jacket type structures. Here a stiffer structure increases the problems with the resonance between the first eigenfrequency and the 3P blade passing frequency. In case a rotor speed exclusion window is required in the partial load range it should be placed as close as possible to the cut-in wind speed, i.e. the disturbing natural frequency should be as low as possible. A parameter study on the effect of the effective tower top mass, obtained with the aeroelastic code HAWC2, on the first eigenfrequency of the reference design is shown in Figure 2-13. In the vicinity of the reference configuration the first eigenfrequency depends approximately linearly inverse on the tower top mass. A +/-10 % change of the RNA mass yields an approximately +/-4 % alternation of the frequency.

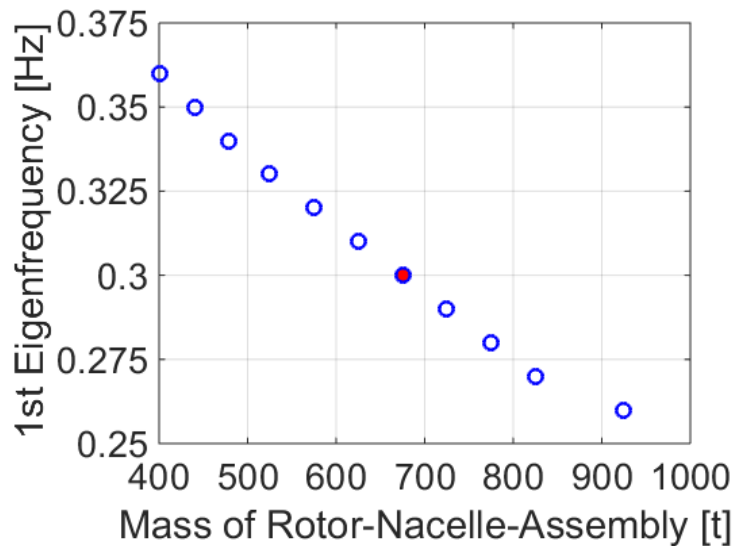


Figure 2-13: First combined eigenfrequency of RNA, tower and jacket over tower top mass; data from (Schwabe 2016)

The tower top mass and the first eigenfrequency also influence the aerodynamic damping of the fundamental fore-aft eigenmode of the RNA-support structure system in an inverse manner, i.e. the damping reduces for heavier tower top masses and stiffer structures.

This effect can be further discussed by an instructive, analytical expression (2-4) for the damping ratio as fraction of critical damping quoted from (Kühn, 2003) and based on (Garrad, 1990). The relation is based on stationary rotor aerodynamics and some simplifications valid for a wind turbine operating with a high tip speed ratio and near the rated wind speed.

$$\xi_{aero} = \frac{N_b \rho \Omega}{8\pi f_0 M_0} \int_{R_{root}}^R \frac{dc_L}{d\alpha} c(r) r dr \quad (2-4)$$

where:

- $\xi_{aero}$  aerodynamic damping ratio as fraction of critical damping
- $N_b$  number of blades
- $\rho$  air density
- $\Omega$  rotational speed of the rotor [rad/s]
- $f_0$  frequency of the first fore-aft mode [Hz]
- $M_0$  modal mass of the single degree of freedom system
- $R_{root}, R$  blade root rotor radius, outer rotor radius
- $dc_L/d\alpha$  slope of the lift coefficient with respect to angle of attack
- $c(r)$  chord length at radius  $r$
- $r$  spanwise coordinate

The modal mass is estimated by the following relation, with  $s$  being the tower top stiffness (2800 kN/m) and the eigenfrequency  $\omega$  as shown in Figure 2-13.

$$M_0 = \sqrt{\frac{s}{\omega^2}} \quad (2-5)$$

In Figure 2-14 the aerodynamic damping ratio for the reference design with a constant first eigenfrequency is plotted as function of the tower top mass. Purely attached flow with a lift slope of  $2\pi$  has been assumed. Two curves are shown for the critical resonating rotor speed of 6 rpm and the rated rotor speed of 9.6 rpm respectively. Since the aerodynamic damping is proportional to the rotational speed, by 1/3 lower damping values are found in the lower partial load range at 6 rpm compared to the rated rotor speed. This highlights another reason why a 3P resonance in this range is rather critical and why a higher operational tip speed ratio can be beneficial in this region.

Such a case of reduced tower top mass at constant first eigenfrequency can happen when a less heavier RNA e.g. with a light-weight drive train is used but the first eigenfrequency is kept constant by slightly lower support structure stiffness in order to not affect the Campbell diagram. Here indeed a lower tower top mass is beneficial also from the dynamic point of view but it improves the aerodynamic damping only slightly.

If the stiffness of the support structure is held constant while the tower top mass is lowered, the first eigenfrequency is increased according to Figure 2-13. While the higher first eigenfrequency amplifies the 3P resonance problem (see Section 4) there is a small positive effect on a slightly higher aerodynamic damping illustrated by Figure 2-16.

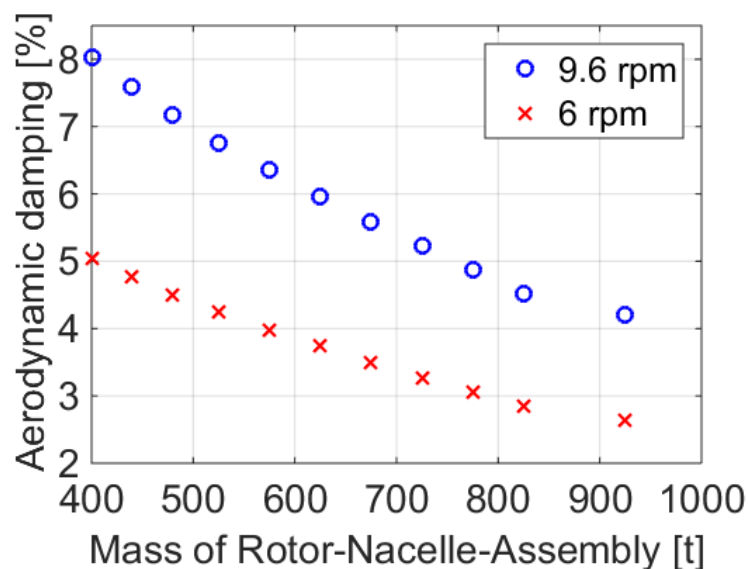


Figure 2-14: Aerodynamic damping estimation over tower top mass for rated revolutions at 9.6 rpm and the resonance case at 6rpm at a constant first eigenfrequency of 0.30 Hz

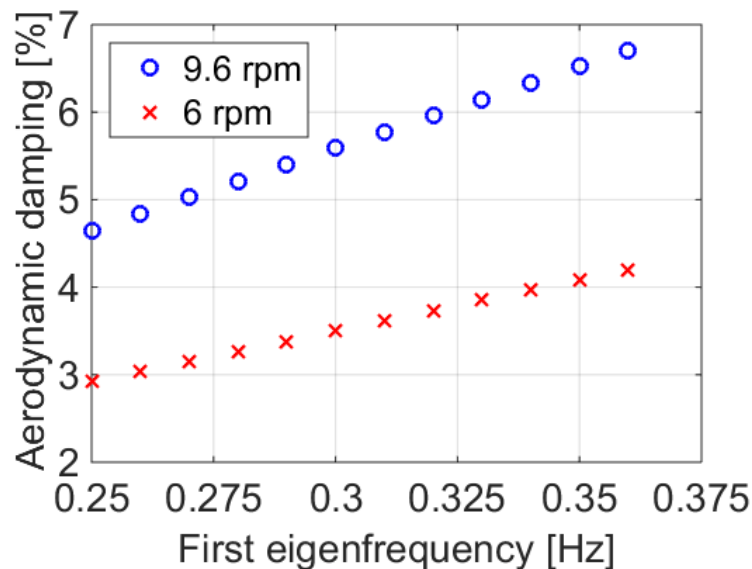


Figure 2-15: Aerodynamic damping over first combined eigenfrequency of RNA, tower and jacket. The different eigenfrequencies result from variation of the tower top mass according to Figure 2-12.

Considering only the overall dynamics of the reference design a heavier tower top mass would be beneficial since it reduces the 3P resonance problem with only a small penalty on the aerodynamic damping. From a levelised cost of energy (LCOE) point of view however it is hard to argue that a more heavy and consequently more expensive rotor or drive train will reduce the resonance problems in the support structure and the fatigue loads of the support structure so significantly that this would yield overall lower LCOE. On the other hand it is clear that the effort of a lower mass of the rotor and the machinery have to be paid fully by cost reductions in these components and installation costs or by improvement of the energy yield since the support structure loads are affected negatively. Maybe an extra trim mass in the tower top or an extra mass required anyway for a structural tower damper could be a more efficient solution to improve the overall dynamics, loading and LCOE.

## 2.5 Effect of first eigenfrequency of the support structure – RNA system

At the end of this chapter the direct effect of changes of the first combined eigenfrequency on the tower base fatigue loads is studied in the entire production wind speed range. The objective is to investigate the influence of a shift of the first combined frequency to higher and lower values, thus representing a design of a stiffer, respectively softer tower and support structure. In the Campbell diagram this means moving the first combined frequency in a vertical manner and this way influencing the wind turbine system dynamics.

Figure 2-16 and 2-17 illustrate the damage equivalent fatigue loads at the tower base in fore-aft and side-to-side direction respectively over the production wind speed range. The contour plots are normalized with the lower value in each diagram. The vertical red lines are indicating the wind speed at hub height when a rotor speed of 6 rpm is reached and the wind speed with the activation of the pitch control and the rated wind speed respectively. Furthermore the 3P excitation frequency and a  $\pm 10\%$  frequency band is shown. In the vicinity of the curve of the 3P excitation strongly amplified fatigue loads can be seen. Hence the first design eigenfrequency should not be positioned between 0.28 and 0.35 Hz. However, lowering it to a value of 0.275 Hz or below would result in significantly reduced fatigue loads in the entire production wind speed range.

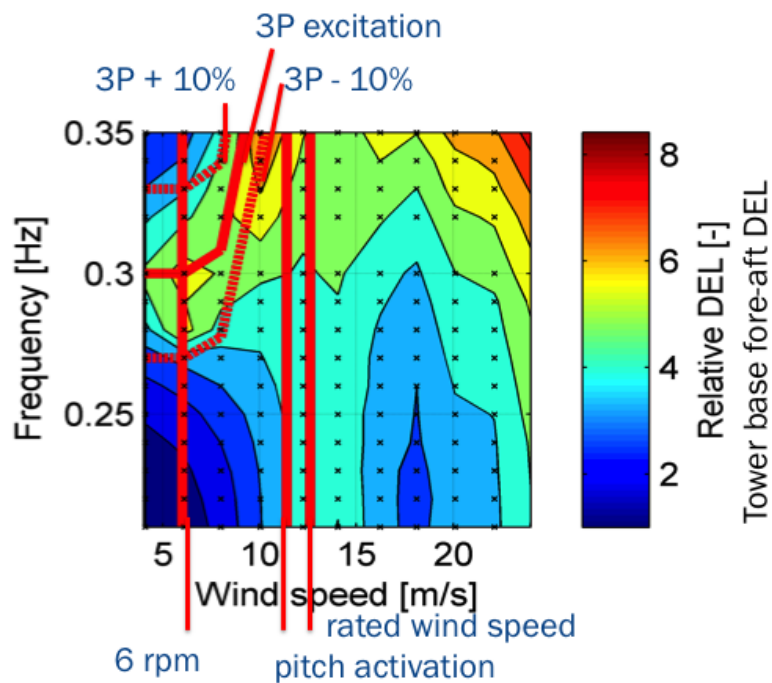


Figure 2-16: Relative damage equivalent loads for  $N_{ref}=10^7$ , SN-slope  $m = 4$  over wind speeds and natural frequency for fore-aft tower base direction (Kuhnle 2015a)

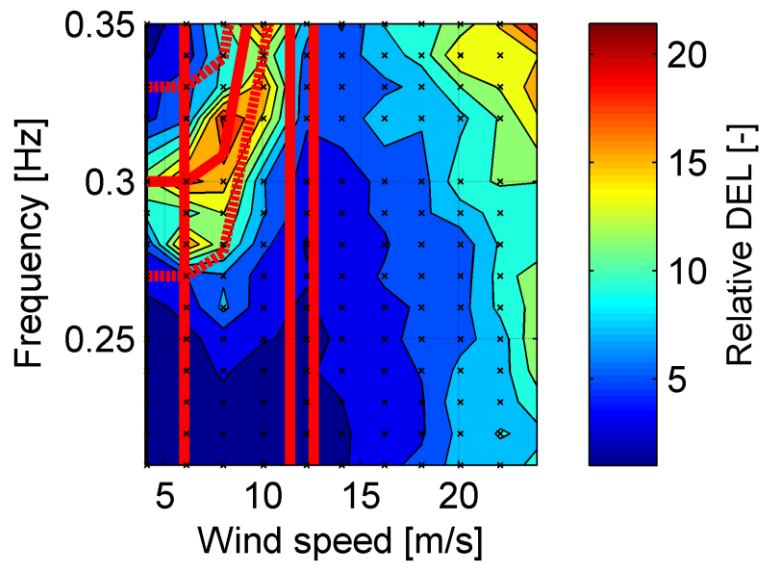


Figure 2-17: Relative damage equivalent loads for  $N_{ref}=10^7$ , SN-slope  $m = 4$  over wind speeds and natural frequency for side-to-side tower base direction (Kuhnle 2015a)

### 3 COST-EFFECTIVE DESIGN METHODOLOGIES

An integrated design of the rotor-nacelle-assembly and the support structure requires detailed design analyses of the overall turbine configuration and its components and the evaluation of the technical and economic key performance indicators. Such an exercise includes cumbersome aero-servoelastic load analyses of the RNA with at least a simplified support structure and aero-hydro-servoelastic analyses of the entire turbine with a detailed substructure and foundation model. In the following only qualitative recommendations without any quantitative load and design analyses can be given with respect to the indented 10 and 20 MW INNWIND wind turbine designs.

Table 3-1 compares five indicative 10 and 20 MW turbine designs.

**Table 3-1: Main parameters of the 10 and 20 MW INNWIND wind turbines. Comparison of up-scaled and adjusted values**

Parameter	INNWIND 10 MW onshore	INNWIND 10 MW offshore	10 MW adjusted	20 MW up-scaled	20 MW adjusted
Rotor diameter [m]	178.3	178.3	205.9	252.2	291.2
Power density [W/m]	400	400	300	400	300
Number of blades	3	3	3	3	2
Maximum tip speed [m/s]	90	90	105	90	100
Aerodynamic design	classical	classical	low induction, low solidity	classical	low induction, low solidity
Rotor speed range [rpm]	6 – 9.6	5.5 – 9.6	6.0 – 9.7	4.9 – 8.0	4.3 – 6.9
Rotor speed variability $1P_{rated} / 1P_{min}$ [-]	1.92	1.92	1.61	1.92	1.92 or larger
rotor speed exclusion zone	no	yes	no	yes	no
Support structure type	tubular tower	jacket with tubular tower	jacket with tubular tower	jacket with tubular tower	jacket with tubular tower
Hub height [m]	119	119	≈ 130 or taller	≈ 170	≈ 170 or shorter
1 <sup>st</sup> eigenfrequency [Hz]	0.25	0.30	≤ 0.275	≈ 0.25	≥ 0.25
Dynamic tower characteristics	soft-stiff	soft-stiff	soft-stiff	soft-stiff	stiff-stiff

The first and the second configuration include the 10 MW onshore INNWIND reference design and the 10 MW design with adjusted cut-in rotor speed and rotor speed exclusion zone combined with the 10 MW reference jacket. The latter configuration has been analysed in Chapter 2 and severe problems with the 3P blade passing resonance have been recognized. Therefore an adjusted 10 MW design is proposed here and described in more detail in the following. The fourth turbine parameter

set corresponds to a direct up-scaling of the 10 MW INNWIND offshore reference design to 20 MW rated power. Since here an even more pronounced 3P resonance is expected also an adjusted 20 MW design is indicated. The dynamic configuration of the 10 and 20 MW up-scaled offshore design respectively (column 3 and 5 in Table 3-1) is shown in Figure 3-1. As expected from the discussion in Chapter 1 a 3P resonance takes place for the 10 MW design close to the cut-in rotor speed and the 20 MW machine would suffer from a likewise resonance more in the centre of the rotor speed range. Both machines feature a high power density of 400 W/m<sup>2</sup>, an aerodynamic design with maximum tip speed of 90 m/s, classical high induction and solidity blade design, a relatively short tower with a soft-stiff dynamic characteristics and a rotor speed exclusion zone in order to mitigate in an insufficient manner the 3P resonance.

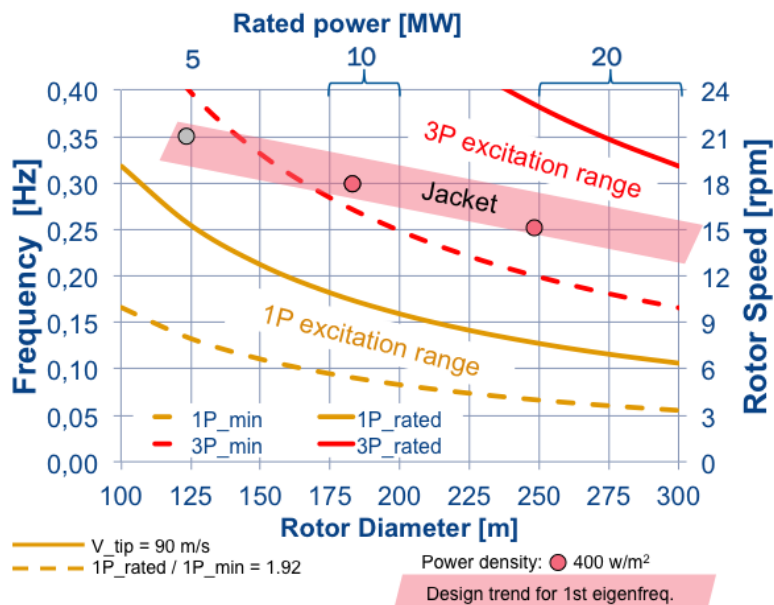


Figure 3-1: Expected frequency configuration for the INNWIND 10 and 20 MW turbine design resulting from direct up-scaling indicated by red dots.

For an optimised 10 MW INNWIND design either a softer substructure like the monotower with bucket foundation (D4.3.2) or a redesigned overall configuration should be aimed for. In order to improve the cost of energy different low induction rotor design partly with increased tip speed have been developed in Task 2.1 (D2.1.1). The gain in energy yield due to an increase of rotor diameter more than compensates the loss in aerodynamic efficiency of the low induction design. Furthermore a preliminary analysis showed that most likely the load level could be maintained, which is very important for the economic design of the support structure. From a dynamic point of view it is very preferable to achieve a classical soft-stiff design with a first eigenfrequency well below the cut-in rotor speed. In order to accomplish this the following design changes are proposed and are indicated by a shift of the red (old) to the green (new) design point in Figure 3-2.

- Increase of the hub height to approximately 130 m or taller in order to lower the first eigenfrequency from 0.30 to 0.275 Hz or below
- Significant increase of the maximum tip speed to approximately 105 m/s. Such a value is relatively high for three-bladed design. Most likely the design tip speed ratio of the rotor should be increase as well which could provide additional benefits as described in Section 2.2.
- Reduction of the rotor speed variability, i.e. ratio between rated rotor speed and cut-in rotor speed from 1.92 down to 1.61. This effect is indicated by dashed and dotted curves respectively in Figure 3-2.
- Advanced controls like higher order individual pitch control (IPC) (see Task 1.4) aiming at the reduction of dynamic loads on both rotor and support structure.

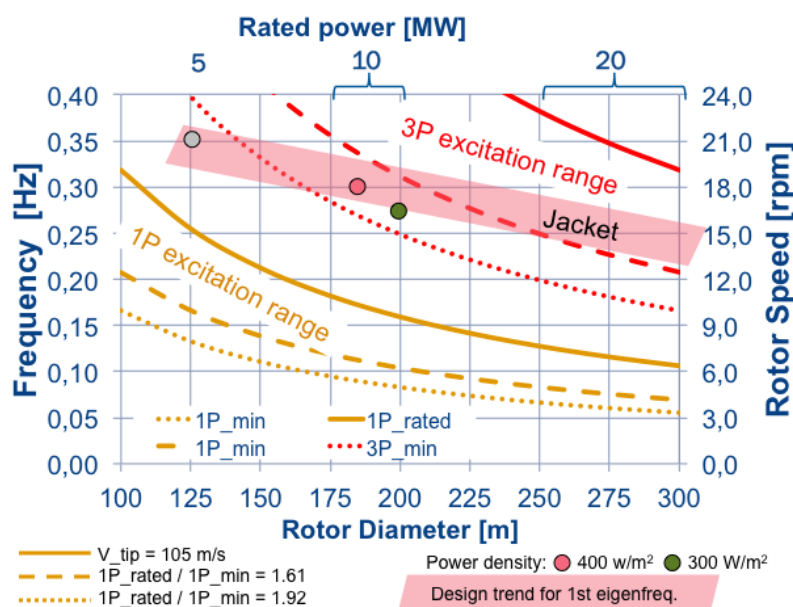


Figure 3-2: Example of the frequency configuration for an adjusted INN WIND 10 MW turbine design. Red dot direct up-scaling, green dot adjusted design.

Despite the fact that the energy yield and cost of energy could be improved by the increase of the rotor diameter from 178.3 to 205.9 m (decrease of the power density from 400 to 300 W/m<sup>2</sup>) this measure is counter active in respect to the dynamic characteristics since it lowers the operational rotor speed range.

In total it should be possible to realize a first design eigenfrequency which is at least 10 % below the cut-in rotor speed in order to facilitate sufficient distance to the strong 3P excitation without any rotor speed exclusion zone.

Even more rigorous design changes are required for an optimised 20 MW INNWIND design. Further investigations in Task 4.1 are required to check the feasibility of a monotower with a large multi-bucket foundation. Such a support structure in combination with a similar rotor design than the above-mentioned optimised 10 MW design might be able to provide a soft-stiff overall configuration as well. From the support structure design point of view straighter forward but still challenging will be a rather stiff jacket substructure with a relatively short tubular tower. Matching such a concept with a two-bladed rotor design could achieve a stiff-stiff dynamic characteristics where the 1<sup>st</sup> eigenfrequency is at least 20 % above the 2P blade passing frequency at rated rotor speed. With the increase of turbine size during the last three decades stiff-stiff tower designs have died out in the wind energy community. The main reason is that for common utility scale turbines it is not economical to build towers with such high stiffness. In addition a stiff-stiff design is experiencing inherently higher dynamic loads compared to a soft-stiff design when the same safety margin, e.g. 10 %, between the first eigenfrequency and the excitation frequency is maintained (see Kühn, 2011, Section 9.3.2). Therefore here a larger safety margin and advanced controls to mitigate the 2P tower excitation will absolutely be required. In total the following main design changes are proposed with respect to a directly up-scaled 20 MW concept.

- Aiming at a light-weight rotor-nacelle-assembly which is opposite to the square-cube law for such a giant turbine.
- Maintaining a low or even a decrease of the hub height to approximately 170 m or lower in order to achieve a first eigenfrequency of at least 20 % above the rated (2P) blade passing frequency.
- Choosing a two-bladed rotor with a moderate or low maximum tip speed to 100 m/s or lower with a low induction, large rotor diameter. Close to the rated wind speed a low maximum tip speed will result in an operational tip speed ratio which is significantly lower than the design tip speed. The reduced aerodynamics efficiency at the high wind speed offshore site will cause extra losses in energy yield. This should be compensated by the above-mentioned increase in rotor diameter.
- A high rotor speed variability of 1.92 or even larger could be maintained.
- Advanced controls like higher order individual pitch control (IPC) and/or smart blades with multiple flaps (see Task 1.4) aiming at the reduction of dynamic loads and especially the 2P excitation by the thrust force and the yaw moment on the support structure.

Again the up-scaled (red) and the adjusted 20 MW design (green) are indicated by dots in the frequency diagram in Figure 3-3.

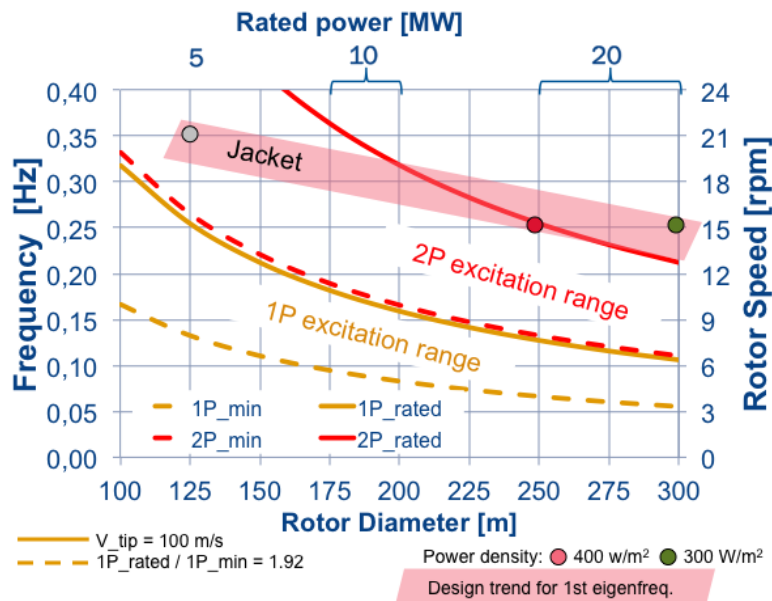


Figure 3-3: Example of the frequency configuration for an adjusted INNWIND 20 MW turbine design. Red dot direct up-scaling, green dot adjusted design.

## 4 CONCLUSIONS

A strong and severe resonance in the operational range is expected for very large offshore turbines in the 10 to 20 MW class between the 1<sup>st</sup> eigenfrequency of the combined rotor-nacelle-assembly and support structure system and the 3P (blade passing) frequency. The problem has been analysed at the example of the 10 MW INNWIND reference wind turbine on top of the INNWIND reference jacket. The damage equivalent fatigue loads at the tower base in fore-aft and especially in the side-to-side direction are significantly increased in the lower partial load range despite the fact that a rotor speed exclusion zone is employed.

A parameter study has been carried out which highlighted the following mitigation aspects:

- Lowering the first combined eigenfrequency below the cut-in rotor speed. This could be achieved by a combination of taller structure with larger hub height, higher RNA mass (if acceptable), increase of the cut-in rotor speed by reduced rotor speed variability and/or increased rated rotor speed.
- Rotor design for a higher design tip speed ratio resulting in load reduction and only moderate losses in the annual energy yield.

The effect of such design changes on the damage equivalent fatigue loads at the tower base, the energy yield and the aerodynamic damping has been analysed.

Another conceptual design choice could be to replace the stiff jacket with a softer support structure type. Since monopiles are not considered feasible for 10 to 20 MW turbines in large water depth the investigation of a monotower with bucket foundation could be an interesting development attempt.

In order to achieve a more integrated design of the RNA and support structure for the 10 and 20 MW INNWIND turbines the adjustment of several design parameters has been proposed resulting in:

- Three-bladed 10 MW design with a soft-stiff dynamic characteristics
- Two-bladed 20 MW design with a stiff-stiff dynamic characteristics

Both design should maintain or reduce the load level with respect to up-scaled concepts by a low induction rotor with high tip speed and advanced individual pitch control and/or smart blades. The energy yield is improved in both cases through a larger rotor diameter and a lower power density. In total a significant reduction in levelized cost of energy (LCOE) is expected by these conceptual changes which consider the entire system in a more integrated manner. In order to realise this potential more detailed load and design analyses involving the RNA and support structure design and researchers from Work Package 1, 2 and 4 will be required.

## BIBLIOGRAPHY

Berger, F. and Kühn, M.: "Investigating the aerodynamic implications of slender wind turbine blade design". in Proc. Proceedings DEWEK 2015, Bremen, 2015.

INNWIND.EU Deliverable D2.1.1 - "New Aerodynamics rotor concepts specifically for very large offshore Wind turbines", innwind.eu, accessed 2015-15-08

INNWIND.EU Deliverable D4.1.2 - Innovations on component level (interim report), "DeliverableD412\_20150831\_final\_Rev01.pdf", internal teamsite, accessed 2015-09-08

INNWIND.EU Deliverable D4.3.1 - "Reference Jacket", innwind.eu, accessed 2015-15-08

INNWIND.EU Deliverable D4.3.2 - "Innovative Concepts for Bottom-Mounted Structures" Rev.03, forthcoming

Gasch, R. and Twele, J.: "Wind Power Plants", Springer Berlin, 2012

Garrad, A.D, Forces and Dynamics of Horizontal Axis Wind Turbines. In: Freris, L.L. (Ed.), Wind Energy Conversion Systems. Prentice Hall Int., 119 - 144, 1990.

Kühn, M.: "Dynamics and Design Optimization of Offshore Wind Energy Conversion Systems". PHD thesis, TU Delft, 2001.

Kuhnle, B., Kühn, M.: "Strukturelle Dämpfer - Ein alter Hut oder Innovation für große Windenergieanlagen?", 6.VDI-Fachtagung Schwingungen in Windenergieanlagen 2015, Bremen, Germany

Kuhnle, B., Kühn, M.: "Unfavourable trends of rotor speed and systems dynamics for very large offshore wind turbines - Analysis of the 10MW INNWIND.EU reference turbine", EWEA Offshore Conference 2015, Copenhagen, Denmark

Schwabe, R.: "Aerodynamic analysis and optimisation of a reference rotor for a 10 MW offshore wind turbine with respect to the support structure", Master thesis, University of Oldenburg, in preparation for 2016.

## PART B - O&M FOR INNOVATIVE SUPPORT STRUCTURES (AAU)

### 1 INTRODUCTION

Reliability and risk based inspection planning (RBI) for offshore structures have been an area of practical interest over the last decades. The first developments were within inspection planning for welded connections subject to fatigue crack growth in fixed steel offshore platforms. This application area for RBI is now the most developed. Initially practical applications of RBI required a significant expertise in the areas of structural reliability theory and fatigue and fracture mechanics, see e.g. (Aker Partner Engineering, 1990). This made practical implementation in industry difficult. Recently generic and simplified approaches for RBI have been formulated making it possible to base inspection planning on a few key parameters commonly applied in deterministic design of structures, e.g. the Fatigue Design Factor (FDF) and the Reserve Strength Ratio (RSR), see Faber et al. (Faber, et al., 2005), (Faber, et al., 2000).

Based on the results of detailed sensitivity studies with respect to the “generic parameters” such as the bending to membrane stress ratio, the design fatigue life and the material thickness, a significant number of inspection plans are computed by a simulation technique for fixed generic parameters (pre-defined generic plans). These generic plans are collected in a database and used in such a way that inspection plans for a particular application can be obtained by interpolation between the pre-defined generic plans. The database facilitates the straightforward production of large numbers of inspection plans for structural details subject to fatigue deterioration.

The basic assumption made in risk / reliability based inspection planning is that a Bayesian approach can be used. This implies that probabilities of failure can be updated in a consistent way when new information (from inspections) becomes available. Further the RBI approach for inspection planning is based on the assumption that at all future inspections no cracks are detected. If a crack is detected then a new inspection plan should be developed. The Bayesian approach and the no-crack detection assumption imply that the inspection time intervals usually become longer and longer.

Further, inspection planning based on the RBI approach implies that single components are considered, one at the time, but with the acceptable reliability level assessed based on the consequence for the whole structure in case of fatigue failure of the component.

Examples and information on reliability-based inspection and maintenance planning can be found in a number of papers, e.g. (Thoft-Christensen & Sørensen, 1987), (Madsen, et al., 1989), (Madsen & Sørensen, 1990), (Fujita, et al., 1989), (Skjong, 1985), (Sørensen, et al., 1991) (Faber & Sørensen, 1999), (Ersdal, 2005), (Sørensen, et al., 2005), (Moan, 2005), (Kübler & Faber, 2004), (Straub & Faber, 2005), (Rouhan & Schoefs, 2003), (Faber, et al., 2005), (Aker Partner Engineering, 1990) and (Faber, et al., 2000). Important aspects are systems considerations, design using robustness considerations by accidental collapse limit states and use of monitoring by the leak before break principle to identify damages.

Based on the above considerations the following aspects are considered in this report with the aim to develop the risk based inspection approach for application within offshore wind turbine foundations, namely:

- For new (innovative) wind turbine fixed support structures design is generally performed using safety factors that assume no inspections during the design lifetime. However, it could be cost-effective to plan for operation & maintenance actions (especially inspections) during the operational lifetime if the associated (discounted) costs are smaller than the initial costs that can be saved by using smaller safety factors for the design. In order to account for the possible, future inspections, maintenance and repair actions rational decisions have to be made. This report presents an approach for how this can be done using pre-posterior Bayesian decision theory. Further, application of a design approach where inspections (and other) condition monitoring are performed for innovative wind turbine substructures has the potential to discover unexpected behavior of the substructures before failures happen.
- For ageing wind turbine support structure several small cracks are often observed – implying an increased risk for crack initiation (and coalescence of small cracks) and increased growth – thus modelling a bath-tub effect, and implying shorter inspection time intervals for ageing structures. Note, that for non-ageing structures longer inspection intervals can be expected.
- Systems effects including
  - Assessment of the acceptable annual fatigue probability of failure for a particular component taking into account that there can be a number of fatigue critical components in a structure.
  - Effects due to common loading, common model uncertainties and correlation between inspection qualities implying that information obtained from inspection of one component can be used not only to update the inspection plan for that component, but also for other nearby components.
- Illustration in numerical examples of the RBI methodology for planning of O&M activities related to inspections of support structures for offshore wind turbines. This includes generic examples and cases where stress range spectra for specific types of fatigue critical details are considered. The Reference Jacket in WP4 will be used for this illustration.

In Section 2 a state-of-the art of reliability and risk-based (RBI) planning of O&M for offshore wind turbine support structures is presented. The presentation is partly based on (Faber & Sørensen, 1999), (Sørensen, et al., 2005), (Straub & Faber, 2005), (Faber, et al., 2005), and (Faber, et al., 2000). In Section 3 a methodology is presented for cost-optimal, reliability and risk-based planning of O&M with focus on inspections and repair planning for innovative support structures for offshore wind turbines. Finally in Section 4 the methodology is illustrated considering critical tubular K- and X-joints identified in the InnWind D4.3.1 deliverable on the Reference Jacket support structure. Here the actual stress range distributions are applied together with the design SN-cures to obtain general recommendations on needed inspections during the design lifetime for different inspection techniques. Further, in Appendix A results are shown for generic examples linked to the

requirements and assumptions made in the recent revision of the IEC 61400-1 standard. Appendix B presents some detailed results related to the illustration in Section 4.

## 2 RELIABILITY AND RISK-BASED PLANNING FOR O&M FOR OFFSHORE WIND TURBINE SUPPORT STRUCTURES

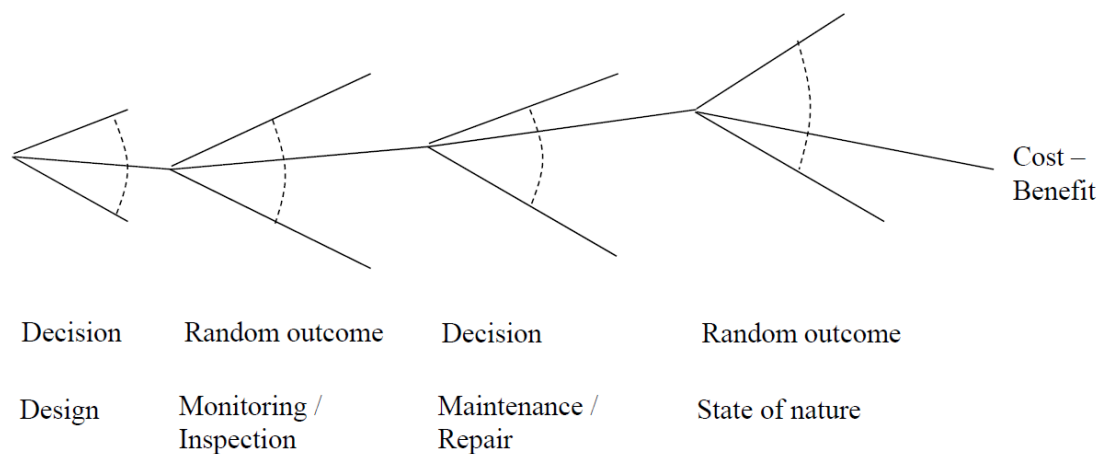


**Figure 2.1. Decision tree – Pre-posterior Bayesian decision theory**

This section describes the basis for cost-optimal planning of design and operation & maintenance (O&M) which includes planning of inspections, maintenance and repairs. The theoretical basis is illustrated in Figure 2.1, based on the pre-posterior analysis from classical Bayesian decision theory, see e.g. (Raiffa and Schlaifer 1961) and (Benjamin and Cornell 1970).

For new structures design is generally performed using safety factors that assume no inspections during the design lifetime. However, as an alternative operation & maintenance actions (especially inspections) during the operational lifetime could be cost-optimal. This may occur if the total (discounted) costs of design and O&M with smaller safety factors are smaller than the initial costs with on O&M activities but larger safety factors. In order to account for the possible, future inspections, maintenance and repair actions rational decisions have to be made and the theoretical basis is illustrated in Figure 2.1 based on Bayesian decision theory, see description below. Application of a design approach where inspections (and other types of condition / health monitoring) are performed for innovative wind turbine substructures has the potential to discover unexpected behaviour of the substructures before failures happen.

In addition to decision making from only a cost-benefit perspective acceptance criteria from e.g. codes and standards often has to be fulfilled. Such acceptance criteria for individual critical details / joints are described in subsection 2.1. Next, subsection 2.2 describes how optimal planning of inspections and repair for fatigue cracks can be performed based on the above risk-based Bayesian approach. It is noted that the methodology described in subsection 2.1 can also be used for other deterioration mechanisms. In subsection 2.3 it is described how a simplified reliability-based approach can be formulated.

An important part of modelling inspections (and equivalently for other methods for obtaining information of the health of a structure) is to model the reliability of the inspections. Subsection 2.4 describes how Probability of Detection models can be formulated and incorporated in the probabilistic modelling. Stochastic modelling of the deterioration process is needed in order to perform the planning. Section 2.5 describes how fatigue can be modelled by the SN-approach used in standards such as IEC 61400-1 and by a fracture mechanics approach needed in order to perform the inspection planning. Finally subsection 2.6 discuss various system aspects relevant when considering one structure with many correlated fatigue critical details and when considering wind farms with many correlated substructures.

## 2.1 Acceptance criteria for individual joints

Requirements to the safety of offshore structures are commonly given in two ways. In the North Sea it is a requirement that the offshore operator demonstrates to the authorities that risk to personnel and risk to the environment are controlled and maintained within acceptable limits throughout the operational service life of the installation. The limits are usually determined in agreement between the authorities and the offshore operator. Normally, the requirements to the acceptable risk are given in terms of an acceptable Fatal Accident Rate (FAR) for the risk of personnel and in terms of acceptable frequencies of leaks and outlets of different categories for the risk to the environment. These acceptance criteria address in particular risk associated with the operation of the facilities on the topside and cannot be applied directly as a basis for the inspection planning of the structural components.

In addition to the general requirements stated above also indirect and direct specific requirements to the safety of structures and structural components are given in the codes of practice for the design of structures. For manned offshore steel jacket structures for oil & gas production typically a maximum annual probability of failure in the range  $10^{-5}$  -  $5 \cdot 10^{-5}$  is accepted and for unmanned structures a maximum annual probability of failure in the range  $10^{-4}$  -  $2 \cdot 10^{-4}$  is accepted, see e.g. (ISO 19902, 2007) and OS-J101 (DNV, 2011). In regard to fatigue failures the requirements to safety are typically given in terms of a required Fatigue Design Factor (FDF). The deterministic, nominal fatigue design life is obtained as FDF multiplied to the service life, usually 20-25 years. More details on FDF can also be found in (DNV-GL, 2015).

Required FDF values are shown in Table 2.1 for fatigue design for in various standards: (ISO 19902, 2007) and (NORSOK, 1998) for fixed offshore steel structures for oil & gas platforms, GL Guideline for the certification of offshore wind turbines (GL, 2005) DNV Design of offshore wind turbine structures, OS-J101 (DNV, 2011) and Eurocode 3: Design of steel structures - Part 1-9: Fatigue, (EN 1993-1-9, 2005). The FDF values shown for GL / DNV and EN 1993-1-9 are determined using a linear SN-curve with slope equal to 3 – the corresponding FDF values obtained using a slope equal to 5 are shown in Table 2.1. Fatigue Design Factors required. The FDF values are specified for critical and non-critical details and for details than can or cannot be inspected.

Table 2.1. Fatigue Design Factors required.

Failure critical detail	Inspections	ISO 19902	GL / DNV	EN 1993-1-9
Yes	No	10	2.0 (3.0)	2.5 (4.5)
Yes	Yes	5	1.5 (2.0)	1.5 (2.0)
No	No	5	1.5 (2.0)	1.5 (2.0)
No	Yes	2	1.0 (1.0)	1.0 (1.0)

From the FDF's specified in Table 2.1 it is possible to establish the corresponding annual probabilities of failure for a specific year. In principle the relationship between the FDF and the annual probability of failure has the form shown in Figure 2.2.

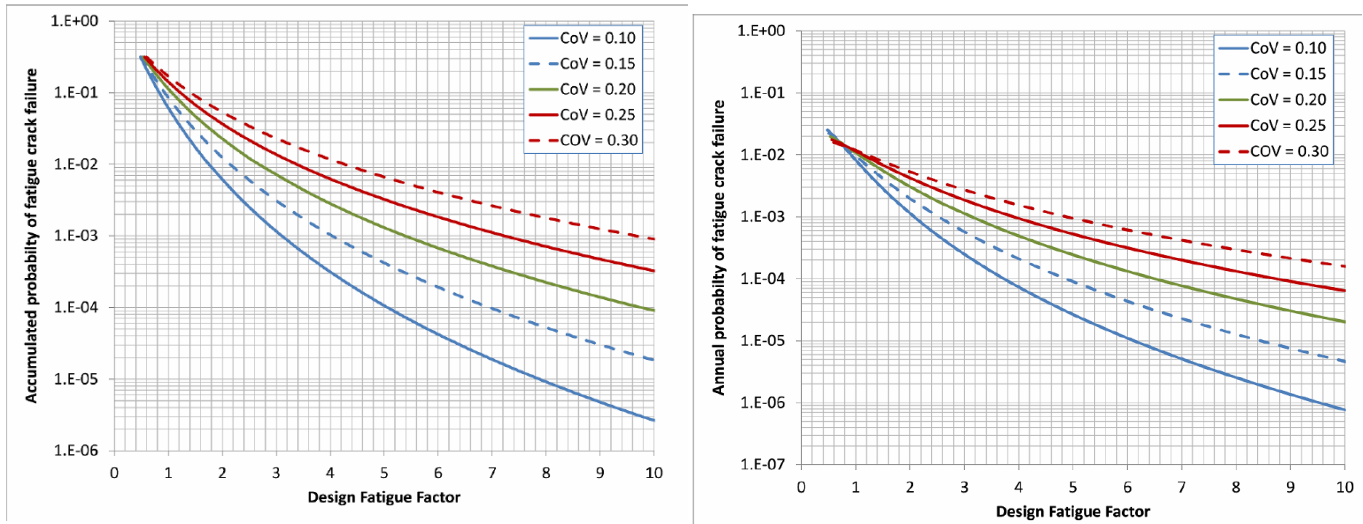


Figure 2.2. Example relationship between FDF and probability of fatigue failure, adopted from (DNV-GL, 2015).

For the joints to be considered in an inspection plan, the acceptance criteria for the annual probability of fatigue failure may be assessed through the RSR given failure of each of the individual joints to be considered together with the annual probability of joint fatigue failure. Application of RSR values is one way to account for redundancy in the structure, especially for jacket type of support structures and for substructures where extreme eave load is dominant, see below. If the RSR given joint fatigue failure is known (can be obtained from e.g. an USFOS analysis), it is possible to establish the corresponding annual collapse failure probability given fatigue failure,  $P_{COL|FAT}$  if information is available on

- applied characteristic values for the capacities
- applied characteristic values for the live loads
- applied characteristic values for the wave height, period, ... (environmental load)
- ratios of the environmental load to the total load
- coefficient of variation of the capacity and the load

In order to assess the acceptable annual probability of fatigue failure for a particular joint in a platform the reliability of the considered platform must be calculated conditional on fatigue failure of the considered joint. The importance of a fatigue failure is measured by the Residual Influence Factor defined as:

$$RIF = \frac{RSR^{\text{damaged}}}{RSR^{\text{intact}}} \quad (1)$$

where  $RSR^{\text{intact}}$  is the  $RSR$  value for the intact structure and  $RSR^{\text{damaged}}$  is the  $RSR$  value for the structure damaged by fatigue failure of a joint.

The principal relation between RIF and annual collapse probability is illustrated in Figure 2.3.

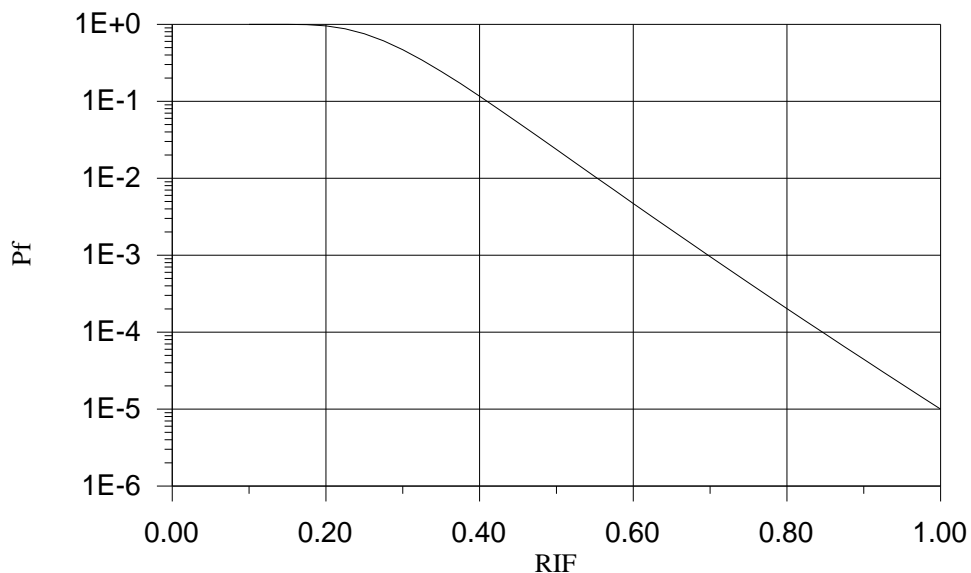


Figure 2.3. Example relationship between Residual Influence Factors (RIF) and annual collapse probability of failure, (Faber, et al., 2005).

The implicit code requirement to the safety of the structure in regard to total collapse may be assessed through the annual probability of joint fatigue failure (in the last year in service)  $P_{FAT_j}$  for a joint for which the consequences of failure are “substantial” (i.e. design fatigue factor 10). This probability can be regarded an acceptance criteria i.e.  $P_{AC}$ . A typical maximal allowed annual probability of collapse failure is in the in the range  $10^{-4}$  -  $2 \cdot 10^{-5}$  for unmanned structures.

On this basis it is possible to establish joint & member specific acceptance criteria in regard to fatigue failure. For each joint  $j$  the conditional probabilities of structural collapse give failure of the considered joint  $P_{COL|FAT_j}$  are determined and the individual joint acceptance criteria for the annual probability of joint fatigue failure are found as:

$$P_{AC_j} = \frac{P_{AC}}{P_{COL|FAT_j}} \quad (2)$$

The inspection plans must then satisfy that

$$P_{FAT_j} \leq P_{AC_j} \quad (3)$$

for all years during the operational life of the structure.

The annual probability of joint fatigue failure  $P_{FAT_j}$  may in principle be determined on the basis of either a simplified probabilistic SN approach or a probabilistic fracture mechanics approach provided the fracture mechanical model has been calibrated to the appropriate SN model.

As an alternative to the above approach where basis is taken in annual probabilities of failure it is equally possible to take basis in service life probabilities. However, as most installation concept risk analysis give requirements to the maximum allowable risk for structural collapse in terms of annual failure probabilities, these are used in the following.

In addition to the acceptance criteria relating to the maximum allowable annual probabilities of joint fatigue failure, economic considerations can be applied as basis for the inspection planning. The aim is to plan inspections such that the overall service life costs are minimized. The costs include costs of failure, inspections, repairs and production losses, see next section. (Ersdal, 2005) considered life extension of existing offshore jacket structures including fatigue degradation and inspection effects in a life extension. A predictive Bayesian approach is used.

## 2.2 Optimal reliability-based inspection planning

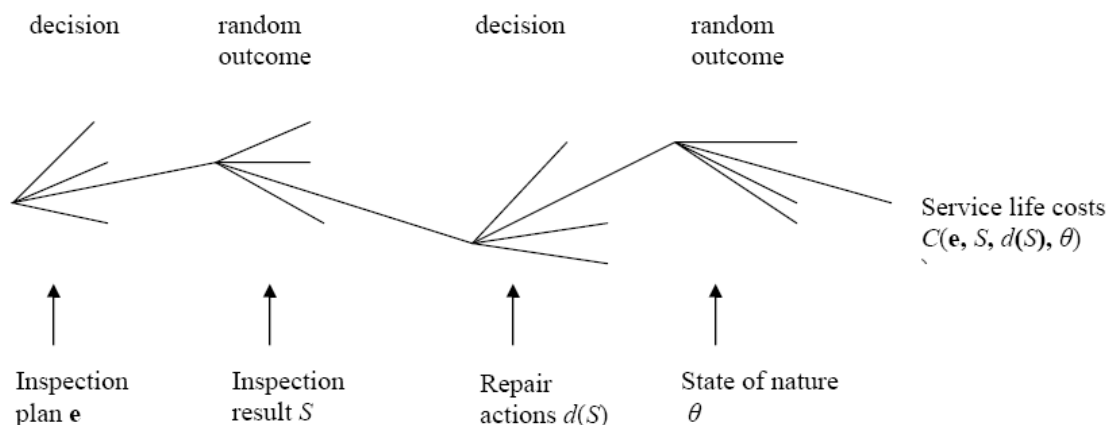


Figure 2.4. Inspection planning decision tree.

The decision problem of identifying the cost optimal inspection plan may be solved within the framework of pre-posterior analysis from the classical Bayesian decision theory see e.g. (Raiffa &

Schlaifer, 1961) and (Benjamin & Cornell, 1970). Here a short summary is given following (Sørensen, et al., 1991). The inspection decision problem may be represented as shown in Figure 2.4.

In the general case the parameters defining the inspection plan are:

- the possible repair actions i.e. the repair decision rule  $d$
- the number of inspections  $N$  in the service life  $T_L$
- the time intervals between inspections  $\mathbf{t} = (t_1, t_2, \dots, t_N)$
- the inspection qualities  $\mathbf{q} = (q_1, q_2, \dots, q_N)$ .

These inspection parameters are written as  $\mathbf{e} = (N, \mathbf{t}, \mathbf{q})$ . The outcome, typically a measured crack size, of an inspection is modelled by a random variable  $S$ . A decision rule  $d$  is then applied to the outcome of the inspection to decide whether or not repair should be performed. The different uncertain parameters (stochastic variables) modelling the state of nature such as load variables and material characteristics are collected in a vector  $\mathbf{X} = (X_1, X_2, \dots, X_n)$ .

If the total expected costs are divided into inspection, repair, strengthening and failure costs and a constraint related to a maximum yearly (or accumulated) failure probability  $\Delta P_F^{\max}$  related to  $P_{AC_j}$  for joint  $j$  is added, then the optimization problem can be written:

$$\begin{aligned} \min_{\mathbf{e}, d} \quad & C_T(\mathbf{e}, d) = C_{IN}(\mathbf{e}, d) + C_{REP}(\mathbf{e}, d) + C_F(\mathbf{e}, d) \\ \text{s.t.} \quad & \Delta P_{F,t} \leq \Delta P_F^{\max} \quad t = 1, 2, \dots, T_L \end{aligned} \quad (4)$$

$C_T(\mathbf{e}, d)$  is the total expected cost in the service life  $T_L$ ,  $C_{IN}$  is the expected inspection cost,  $C_{REP}$  is the expected cost of repair and  $C_F$  is the expected failure cost. The annual probability of failure in year  $t$  is  $\Delta P_{F,t}$ . The  $N$  inspections are assumed performed at times  $0 \leq T_1 \leq T_2 \leq \dots \leq T_N \leq T_L$ .

If the repair actions are 1) to do nothing, 2) to repair by welding for large cracks, and 3) to repair by grinding by small cracks, then the number of branches becomes  $3^N$ . It is noted that generally the total number of branches can be different from  $3^N$  if the possibility of individual inspection times for each branch is taken into account.

The total capitalised expected inspection costs are:

$$C_{IN}(\mathbf{e}, d) = \sum_{i=1}^N C_{IN,i}(\mathbf{q})(1 - P_F(T_i)) \frac{1}{(1+r)^{T_i}} \quad (5)$$

The  $i$  th term represents the capitalized inspection costs at the  $i$  th inspection when failure has not occurred earlier,  $C_{IN,i}(q_i)$  is the inspection cost of the  $i$  th inspection,  $P_F(T_i)$  is the probability of failure in the time interval  $[0, T_i]$  and  $r$  is the real rate of interest.

The total capitalised expected repair costs are:

$$C_{REP}(\mathbf{e}, d) = \sum_{i=1}^N C_{R,i} P_{R_i} \frac{1}{(1+r)^{T_i}} \quad (6)$$

$C_{R,i}$  is the cost of a repair at the  $i$  th inspection and  $P_{R_i}$  is the probability of performing a repair after the  $i$  th inspection when failure has not occurred earlier and no earlier repair has been performed.

The total capitalised expected costs due to failure are estimated from:

$$C_F(\mathbf{e}, d) = \sum_{t=1}^{T_L} C_F(t) \Delta P_{F,t} P_{COL|FAT_j}(RSR) \frac{1}{(1+r)^t} \quad (7)$$

where  $C_F(t)$  is the cost of failure at the time  $t$  and  $P_{COL|FAT_j}(RSR)$  is the conditional probability of collapse of the structure given fatigue failure of the considered component  $j$ .

Details on the formulation of limit state equations for the modelling of failure, detection and repair events are given in (Sørensen, et al., 1991). Finally, the cumulative probability of failure at time  $T_i$ ,  $P_F(T_i)$  may be found by summation of the annual failure probabilities

$$P_F(T_i) = \sum_{t=1}^{T_i} \Delta P_{t} P_{COL|FAT_j} \quad (8)$$

The solution of the optimization problem (2.4) in its general form is difficult to obtain. However, if as an approximation it is assumed that all the components of  $\mathbf{P}_f^T = (P_{f1}^T, P_{f2}^T, \dots, P_{fT_L}^T)^T$  are identical ( $= P_f^T$ ), i.e. that the same threshold on the annual probability of failure is applied for all years, the problem is greatly simplified. In this case (4) may be solved in a practical manner by performing the optimization over  $P_f^T$  outside the optimization over  $d$  and  $\mathbf{e}$ . The total expected cost corresponding

to an inspection plan evolving from a particular value of  $P_f^T$  is then evaluated over a range of values of  $P_f^T$  and the optimal  $P_f^* = P_f^T$  is identified as the one yielding the lowest total costs.

In order to identify the inspection times corresponding to a particular  $P_f^T$  another approximation is introduced, namely that all the future inspections will result in no-detection. Thereby the inspection times are identified as the times where the annual conditional probability of fatigue failure (conditional on no-detection at previous inspections) equals  $P_f^T$ . This is clearly a reasonable approximation for components with a high reliability, see (Straub, 2004).

Having identified the inspection times the expected costs are evaluated. It is important to note that the probabilities entering the cost evaluation are not conditioned on the assumed no-detection at the inspection times. This in order to include all possible contributions to the failure and repair costs.

The process is repeated for a range of different values of  $P_f^T$  and the value  $P_f^*$ , which minimizes the costs and at the same time fulfills the given requirements to the maximum acceptable  $P_f^T$  is selected as the optimal one. The optimal inspection plan is then the inspection times  $0 \leq T_1 \leq T_2 \leq \dots \leq T_N \leq T_L$  corresponding to  $P_f^*$ , the related optimal repair decision rule  $d$  together with the inspection qualities  $q$ .

Following the approach outlined above it is possible to establish so-called generic inspection plans. The idea is to pre-fabricate inspection plans for different joint types designed for different fatigue lives. For given

- Type of fatigue sensitive detail – and thereby code-based SN-curve
- Fatigue strength measured by *FDF* (Fatigue Design Factor)
- Importance of the considered detail for the ultimate capacity of the structure, measured by e.g. *RIF* (Residual Influence Factor)
- Member geometry (thickness)
- Inspection, repair and failure costs

the optimal inspection plan i.e. the inspection times, the inspection qualities and the repair criteria, can be determined. This inspection plan is generic in the sense that it is representative for the given characteristics of the considered detail, i.e. SN-curve, *FDF*, *RSR* and the inspection, repair and failure costs.

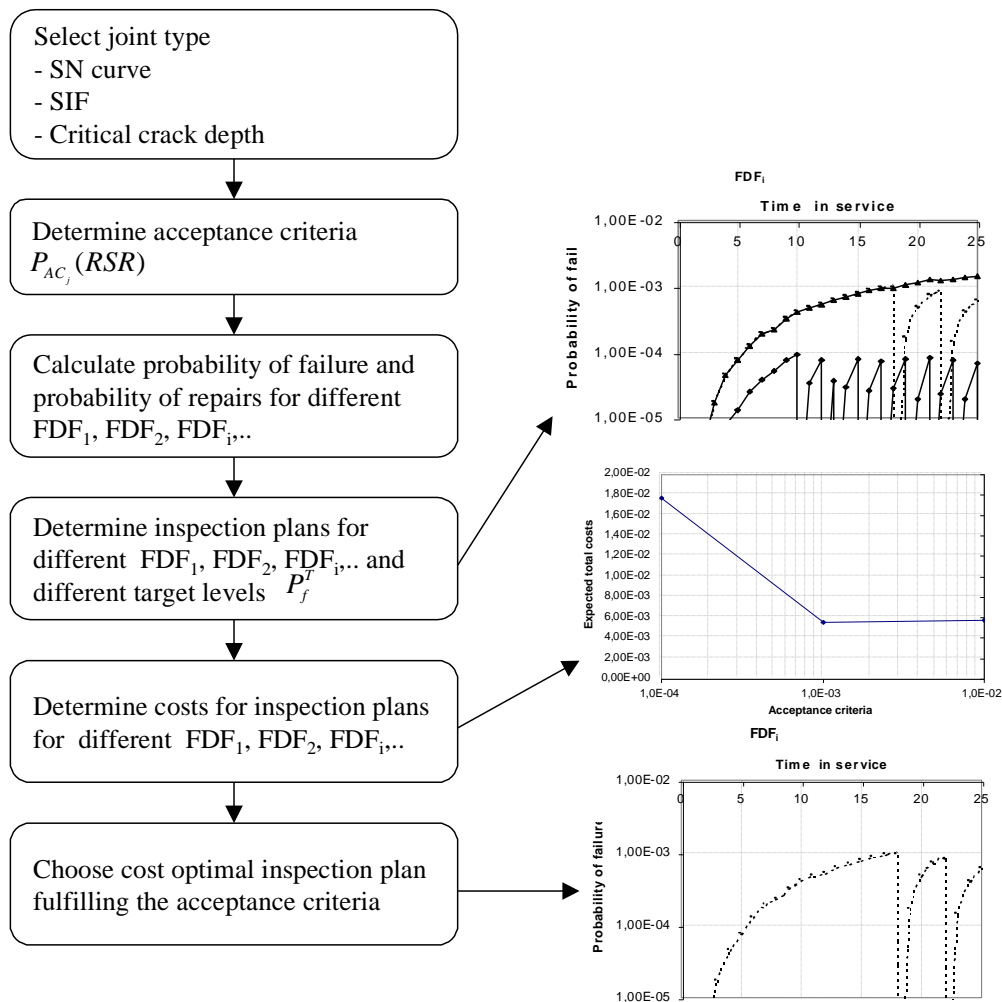


Figure 2.5. Illustration of the flow of the generic inspection planning approach, (Faber, et al., 2005).

For given SN-curve, member geometry,  $FDF$  and cost structure the procedure may be summarized as follows:

1. Identify inspection times by assuming inspections at times when the annual failure probability exceed a certain threshold.
2. Calculate the probabilities of repairs corresponding to the times of inspections
3. Calculate the total expected costs.
4. Repeat steps 1-3 for a range of different threshold values and identify the optimal threshold value as the one yielding the minimum total costs.

The inspection times corresponding to the optimal threshold value then represent the optimal inspection plan. For the identification of optimal inspection methods and repair strategies the above

mentioned procedure may be looped over different choices of these. The procedure is illustrated in Figure 2.5.

As the generic inspection plans are calculated for different values of the FDF it is possible to directly assess the effect of design changes or the effect of strengthening of joints on existing structures as such changes are directly represented in changes of the FDF. It is furthermore interesting to observe that the effect of service life extensions on the required inspection efforts may be directly assessed through the corresponding change on the FDF. Given the required service life extension, the FDF for the joint is recalculated and the corresponding pre-fabricated inspection plan identified.

### 2.3 Reliability-based inspection planning

The inspection planning procedure described in the above section requires information on costs of failure, inspections and repairs. Often these are not available, and the inspection planning is based on the requirement that the annual probability of failure in all years has to satisfy the reliability constraint in (4). This implies that the annual probabilities of fatigue failure has to fulfill (3). Further, in risk-based inspection planning the planning is often made with the assumption that no cracks are found at the inspections. If a crack is found, then a new inspection plan has to be made based on the observation.

If all inspections are made with the same time intervals, then the annual probability of fatigue failure could be as illustrated in Figure 2.6.

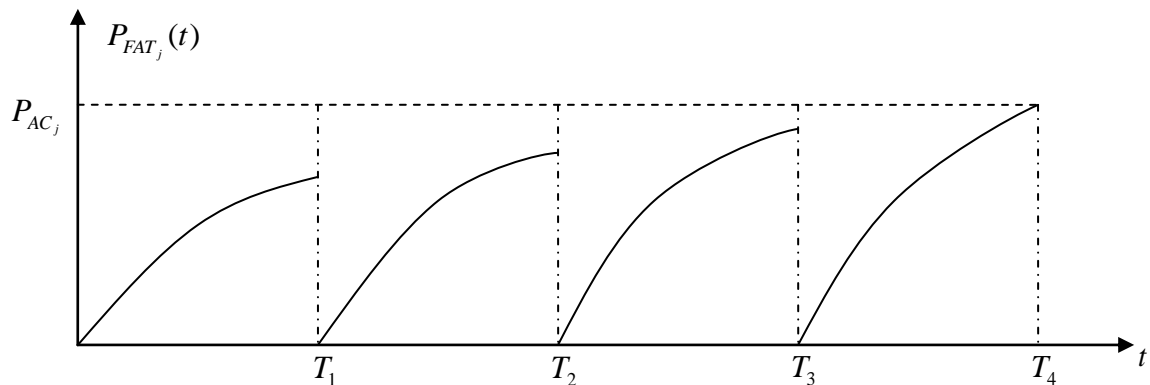


Figure 2.6. Illustration of inspection plan with equidistant inspections.

If inspections are made when the annual probability of fatigue failure exceeds the critical value then inspections are made with different time intervals, as illustrated in Figure 2.7. The inspection planning is based on the no-find assumption. This way of inspection planning is the one which is most often used. Often this approach results in increasing time intervals between inspections.

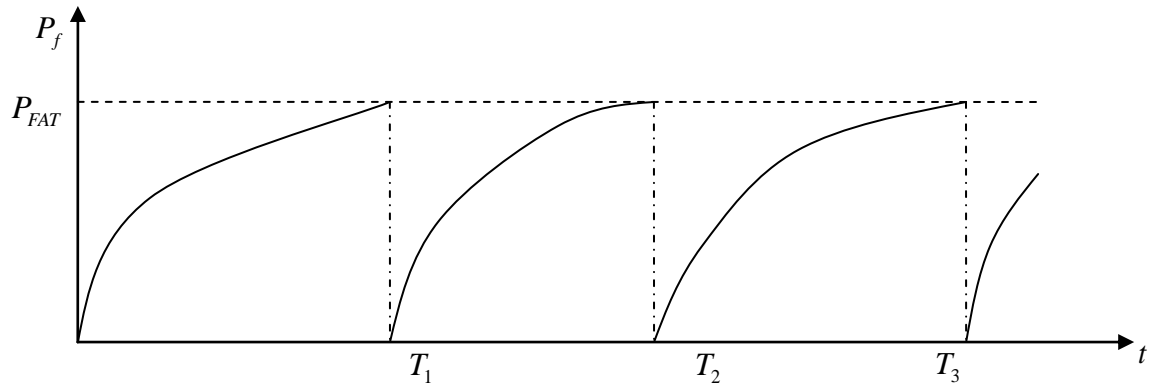


Figure 2.7. Illustration of inspection plan where inspections are performed when the annual probability of failure exceeds the maximum acceptable annual probability of failure.

## 2.4 Probabilistic modelling of inspections

The reliability of inspections can be modelled in many different ways. Often POD (Probability of Detection) curves are used to model the reliability of the inspections. If inspections are performed using an Eddy Current technique (below or above water) or a MPI technique (below water) the inspection reliability can be represented by following Probability Of Detection (POD) curve:

$$POD(x) = 1 - \frac{1}{1 + \left(\frac{x}{x_0}\right)^b} \quad (9)$$

where e.g.  $x_0 = 12.28$  mm and  $b = 1.785$ .

Other models such as exponential, lognormal and logistics models can be used, see next sections. The measurement uncertainty may be modelled by a Normal distributed random variable  $\varepsilon$  with zero mean value and standard deviation  $\sigma_\varepsilon = 0.5$  mm. Also the Probability of False Indication (PFI) can be introduced and modelled probabilistically.

For more detailed description on different types of POD curves for different types of inspections and types of structures, refer to (DNV-GL, 2015) Section 11.

## 2.5 Reliability modelling of fatigue

In this section probabilistic models are described for reliability assessment of wind turbines where wind load is dominating (over wave loads). The models are mainly based on (Sørensen, et al., 2008). Alternatively, the models could be established using (JCSS, 2011) where a more detailed approach is described with respect to stress concentration and weld geometry. Furthermore, a detailed standardized approach can also be found in (DNV-GL, 2015).

First design by linear SN-curves is considered. The SN relation is written:

$$N = K(\Delta\sigma)^{-m} \quad (10)$$

where  $N$  is the number of stress cycles to failure with constant stress ranges  $\Delta\sigma$ .  $K$  and  $m$  are dependent on the fatigue critical detail.

For a wind turbine in free wind flow the design equation in deterministic design is written:

$$G(z) = 1 - \int_{U_{in}}^{U_{out}} \frac{\nu \cdot FDF \cdot T_L}{K_C} D_L(m; \alpha_{\Delta\sigma}(U) \hat{\sigma}_u(U) / z) f_U(U) dU = 0 \quad (11)$$

where  $z$  is a design parameter (e.g. proportional to cross sectional area) and

$$D_L(m; \sigma_{\Delta\sigma}) = \int_0^{\infty} s^m f_{\Delta\sigma}(s | \sigma_{\Delta\sigma}(U)) ds \quad (12)$$

is the expected value of  $\Delta\sigma^m$  given standard deviation  $\sigma_{\Delta\sigma}$  and mean wind speed  $U$ .  $\nu$  is the total number of fatigue load cycles per year (determined by e.g. rainflow counting),  $T_L$  is the design life time,  $FDF$  is the Fatigue Design Factor (equal to  $(\gamma_f \gamma_m)^m$  where  $\gamma_f$  and  $\gamma_m$  are partial safety factors for fatigue load and fatigue strength),  $K_C$  is the characteristic value of  $K$  (here assumed to be obtained from  $\log K_C$  as mean of  $\log K$  minus two standard deviations),  $U_{in}$  is the cut-in wind speed (typically 5 m/s),  $U_{out}$  is the cut-out wind speed (typically 25 m/s) and  $f_{\Delta\sigma}(s | \sigma_{\Delta\sigma}(U))$  is the density function for stress ranges given standard deviation of  $\sigma_{\Delta\sigma}(U)$  at mean wind speed  $U$ . This distribution function can be obtained by e.g. rainflow counting of response, and can generally be assumed to be Weibull distributed, see (Sørensen, et al., 2008) and (DNV, 2010). It is assumed that the standard deviation  $\sigma_{\Delta\sigma}(U)$  can be written:

$$\sigma_{\Delta\sigma}(U) = \alpha_{\Delta\sigma}(U) \frac{\sigma_u(U)}{z} \quad (13)$$

where  $\alpha_{\Delta\sigma}(U)$  is the influence coefficient for stress ranges given mean wind speed  $U$ ,  $\sigma_u(U)$  is the standard deviation of turbulence given mean wind speed  $U$ .

$\sigma_u(U)$  is modeled as LogNormal distributed with characteristic value  $\hat{\sigma}_u(U)$  defined as the 90% quantile and standard deviation equal to  $I_{ref} \cdot 1.4$  [m/s]. The characteristic value of the standard

deviation of turbulence,  $\hat{\sigma}_u(U)$  given average wind speed  $U$  is modeled by, see (IEC 61400-1, 2005)

$$\hat{\sigma}_u(U) = I_{ref} \cdot (0.75 \cdot U + b) ; b = 5.6 \text{ m/s} \quad (14)$$

where  $I_{ref}$  is the reference turbulence intensity (equal to 0.14 for medium turbulence characteristics) and  $\hat{\sigma}_u$  is denoted the ambient turbulence.

The corresponding limit state equation is written

$$g(t) = \Delta - \int_{U_{in}}^{U_{out}} \int_0^{\infty} \frac{v \cdot t}{K} (X_{Wind} X_{SCF})^m D_L(m; \alpha_{\Delta\sigma}(U) \sigma_u(U) / z) f_{\sigma_u}(\sigma_u | U) f_U(U) d\sigma_u dU \quad (15)$$

where  $\Delta$  is a stochastic variable modeling the model uncertainty related to the Miner rule for linear damage accumulation,  $t$  is time in years,  $X_{Wind}$  is the model uncertainty related to wind load effects (exposure, assessment of lift and drag coefficients, dynamic response calculations),  $X_{SCF}$  is the model uncertainty related to local stress analysis and  $\sigma_u(U)$  standard deviation of turbulence given average wind speed  $U$ . The model uncertainties  $X_{Wind}$  and  $X_{SCF}$  are discussed in more details in (Tarp-Johansen, et al., 2003).

The design parameter  $z$  is determined from the design equation (11) and next used in the limit state (15) to estimate the reliability index or probability of failure with the reference time interval  $[0; t]$ , see (Madsen, et al., 1986) for definition and calculation of the reliability index.

For wind turbines in a wind farm wake and non-wake conditions have to be accounted for. In the following the model for effective turbulence in (IEC 61400-1, 2005) and (Frandsen 2005) is used. An effective turbulence standard deviation is calculated as

$$\sigma_{u,eff}(U) \cong \left[ (1 - N_w \cdot p_w) \sigma_u^m + \sum_{j=1}^{N_w} p_w \sigma_{u,j}^m \right]^{\frac{1}{m}} \quad (16)$$

where  $\sigma_{u,j}$  is maximum turbulence standard deviation for wake number  $j$  and  $N_w$  is the number of neighboring wind turbines taken into account and  $p_w \approx 0.06$ .

For a wind turbine in a wind farm the design equation based on (IEC 61400-1, 2005) can then be written:

$$G(z) = 1 - \int_{U_{in}}^{U_{out}} \frac{v \cdot FDF \cdot T_L}{K_C} \cdot \left\{ \begin{array}{l} (1 - N_W \cdot p_W) D_L(m; \alpha_{\Delta\sigma}(U) \hat{\sigma}_u(U)/z) + \\ p_W \sum_{j=1}^{N_W} D_L(m; \alpha_{\Delta\sigma}(U) \hat{\sigma}_{u,j}(U)/z) \end{array} \right\} f_U(U) dU = 0 \quad (17)$$

where  $\hat{\sigma}_u$  is the standard deviation of turbulence given by (14) and  $\hat{\sigma}_{u,j}$  is the standard deviation of turbulence from neighboring wind turbine no j:

$$\hat{\sigma}_{u,j}(U) = \sqrt{\frac{0.9 \cdot U^2}{(1.5 + 0.3d_j \sqrt{U/c})^2} + \hat{\sigma}_u^2} \quad (18)$$

where  $d_j$  is the distance normalized by rotor diameter to neighboring wind turbine no j and c constant equal to 1 m/s.

The limit state equation corresponding to either the of the above design equations is written:

$$g(t) = \Delta - \int_{U_{in}}^{U_{out}} \int_0^t \frac{v \cdot t}{K} (X_{Wind} X_{SCF})^m \times \left\{ \begin{array}{l} (1 - N_W \cdot p_W) D_L(m; \alpha_{\Delta\sigma}(U) \sigma_u(U)/z) + \\ p_W \sum_{j=1}^{N_W} D_L(m; \alpha_{\Delta\sigma}(U) \sigma_{u,j}(U)/z) \end{array} \right\} \times f_{\sigma_u}(\sigma_u|U) f_U(U) d\sigma_u dU \quad (19)$$

where

$$\sigma_{u,j}(U) = \sqrt{X_{wake} \frac{U^2}{(1.5 + 0.3d_j \sqrt{U/c})^2} + \sigma_u^2} \quad (20)$$

and  $X_{wake}$  is model uncertainty related to wake generated turbulence model.

The design parameter  $z$  is determined from the design equation (17) and next used in the limit state equation (19) to estimate the reliability index or probability of failure with the reference time interval  $[0; t]$ .

Next, it is assumed that the SN-curve is bilinear (thickness effect not included) with slope change at  $N_D = 5 \cdot 10^6$ :

$$\begin{aligned}
 N &= K_1 S^{-m_1} \quad \text{for } S \geq \Delta\sigma_D \\
 N &= K_2 S^{-m_2} \quad \text{for } S < \Delta\sigma_D
 \end{aligned}
 \tag{21}$$

where  $K_1, m_1$  are material parameters for  $S \geq \Delta\sigma_D$  and  $K_2, m_2$  are material parameters for  $S < \Delta\sigma_D$  with  $\Delta\sigma_D = (K_1 / 5 \cdot 10^6)^{1/m_1}$ . The fatigue strength  $\Delta\sigma_F$  is defined as the value of  $S$  for  $N_D = 2 \cdot 10^6$ .

In case the SN-curve is bilinear  $D_L(m; \sigma_{\Delta\sigma})$  in design equations and limit state equations is exchanged with

$$\begin{aligned}
 D_{BL}(m_1, m_2, \Delta\sigma_D; \sigma_{\Delta\sigma}) = \\
 \int_0^{\Delta\sigma_D} s^{m_2} f_{\Delta\sigma}(s | \sigma_{\Delta\sigma}(U)) ds + \int_{\Delta\sigma_D}^{\infty} s^{m_1} f_{\Delta\sigma}(s | \sigma_{\Delta\sigma}(U)) ds
 \end{aligned}
 \tag{22}$$

(3.13) can easily be modified to include a lower threshold  $\Delta\sigma_{th}$ . Further, the SN-curves can also be extended with a modification factor taking into account thickness effects.

For a structural detail in an offshore wind turbine where wave load is dominating the design equation in deterministic design is written

$$G(z) = 1 - \frac{\nu \cdot FDF \cdot T_L}{K_C} D_L(m; \sigma_{\Delta M} / z) = 0
 \tag{23}$$

where  $z$  is a design parameter (e.g. proportional to cross sectional area),  $\sigma_{\Delta M}$  is the standard deviation of the relevant cross-sectional force and  $D_L(m; \sigma_{\Delta\sigma})$  is the expected value of  $\Delta\sigma^m$  given standard deviation of stress ranges,  $\sigma_{\Delta\sigma} \cdot f_{\Delta\sigma}(s | \sigma_{\Delta\sigma})$  is the density function for stress ranges given standard deviation. This distribution function can be obtained by e.g. rain flow counting of response, and can generally be assumed to be Weibull distributed, see (Sørensen, et al., 2008) and (DNV, 2010). The other parameters are the same as above.

The design parameter  $z$  is determined from the design equation (23). Next, the reliability index (or the probability of failure) is calculated using this design value and the limit state function associated with (23). The limit state equation can be written:

$$g(t) = \Delta - \frac{\nu \cdot t}{K} D_L(m; X_{wave} X_{SCF} \sigma_{\Delta M} / z) = 0
 \tag{24}$$

where  $\Delta$  is the model uncertainty related to Miner's rule for linear damage accumulation.  $X_{Wave}$  is the model uncertainty related to wave load effects and  $X_{SCF}$  is the model uncertainty related to local stress analysis.

If one fatigue critical detail is considered then the annual probability of failure is obtained from:

$$\Delta P_{F,t} = P_{COL|FAT} P(\text{Fatigue failure in year } t) \quad (25)$$

where  $P(\text{Fatigue failure in year } t) = P(g(t) \leq 0) - P(g(t-1) \leq 0)$  is the probability of failure in year  $t$  determined using the limit state equations above and  $P_{COL|FAT}$  is the probability of collapse of the structure given fatigue failure - modeling the importance of the detail.

Given a maximum acceptable probability of failure (collapse),  $\Delta P_{F,max}$  the maximum acceptable annual probability of fatigue failure (with one year reference time) and corresponding minimum reliability index become:

$$\Delta P_{F,max,FAT} = \Delta P_{F,max} / P_{COL|FAT} \quad (26)$$

$$\Delta \beta_{min,FAT} = -\Phi^{-1}(\Delta P_{F,max,FAT}) \quad (27)$$

where  $\Phi^{-1}(\cdot)$  is the inverse standard Normal distribution function.

If inspections are performed then the required *FDf* values can be decreased. This section describes how much the *FDf* values can be decreased. The theoretical basis for reliability-based planning of inspection and maintenance for fatigue critical details in offshore steel substructures is described in e.g. (Madsen & Sørensen, 1990), (Skjong, 1985), (Faber, et al., 2005), (Moan, 2005), (Straub, 2004) and (Sørensen, 2009). Risk- and reliability-based inspection planning is widely used for inspection planning for oil & gas steel jacket structures. Fatigue reliability analysis of jacket-type offshore wind turbine considering inspection and repair is also considered in (Dong, et al., 2010) and (Rangel-Ramírez & Sørensen, 2010).

For the fatigue sensitive details / joints to be considered in an inspection plan, the acceptance criteria for the annual probability of fatigue failure may be assessed using a measure for the decrease in ultimate load bearing capacity given failure of each of the individual joints to be considered together with the annual probability of joint fatigue failure. For offshore structures the *RSR* (Reserve Strength Ratio) is often used as a measure of the ultimate load bearing capacity, as described above.

If the *RSR* given joint fatigue failure is known (can be obtained from a non-linear FEM analysis), it is possible to establish the corresponding annual collapse failure probability  $P_{COL|FAT}$  if information is available on applied characteristic values for the capacity, live load, wave height, ratio of the environmental load to the total load and coefficient of variation of the capacity.

Inspection planning as described above requires information on costs of failure, inspections and repairs. Often these are not available, and the inspection planning is based on the requirement that the annual probability of failure in all years has to satisfy the reliability constraint, corresponding to the general description in Section 2.1.

$$\Delta P_{F,t} \leq \Delta P_{F,\max,FAT} \quad (28)$$

This implies that the annual probabilities of fatigue failure have to fulfill (28). Further, in risk-based inspection planning the planning is often made with the assumption that no cracks are found at the inspections. If a crack is found, then a new inspection plan has to be made based on the observation.

The Fracture Mechanical (FM) modeling of the crack growth is applied assuming that the crack can be modeled by a 2-dimensional semi-elliptical crack, or simplified models where the ratio between crack width and depth is either a constant or the crack width is a given function of the crack depth. It is assumed that the fatigue life may be represented by a fatigue initiation life and a fatigue propagation life:

$$N = N_I + N_p \quad (29)$$

where:

$N$  number of stress cycles to failure

$N_I$  number of stress cycles to crack propagation

$N_p$  number of stress cycles from initiation to crack through.

The number of stress cycles from initiation to crack through is determined on the basis of a two-dimensional crack growth model. The crack is assumed to be semi-elliptical with length  $2c$  and depth  $a$ , see Figure 2.8.

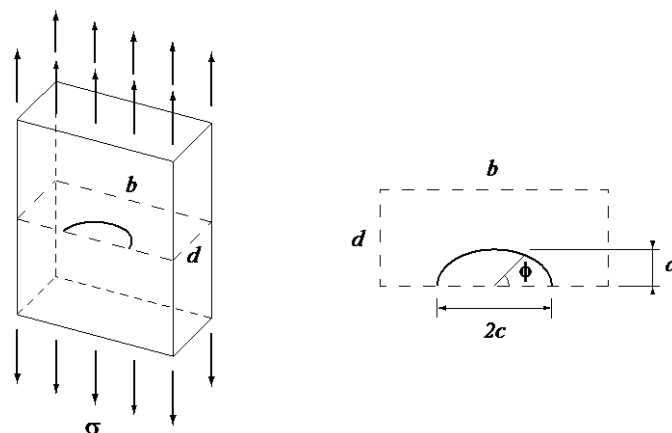


Figure 2.8. Semi-elliptical surface crack in a plate under tension or bending fatigue loads.

The crack growth can be described by the following two coupled differential equations.

$$\begin{aligned} \frac{da}{dN} &= C_A (\Delta K_A)^m & a(N_0) &= a_0 \\ \frac{dc}{dN} &= C_C (\Delta K_C)^m & c(N_0) &= c_0 \end{aligned} \quad (30)$$

where  $C_A$ ,  $C_C$  and  $m$  are material parameters,  $a_0$  and  $c_0$  describe the crack depth  $a$  and crack length  $c$ , respectively, after  $N_I$  cycles and where the stress intensity ranges are  $\Delta K_A(\Delta\sigma)$  and  $\Delta K_C(\Delta\sigma)$ .

The stress range  $\Delta\sigma$  is obtained from

$$\Delta\sigma = X_{Wind} X_{SCF} \cdot Y \cdot \Delta\sigma^e \quad (31)$$

where

- $X_{Wave}, X_{SCF}$  model uncertainties
- $Y$  model uncertainty related to geometry function
- $\Delta\sigma^e$  equivalent stress range:

$$\Delta\sigma^e = \left[ \frac{1}{n} \sum_{i=1}^{n_\sigma} n_i \Delta\sigma_i^m \right]^{1/m} \quad (32)$$

The total number of stress ranges per year,  $n$  is

$$n = \sum_{i=1}^{n_\sigma} n_i \quad (33)$$

The crack initiation time  $N_I$  may be modeled as Weibull distributed with expected value  $\mu_0$  and coefficient of variation equal to 0.35, see e.g. (Lassen, 1997). In some applications of a FM approach  $N_I$  is not included, i.e. it is put equal to 0 years.

**Table 2.2. Uncertainty modelling used in the fracture mechanical reliability analysis. D: Deterministic, N: Normal, LN: LogNormal, W: Weibull.**

Variable	Dist.	Expected value	Standard deviation
$N_I$	W	$\mu_0$ (reliability based fit to SN approach)	$0.35 \mu_0$
$a_0$	D	0.1 mm (high material control) / 0.5 mm (low material control)	
$\ln C_C$	N	$\mu_{\ln C_C}$ (reliability based fit to SN approach)	0.77
$m$	D	$m$ -value (reliability based fit to SN approach)	
$Z_{SCF}$	LN	1	0.05
$X_{Wave}$	LN	1	0.20
$n$	D	Total number of stress ranges per year	
$a_c$	D	T (thickness)	
$Y$	LN	1	0.1
$T$	D	Thickness	
$T_L$	D	25 years	
$T_F$	D	Fatigue life	
$\ln C_C$ and $N_I$ are correlated with correlation coefficient $\rho_{\ln(C_C), N_I} = -0.5$			

It is noted that more refined fracture mechanics models are described in (BS 7910, 2013), (JCSS , 2012), and (Maljaars, et al., 2012). This includes application of the stress intensity factor in a limit state equation to model unstable crack growth; and a Failure Assessment Diagram (FAD) in the limit state equation for a more general modelling of fatigue failure.

The limit state function is written

$$g(\mathbf{X}) = N - n t \quad (34)$$

where  $t$  is time in the interval from 0 to the service life  $T_L$ .

To model the effect of different weld qualities, different values of the crack depth at initiation  $a_0$  can be used. The corresponding assumed length is 5 times the crack depth. The critical crack depth  $a_c$  is taken as the thickness of the tubular member. The parameters  $\mu_{\ln C_C}$  and  $\mu_0$  are now fitted such that difference between the probability distribution functions for the fatigue live determined using the SN-approach and the fracture mechanical approach is minimized as illustrated in the example below.

Alternatively, or in addition to the above modeling the initial crack length can be modeled as a stochastic variable, for example by an exponential distribution function, and the crack initiation time  $N_I$  can be neglected.

The reliability of inspections can be modeled in many different ways, see subsection 2.4. In addition to the POD curve shown by (9) also an exponential model is often applied:

$$POD(x) = 1 - \exp\left(-\frac{x}{\lambda}\right) \quad (35)$$

where  $\lambda$  is the expected value of the smallest detectable crack size.

The crack width  $2c$  is obtained from the following model for  $a/2c$  as a function of the relative crack depth  $a/B$ , where  $B$  is the thickness:

$$\frac{a}{2c} = 0.06 - 0.03 \ln\left(\frac{a}{B}\right) \quad (36)$$

If an inspection has been performed at time  $T_I$  and no cracks are detected then the probability of failure can be updated by

$$P_F^U(t | \text{no-detection at time } T_I) = P(g(t) \leq 0 | h(T_I) > 0), \quad t > T_I \quad (37)$$

where  $h(t)$  is a limit state modeling the crack detection. If the inspection technique is related to the crack length then  $h(t)$  is written:

$$h(t) = c_d - c(t) \quad (38)$$

where  $c(t)$  is the crack length at time  $t$  and  $c_d$  is smallest detectable crack length.  $c_d$  is modelled by a stochastic variable with distribution function equal to the POD-curve:

$$F_{c_d}(x) = POD(x) \quad (39)$$

Similarly if the inspection technique is related to the crack depth then  $h(t)$  is written:

$$h(t) = a_d - a(t) \quad (40)$$

where  $a(t)$  is the crack length at time  $t$  and  $a_d$  is smallest detectable crack length.  $a_d$  is modelled by a stochastic variable with distribution function equal to the POD-curve:

$$F_{a_d}(x) = POD(x) \quad (41)$$

If two independent inspections are performed at time  $T_I$  and no cracks are detected then the probability of failure can be updated by

$$P_F^U(t|\text{no-detection at time } T_I) = P(g(t) \leq 0 | h_1(T_I) > 0 \cap h_2(T_I) > 0), t > T_I \quad (42)$$

where  $h_1(t) = a_{d_1} - a(T_I)$  and  $h_2(t) = a_{d_2} - a(T_I)$  are the limit states modeling the inspections.

The inspection planning is based on the requirement that the annual probability of failure in all years has to satisfy the reliability constraint

$$\Delta P_F \leq \Delta P_{F,MAX} \quad , \quad t > T_I \quad (43)$$

where  $\Delta P_{F,MAX}$  is the maximum acceptable annual probability of failure.

Further, the planning is often made with the assumption that no cracks are found at the inspections. If a crack is found, then a new inspection plan has to be made based on the observation.

It is emphasized that the inspection planning is based on the no-find assumption. This way of inspection planning is the one which is most often used. Often this approach results in increasing time intervals between inspections.

## 2.6 System effects

In many situations there will be a number of fatigue crack critical details (components) in an offshore wind turbine substructure, including both monopile and jacket type of structures. In this subsection different systems effects are discussed. The following aspects are considered:

- a. Assessment of the acceptable annual fatigue probability of failure for a particular component can be dependent on the number of fatigue critical details. The acceptable annual probability of fatigue failure is obtained considering the importance of the detail through the conditional probability of failure given failure of the detail / component.
- b. Due to common loading, common model uncertainties and correlation between inspection qualities it can be expected that information obtained from inspection of one component can be used not only to update the inspection plan for that component, but also for other nearby components.
- c. In some cases the development of a crack in one component causes a stiffness reduction and an increased damping which imply that loads could be redistributed and thereby increase (or decrease) the stress ranges in some of the other fatigue critical details.

### Aspect a – acceptable annual fatigue probability of failure

In order to assess the acceptable annual probability of fatigue failure for a component in a platform the probability of failure of the considered substructure must be calculated conditional on fatigue failure of the considered detail / component / joint. In Section 2.5 the basic consideration for one component / critical detail is described. In this section systems effects is included.

The ‘deterministic’ importance of a fatigue failure is measured by the Residual Influence Factor, RIF defined by (1). The principal relation between RIF and annual collapse probability is illustrated in Figure 2.3.

In Section 2.2 it is also described how the individual joint acceptance criteria for the annual probability of joint fatigue failure can be determined as

$$\Delta P_F^{\max} = \frac{P_{AC}}{P_{COL|FAT_j}} \quad (44)$$

Such that the inspection plans must then satisfy

$$P_{FAT_j} \leq \Delta P_F^{\max} \quad (45)$$

for all years during the operational life of the platform.

A general relation between  $RSR$  and the probability of failure can be obtained considering e.g. the following general limit state function:

$$g(x) = R - bH^a \quad (46)$$

where  $R$  is the effective capacity of the platform,  $a$  is a shape factor typically equal to 2,  $b$  is an influence coefficient taking into account model uncertainty parameter and  $H^a$  is a stochastic variable modeling the maximum annual value of the environmental load parameter.

The  $RSR$  value as evaluated by a push-over analysis can be related to characteristic values of  $R$ ,  $a$ ,  $b$  and  $H$  i.e.  $R_c$ ,  $b_c$  and  $H_c$  in the following way

$$RSR = \frac{R_c}{b_c H_c^a} \quad (47)$$

Typically, it can be assumed that  $R$  and  $b$  can be modeled probabilistically as log-Normal distributed random variables and  $H^a$  as a Gumbel distributed random variable. The characteristic value for  $R$ ,  $b$  and  $H^a$  could be defined as 5 %, 50 % and 99 % quantile values of their probability distributions. The example relationship in Figure 2.3 is obtained using  $RSR = 1.8$ .

In the considerations above only one fatigue critical component is considered. Often a number of components will be critical with respect to fatigue failure. In codes of practice usually requirements are only specified to check that individual fatigue critical components have a satisfactory safety. It is therefore not clear how to relate the code requirements to an acceptable system probability of failure for the whole structure considering more than one fatigue critical component. However, a first

estimate can be obtained if it is assumed that  $N$  members are critical, the members contribute equally to the probability of failure and the system probability of failure is estimated by one of the following two possibilities:

- simple upper bound on the system probability of failure. Then

$$P_{AC,FAT} = \frac{1}{N} \frac{P_{AC}}{P_{COL|FAT}} \quad (48)$$

$P_{AC,FAT}$  is shown in Figure 28 for  $N = 1, 2, 5$  and  $10$  critical components.

- approximate estimate of the system probability of failure. Then

$$P_{AC,FAT} = \frac{P_{AC}}{P_{SYS}} \quad (49)$$

where

$$P_{SYS} = 1 - \Phi_N(\beta_1, \beta_2, \dots, \beta_N; \boldsymbol{\rho}) \quad (50)$$

with the reliability index for each member,  $\beta_i$  given fatigue failure is  $\beta_i = -\Phi^{-1}(P_{COL|FAT_i})$  and the correlation coefficients in the correlation coefficient matrix,  $\boldsymbol{\rho}$  are obtained assuming that only the wave loading is common in different components.  $P_{AC,FAT}$  estimated by (2.49) is shown in Figure 2.10.

It is seen that the simple upper bounds in Figure 2.9 for  $N = 1, 2, 5$  and  $10$  critical components give reasonable conservative estimates of the acceptable probability of fatigue failure.

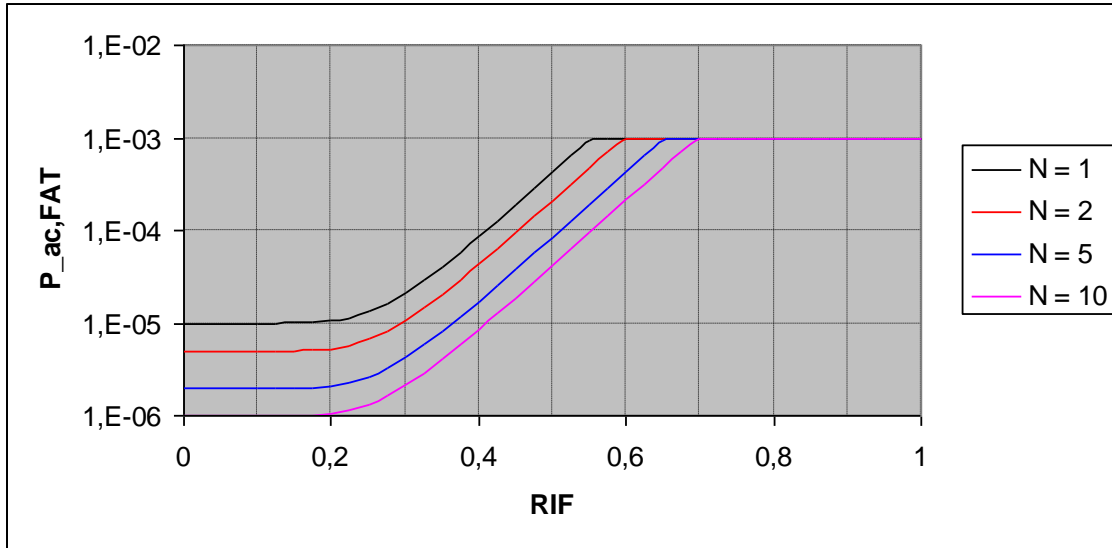


Figure 2.9. Maximum acceptable annual probability of fatigue failure,  $P_{ac,FAT}$  as function of RIF (Residual Influence Factor) based on an upper bound on the probability of failure.

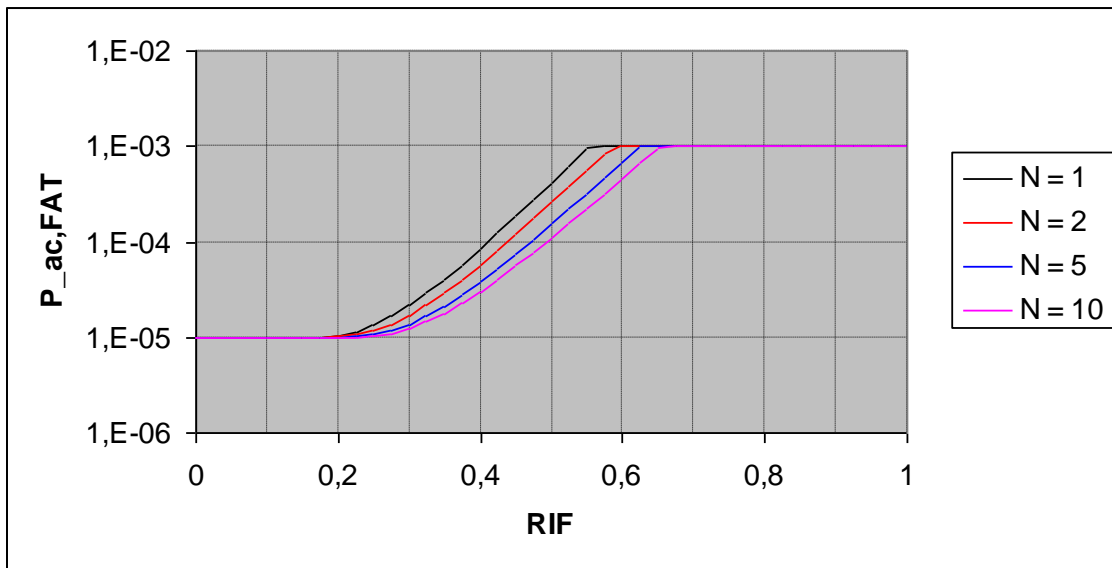


Figure 2.10. Maximum acceptable annual probability of fatigue failure,  $P_{ac,FAT}$  as function of RIF (Residual Influence Factor) based on an approximate estimate of the probability of failure.

For offshore wind turbines this approach of accounting for the consequence of fatigue failure in a support structure with redundancy can be applied if wave load is the dominant extreme load for the support structure. This can be expected to be the case for offshore wind turbines placed at water levels larger than approximately 25-30m, especially if loads from (plunging) breaking waves are important (as recent studies indicate). If wind load is the dominating extreme load then a different type of extreme push-over analysis is required – outside the scope of this deliverable.

### Aspect b – update inspection plan based on inspection of other components

Due to common loading, common model uncertainties and correlation between inspection qualities it can be expected that information obtained from inspections of one or more details / components can be used not only to update the inspection plan for these components, but also for other nearby components.

**Table 2.3. Stochastic variables for fracture mechanical analysis.**

	Variable	Description	Distribution
Strength Variables	$N_I$	Number of stress cycles to initiation of crack	Weibull
	$a_0$	Initial crack length	Exponential
	$\ln C_C$	Crack growth parameter	Normal
	$Y$	Geometry function	LogNormal
Load Variables	$X_{SCF}$	Uncertainty stress range calculation	LogNormal
	$X_{wave}$	Uncertainty wave load	LogNormal
	$a, b$	Weibull parameter in long term stress range distribution	LogNormal
Inspection quality	$c_d$	Probability Of Detection curve POD – smallest detectable crack length	POD

Table 2.3 shows the stochastic variables typically used in the fracture mechanical model. Considering as an example two fatigue critical components, the limit state functions corresponding to fatigue failure can be written:

$$g_1(\mathbf{X}_{Load,1}, \mathbf{X}_{Strength,1}, t) = a_{c,1} - a_1(\mathbf{X}_{Load,1}, \mathbf{X}_{Strength,1}, t) = 0 \quad (51)$$

$$g_2(\mathbf{X}_{Load,2}, \mathbf{X}_{Strength,2}, t) = a_{c,2} - a_2(\mathbf{X}_{Load,2}, \mathbf{X}_{Strength,2}, t) = 0 \quad (52)$$

where

$a_j(\mathbf{X}_{Load,j}, \mathbf{X}_{Strength,j}, t)$  crack depth at time  $t$  for component  $j$

$a_{c,j}$  critical crack depth for component  $j$

$\mathbf{X}_{Load,j}$  load variables ( $X_{SCF}$ ,  $X_{wave}$ ,  $a$  and  $b$ ) for component  $j$

$\mathbf{X}_{Strength,j}$  strength variables ( $N_I$ ,  $a_0$ ,  $\ln C_C$  and  $Y$ ) for component  $j$

The events corresponding to detection of a crack at time  $T$  can be written:

$$h_1(\mathbf{X}_{Load,1}, \mathbf{X}_{Strength,1}, c_{d,1}, T) = c_{d,1} - c_1(\mathbf{X}_{Load,1}, \mathbf{X}_{Strength,1}, T) \leq 0 \quad (53)$$

$$h_2(\mathbf{X}_{Load,2}, \mathbf{X}_{Strength,2}, c_{d,2}, T) = c_{d,2} - c_2(\mathbf{X}_{Load,2}, \mathbf{X}_{Strength,2}, T) \leq 0 \quad (54)$$

Where

$c_j(\mathbf{X}_{Load,j}, \mathbf{X}_{Strength,j}, c_{d,j}, T)$  crack length at time  $T$  for component  $j$

$c_{d,j}$  smallest detectable crack length for component  $j$

It is noted that the crack depth  $a_j(t)$  and crack length  $c_j(t)$  are related through the coupled differential equations in (30).

The stochastic variables in different components will typically be dependent as follows:

- The load related variables can be assumed fully dependent since the loading is common to most components. However, in special cases different types of components and components placed with a long distance between each other can be less dependent.
- The strength variables  $N_I$ ,  $a_0$  and  $\ln C_C$  will typically be independent since the material properties are varying from component to component. However, some dependence can be expected for components fabricated with the same production techniques and from the same basic materials.
- The geometry function uncertainty modelled by  $Y$  will be fully dependent if the same type of fatigue critical details / components is considered and independent if two different types of fatigue critical details / components are considered.

Updated probabilities of failure of component 1 and 2 given no detection of cracks in detail 1 and 2 are

$$P_{F,1|1} = P(\text{failure of component 1 in time interval } [0, t] | \text{no detection in component 1 at time } T) = P(g_1(\mathbf{X}_{Load,1}, \mathbf{X}_{Strength,1}, t) \leq 0 | h_1(\mathbf{X}_{Load,1}, \mathbf{X}_{Strength,1}, c_{d,1}, T) > 0) \quad (55)$$

$$P_{F,2|2} = P(\text{failure of component 2 in time interval } [0, t] | \text{no detection in component 2 at time } T) = P(g_2(\mathbf{X}_{Load,2}, \mathbf{X}_{Strength,2}, t) \leq 0 | h_2(\mathbf{X}_{Load,2}, \mathbf{X}_{Strength,2}, c_{d,2}, T) > 0) \quad (56)$$

$$\begin{aligned}
 P_{F,2|1} &= \\
 &P(\text{failure of component 2 in time interval } [0, t] | \text{no detection in component 1 at time } T) = \\
 &P(g_2(\mathbf{X}_{Load,2}, \mathbf{X}_{Strength,2}, t) \leq 0 | h_1(\mathbf{X}_{Load,1}, \mathbf{X}_{Strength,1}, c_{d,1}, T) > 0)
 \end{aligned}
 \tag{57}$$

$$\begin{aligned}
 P_{F,1|2} &= \\
 &P(\text{failure of component 1 in time interval } [0, t] | \text{no detection in component 2 at time } T) = \\
 &P(g_1(\mathbf{X}_{Load,1}, \mathbf{X}_{Strength,1}, t) \leq 0 | h_2(\mathbf{X}_{Load,2}, \mathbf{X}_{Strength,2}, c_{d,2}, T) > 0)
 \end{aligned}
 \tag{58}$$

(55) and (56) represent situations where a component is updated with inspection of the same component. (57) and (58) represent situations where a component is updated with inspection of another component. The above formulas can easily be extended to cases where both components are inspected to where more components are inspected.

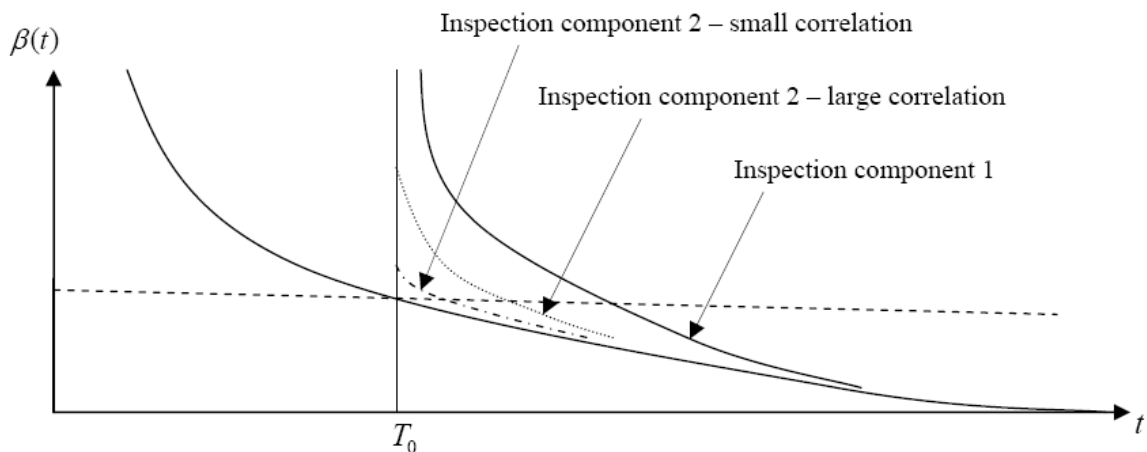


**Figure 2.11. Reliability index as function of time for component no. 1 and updated reliability if inspection of component no. 1 at time  $T_0$ , or of component no. 2 at time  $T_0$  with large and small positive correlation with component no. 1.**

The efficiency of updating the probability of fatigue failure for one component by inspection of another component depends on the degree of correlation between the stochastic variables as discussed above. Further, the relative importance of the load and the strength variables is important. If the load variables are highly uncertain and thus have high COVs then it can be expected that inspection of another components is efficient, because the highly correlated load variables accounts for a large part of the uncertainty in the failure events considered.

In Figure 2.11 is illustrated the effect on inspection planning for a component if this component is inspected or if another nearby component is inspected. The largest effect on reliability updating and thus inspection planning is obtained inspecting the same component or inspection of another component with a large correlation with the considered component.

Thus, inspection of a few details / components can be expected to be of high value for all components if:

- The strength variables are correlated – and this can be the case if
  - the fatigue critical details / components are of the same type (e.g. cracks in tubular K-joints) and the components are placed geometrical close to each other,
  - the components are fabricated under similar conditions and with the same basic material.
- The load variables have a relatively high uncertainty compared to the strength variables, and the components are placed geometrical close to each other.

Considering a group of components the reliability-based inspection planning problem can now be generalized to

- choosing the components to be inspected
- determining the time intervals between inspections – time intervals are not necessary the same for all components
- choosing the inspection method(s) to be used (often the same inspection methods will be used for all inspections)

The generic inspection planning technique could be generalized such that inspection times are planned for all  $N$  components by including a few more generic parameters:

- number  $N$  of components which could be inspected
- correlation between all  $N$  components

A simplified generic inspection planning technique could be obtained if only inspection planning for one component at the time is made but using information from other inspected components. The following information is needed:

- number  $N-1$  of other details / components with inspection information
- correlation the considered details / components and the other  $N-1$  components
- inspection times for the other  $N-1$  details / components (no detection of cracks are assumed)

The information on correlation between components could e.g. be given using the simplified scheme in Table 2.4 where three levels of correlation are assumed.

Table 2.4. Levels of correlation between fatigue critical components.

Uncertainty type	Level 1	Level 2	Level 3
common load uncertainties (assuming the same level of $COV_{wave}$ and $COV_{SCF}$ in the considered components)	Yes	Yes	Yes
common strength model uncertainties related to $\Delta$ and $Y$	No	Yes	Yes
partly correlated material fatigue parameters $\ln C$ (e.g. correlation coefficient equal to 0.5)	No	No	Yes

**Aspect c – effect of redistribution of load effects due to growing cracks**

In some cases the development of a crack in one component causes a stiffness reduction which imply that loads are redistributed and thereby increased stress ranges in other fatigue critical details. This effect can be modelled in the limit state equation by introducing a multiplier  $\alpha_1(a_2(t), a_3(t), \dots)$  on the stress ranges for component 1:

$$g_1(\mathbf{X}_{Load,1}, \mathbf{X}_{Strength,1}, \alpha_1(a_2(t), a_3(t), \dots), t) = 0 \quad (59)$$

As a simplification a multiplier corresponding to the redistribution when the crack depths in the relevant nearby details are equal to e.g. half the critical depth.

### 3 METHODOLOGY FOR COST-OPTIMAL PLANNING OF O&M FOR INNOVATIVE SUPPORT STRUCTURES

This section describes a methodology that can be used for new, innovative wind turbine support structures to account for O&M actions related to inspections and repairs at the design stage. The objective is to determine cost-effective plans for operation & maintenance actions (especially inspections) during the operational lifetime. In order to account for the possible, future inspections, maintenance and repair actions rational decisions have to be made. This section describes how this can be done using the pre-posterior Bayesian decision theoretical basis described in Section 2. It is noted that the application of a design approach where inspections (and other) condition monitoring are performed for innovative wind turbine substructures has the potential to discover unexpected behavior of the substructures before failures happen.

The proposed methodology consists of the following steps:

Step 1 – Decision theoretical and probabilistic basis

- Application of the theoretical approach in Section 2 to formulate the basic pre-posterior decision problem and the probabilistic basis for cost optimal planning of O&M, incl. inspections and maintenance actions.

Step 2 - Determination of safety factors to be used in design

- Calculation of safety factors (partial safety factors or *FDF*-values) for specific applications, including fatigue models (fracture mechanics models and SN-curves), inspection plans, repair & maintenance plans, other relevant deterioration models and cost models.

Step 3 - Design in practice

- Design using safety factors linked to required operation & maintenance actions, i.e. inspection plans and maintenance & repair actions to be performed if cracks / defects are discovered.

Step 1 and 2 have to be performed only once considering the application area (types of structures and critical details) and is not intended to be used in practical design. It results in combinations of inspection & repair plans with reduced fatigue safety factors. In practical design these are used considering and minimizing the total expected costs including initial costs and cost of inspections and possible repairs.

#### 4 ILLUSTRATION OF METHODOLOGY

This section is an illustration of the methodology described in previous sections. The focus is on the Reference INNWIND.EU 10MW wind turbine jacket substructure. The fatigue resistances (lives) of the circumferential welds in tubular K and X type joints are used as basis for inspection planning. The following figure shows the locations of the selected joints on the jacket substructure, for more detail see INNWIND D4.3.1 (Schuman & Kaufer, 2015).

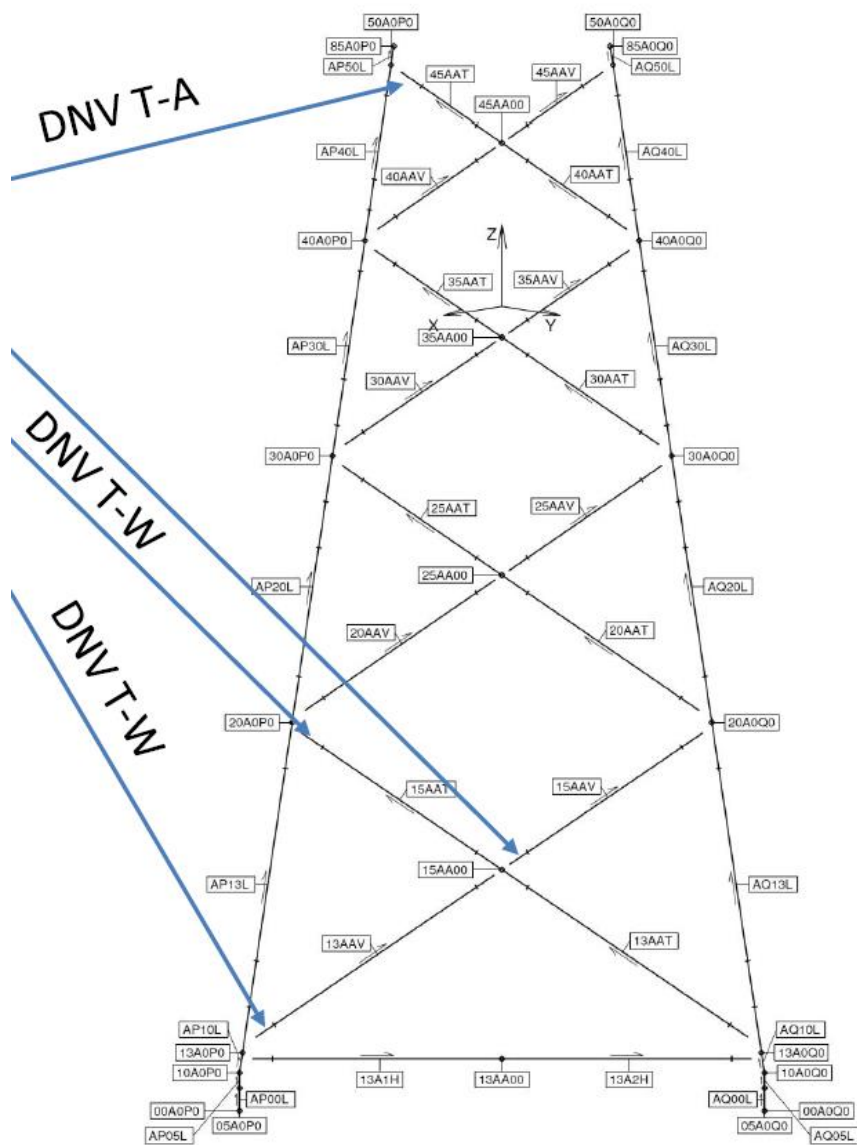
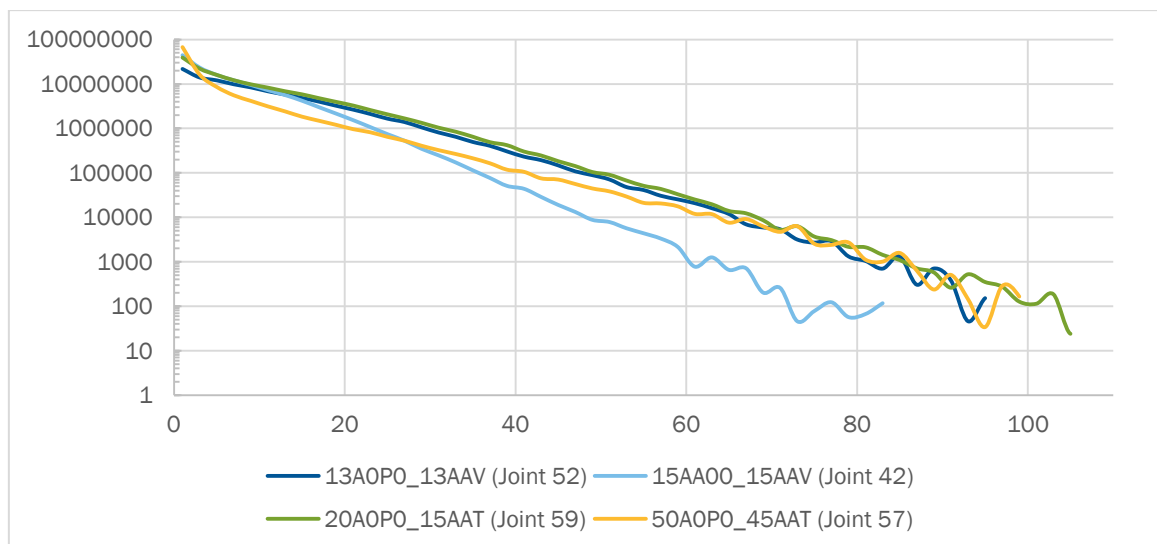


Figure 4.1. Examined joints.

The considered joints are the following:

- **Node 50AOP0, brace 45AAT (joint 57).**  
Fatigue life from (Schuman & Kaufer, 2015) – 28 years
- **Node 15AA00, brace 15AAV (joint 42).**  
Fatigue life from (Schuman & Kaufer, 2015) – 29 or 41 years (depending on which side of X joint)
- **Node 20A000, brace 15AAT (joint 59).**  
Fatigue life from (Schuman & Kaufer, 2015) – 4 or 8 years (depending if at node or at tubular element)
- **Node 13AOP0, brace 13AAV (joint 52).**  
Fatigue life (Schuman & Kaufer, 2015) - 22 or 14 (depending if at node or at tubular element)

Stress range distributions were provided from WP4 for the above joints (related to one of the braces) in terms of half-cycle counts per stress range for 12 different locations around the tubular cross-sections. Figure 4.2 shows the stress range (in MPa) distributions for the locations with the largest stress ranges.



**Figure 4.2. Stress range distributions at different joints.**

Using the stress range distribution data, structural reliability is used to determine the reliability levels and the fatigue life of the 4 selected joints using the SN-curve approach together with Miner's rule, see description in Section 2.5.

For the fatigue design of these joints the SN-curves in Table 4.1 from (DNV RP-C203, 2014) are used. The stochastic model applied in the following is shown in Table 4.3 with COV values chosen according to the general values used in (Sørensen & Toft, 2014) for calibration studies in relation to revision of (IEC 61400-1, 2005).

**Table 4.1. SN-curves: characteristic values.**

SN-curve		$\log K_{1,c}$	$m_1$	$\log K_{2,c}$	$m_2$
DNV-T-A	In air	12.164	3	15.606	5
DNV-T-W	In seawater with cathodic protection	11.764	3	15.606	5

In deterministic design using SN-curves the following design equation is assumed to represent a design situation where the fatigue stress range distribution is given as in Figure 4.2.

$$G(z) = 1 - \sum_{i,1} \frac{T_L n_i (\gamma_F \Delta \sigma_i)^{m_1}}{K_{1,c}} - \sum_{i,2} \frac{T_L n_i (\gamma_F \Delta \sigma_i)^{m_2}}{K_{2,c}} \geq 0 \quad (60)$$

where  $\Delta \sigma_i = \frac{\Delta Q_i}{z}$  is the stress range obtained for load effect range  $\Delta Q_i$  for stress range group  $i$  with  $n_i$  stress ranges per year.  $z$  is the design variable e.g. the cross-sectional section modulus. It is noted that in cases where the input to the fatigue assessment is stress ranges then the design variable acts as a scaling factor. It is assumed that the design lifetime is  $T_L = 25$  years.  $K_{1,c}$  and  $K_{2,c}$  are the characteristic values of  $K_1$  and  $K_2$ .  $\gamma_F$  is the partial safety factor.  $i,1$  and  $i,2$  indicate summations over the two branches of the SN-curve.

The corresponding limit state equation is written in accordance with the limit state equation in Section 2.5:

$$g = \Delta - \sum_{i,1} \frac{t n_i (X_{SCF} X_W \Delta \sigma_i)^{m_1}}{K_1} - \sum_{i,2} \frac{t n_i (X_{SCF} X_W \Delta \sigma_i)^{m_2}}{K_2} \geq 0 \quad (61)$$

where  $X_{SCF}$  and  $X_W$  are model uncertainties related to stress concentration factors and fatigue load;  $\Delta$  models model uncertainty related to Miner's rule.  $K_1$  and  $K_2$  are stochastic variables modelling uncertainty related to the SN-curve.  $t$  is the time in years.

For reliability analysis the  $z$  value is obtained from the design equation (with given safety factor) and the probability of failure is obtained using the limit state equation. The probability of failure is

estimated by the FORM (First Order Reliability Method). This gives a generic link between the safety factor and the reliability level as a function of time  $t$ .

Table 4.2 shows an approximate relationship between the safety factor  $\gamma_F$  and the 'safe', design fatigue life. The fatigue lives are obtained using the stress range distributions in Figure 4.2 and assuming that most of the fatigue life is related to the slope of the SN-curve where  $m = 5$ .

**Table 4.2. Relationship between fatigue life and safety factor**

Safety factor	Design fatigue life [years]
0.7	1.5
0.8	3
0.9	5
1.0	8
1.1	13
1.25	25

It is noted that in INNWIND D4.3.1 fatigue lives as low as 4 years are obtained for K-joints and 29 years for X-joints implying that especially K-joints have problems with sufficient fatigue reliability. In the following it is investigated how often and which inspection techniques could be applied to secure sufficient reliability. Such inspections and possible repairs will have a, Operational & Maintenance (OM) cost to be included in the overall design decision following the principles in Section 2.2. However, since information about these cost contributions are not available, 'only' a reliability based approach is applied in the following.

Table 4.3. Stochastic model.

Variable	Distribution	Expected value	Standard deviation / Coefficient Of variation	Comment
$\Delta$	N	1	$COV_{\Delta} = 0.30$	Model uncertainty Miner's rule
$X_w$	LN	1	$COV_{X_w}$ see below	Model uncertainty fatigue load
$X_{scf}$	LN	1	$COV_{X_{scf}}$ see below	Model uncertainty stress concentration factor
$m_1$	D	3		Slope SN curve
$\log K_1$	N	see Table 4.1	$\sigma_{\log K_1} = 0.2$	Parameter in SN curve
$m_2$	D	5		Slope SN curve
$\log K_2$	N	see Table 4.1	$\sigma_{\log K_2} = 0.2$	Parameter in SN curve
$\log K_1$ and $\log K_2$ are fully correlated				

The stochastic model in Table 4.1 is applied in the following and is equivalent with the stochastic model in (Sørensen & Toft, 2014). The total COV for the model uncertainty and the fatigue load is chosen to  $\sqrt{COV_{X_w}^2 + COV_{X_{scf}}^2} = 0.08$ . This represents a case where the fatigue load is estimated quite good and where the stress concentration factors are obtained based on detailed finite element analyses, see (Sørensen & Toft, 2014) for more details.

Figure 4.3 to Figure 4.6 shows how the reliability level obtained from the accumulated probability of failure in the time interval  $[0; t]$  is decreasing with respect to life,  $t$  (in years). The differently colored lines represent different safety factors,  $\gamma_F$  used in the analysis (0.7, 0.85, 1.0, 1.15 and 1.25).

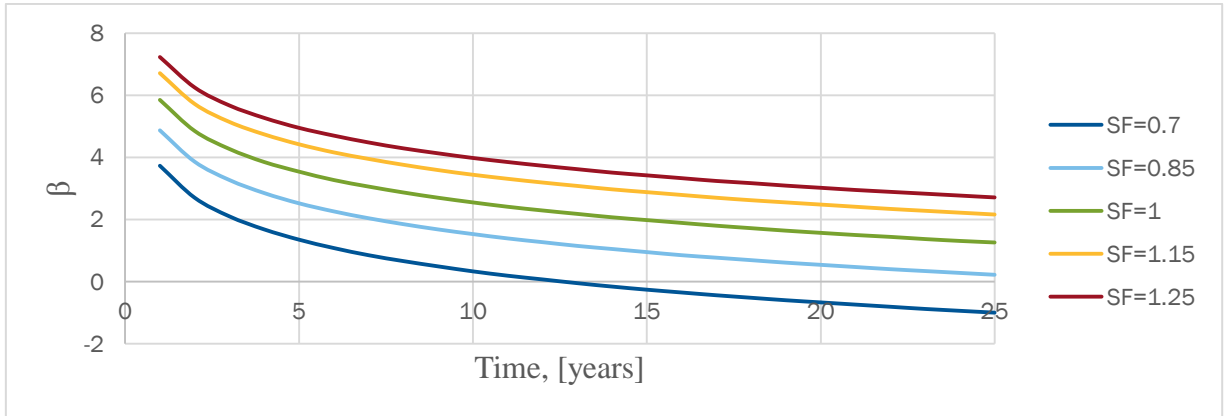


Figure 4.3. Joint 59, accumulated  $\beta$ .

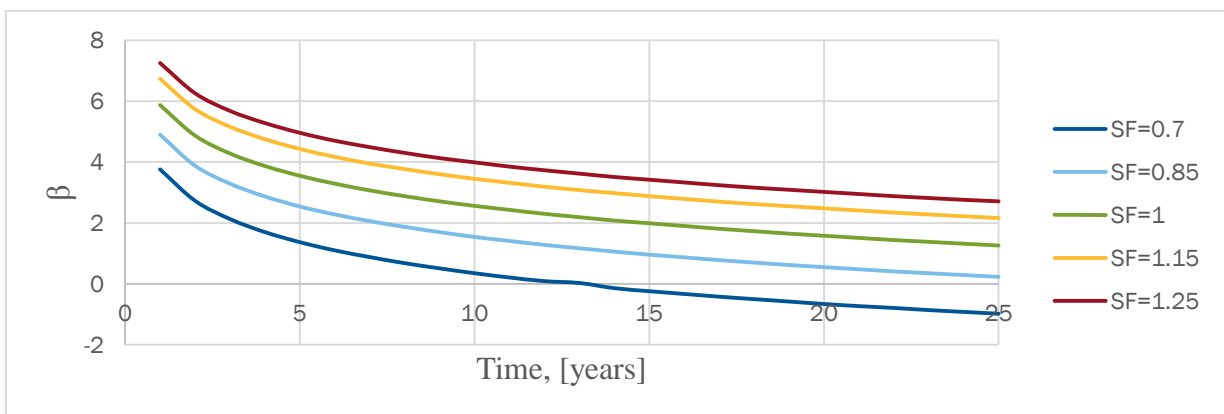


Figure 4.4. Joint 42, accumulated  $\beta$ .

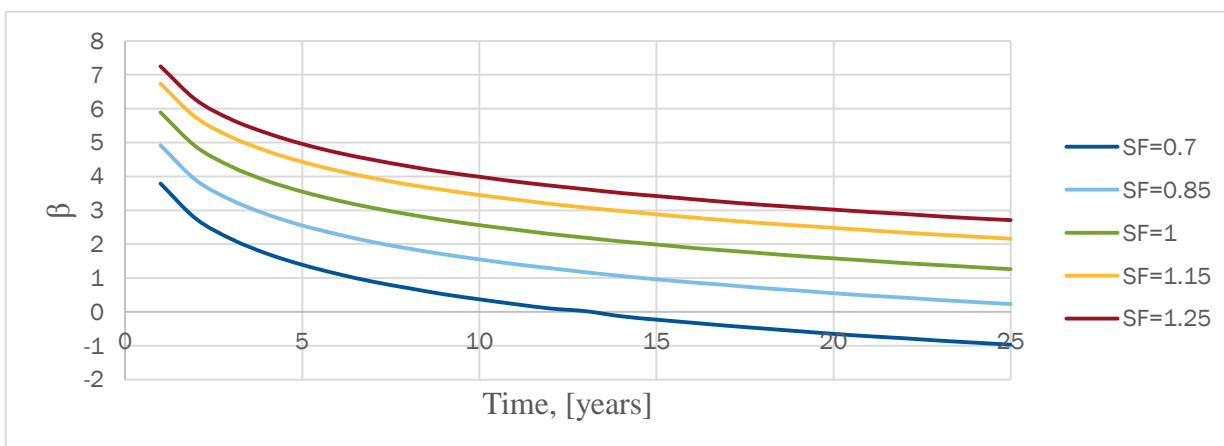


Figure 4.5. Joint 52, accumulated  $\beta$ .

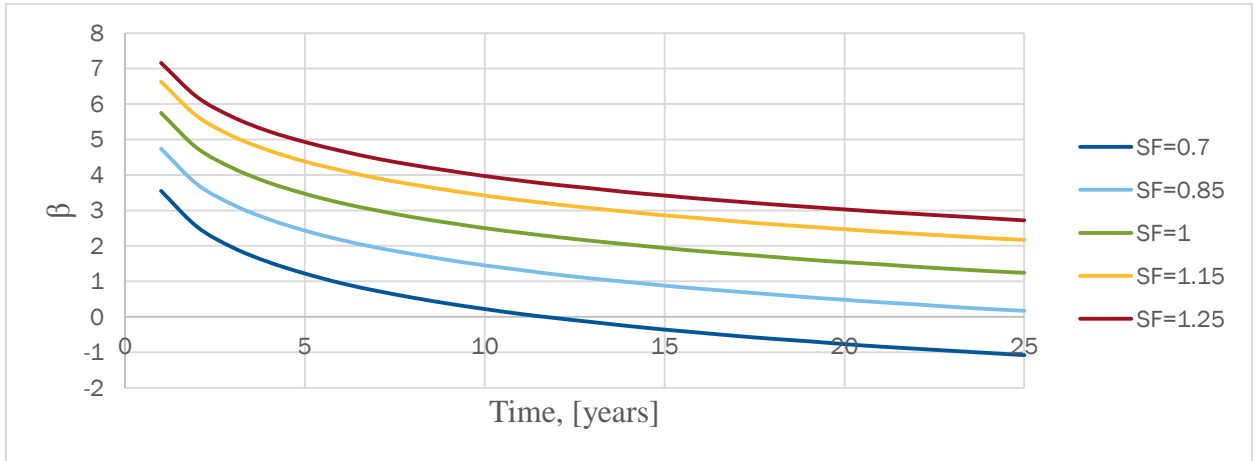


Figure 4.6. Joint 57, accumulated  $\beta$ .

The annual probability of failure in year  $t$  given survival up to year  $t$  is estimated by

$$\Delta P_{F,t} = P_{COL|FAT} (P(g(t) \leq 0) - P(g(t-1) \leq 0)) / P(g(t) \leq 0) \quad (62)$$

The annual reliability indices obtained from (62) corresponding to the accumulated reliability indices in Figure 4.3 to Figure 4.6 are shown in Figure 4.7 to Figure 4.10.

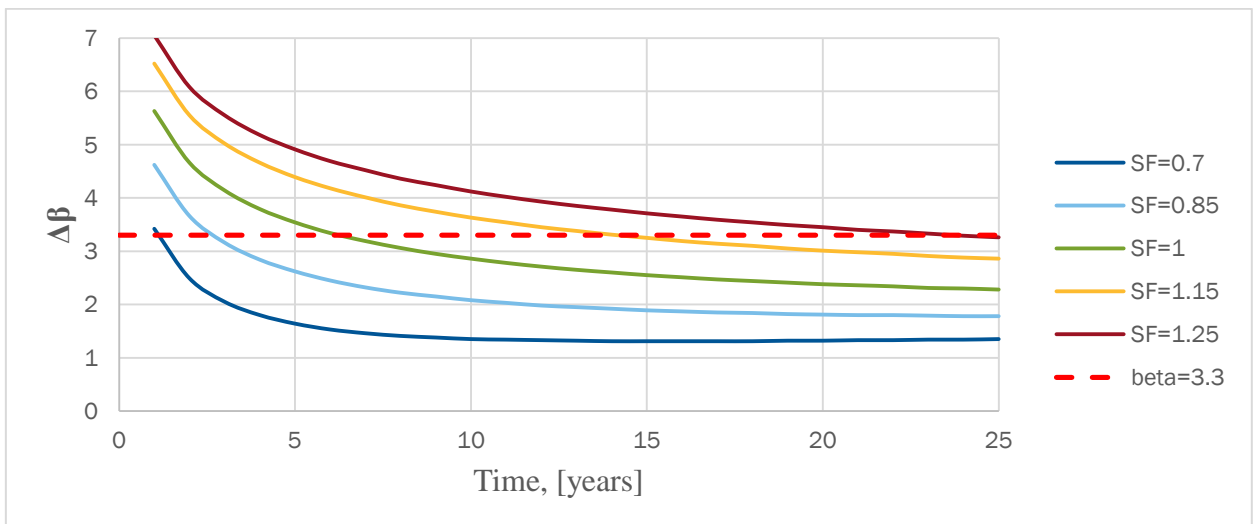


Figure 4.7. Joint 59, annual  $\beta$ .

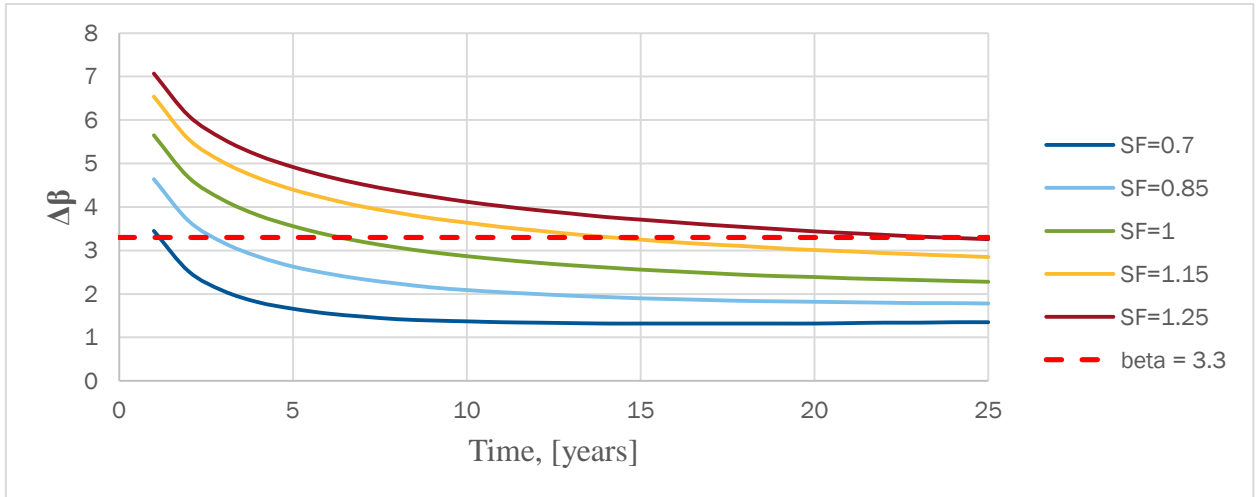


Figure 4.8. Joint 42, annual  $\beta$ .

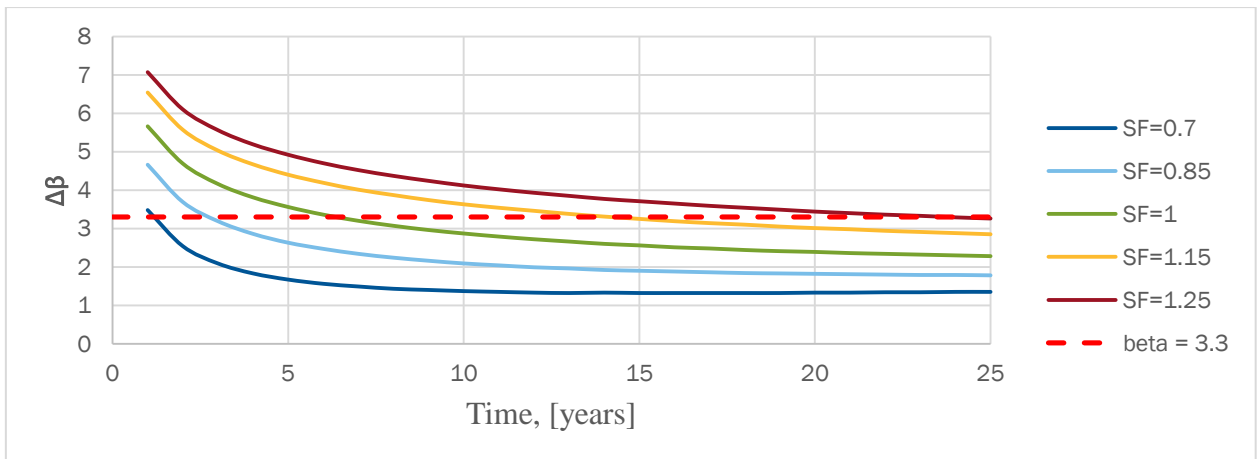


Figure 4.9. Joint 52, annual  $\beta$ .

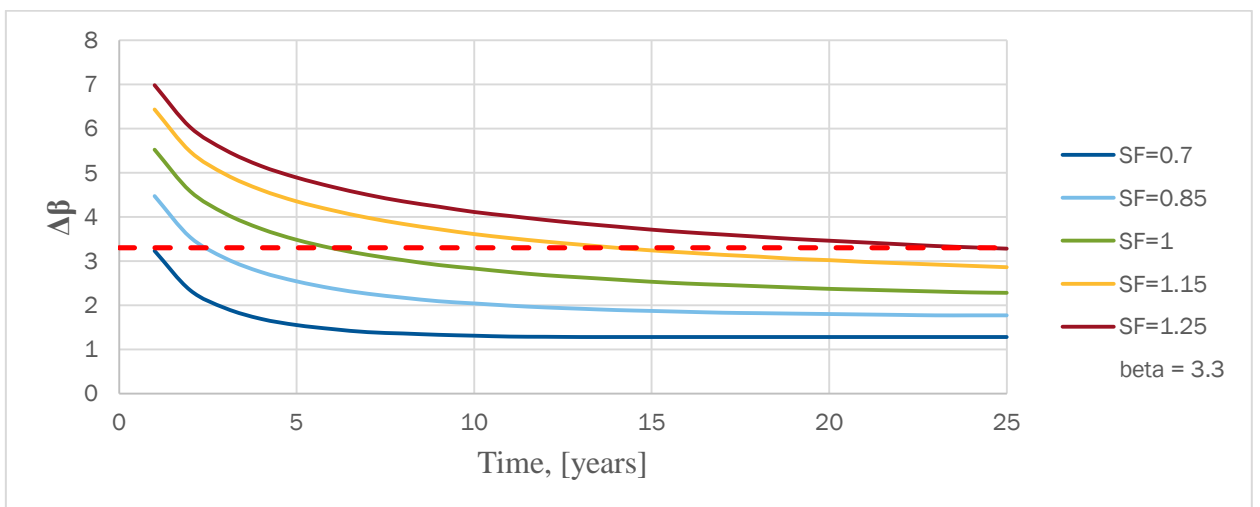


Figure 4.10. Joint 57, annual  $\beta$ .

It is seen that:

- When the safety factor is equal to 1.25 then an annual reliability index equal to approximately 3.3 is obtained after 25 years. This corresponds to the target reliability level in the CD IEC 61400-1 ed. 4 standard, Annex K.
- If the safety factor is lower than 1.25 (corresponding to design fatigue lives lower than 25 years) the reliability level becomes too low – and inspections are needed during the design lifetime in order to secure the required reliability level.

As described in Section 2.5 a Fracture Mechanics (FM)-model is calibrated to give approximately the same annual reliability indices as function of time as obtained above with SN-curves from the (DNV RP-C203, 2014) resulting in the illustrative results in Figure 4.11 and Figure 4.12. The calibration is performed such that the reliability curves have the best fit at the end of the lifetime (approximately from year 15 to year 25). It is seen that the fits are not perfect, but are considered to be of sufficient accuracy for inspection planning.

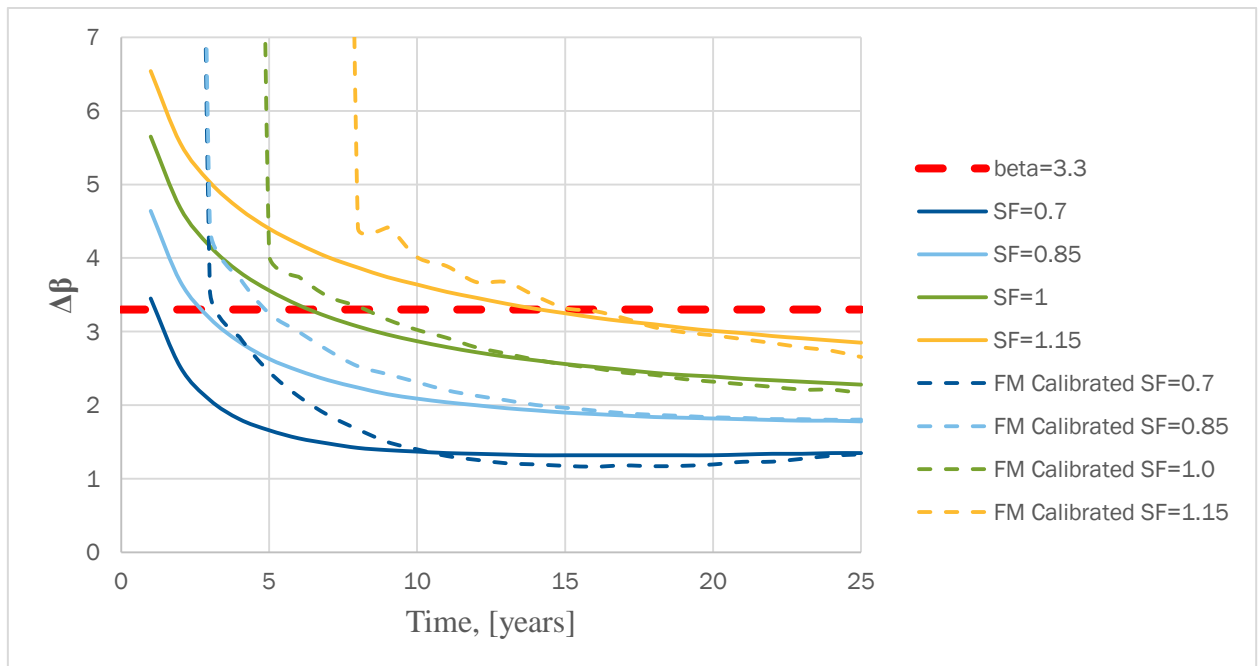


Figure 4.11. Joint 42, annual reliability levels using different methods (SN – solid line, FM – dashed line).

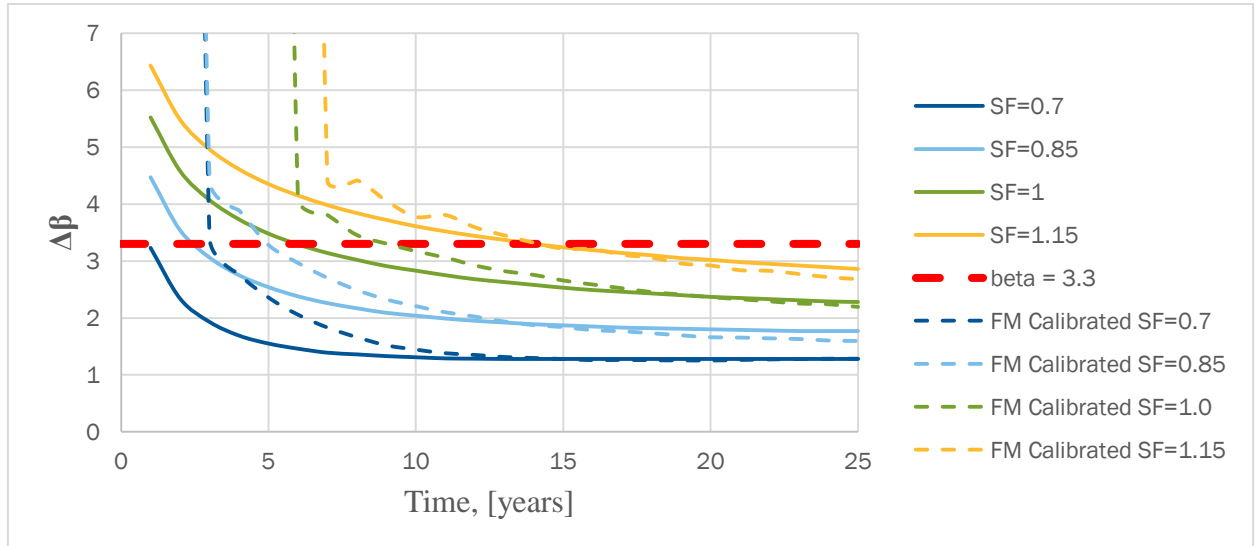


Figure 4.12. Joint 57, annual reliability levels using different methods (SN – solid line, FM – dashed line).

The calibrated FM models are used to introduce inspections and thus reduce the initial reliability level necessary to ensure that the joints survive the 25 year lifetime of the structure with sufficient reliability.

Three different inspection methods are applied:

- Eddy current:  
POD curve: eq. (2.9)
- Very close visual inspection:  
POD curve: eq. (2.35) with  $\lambda = 5$  mm
- Close visual inspection:  
POD curve: eq. (2.35) with  $\lambda = 10$  mm

The following figures show how the reliability level changes throughout the lifetime of the joint when inspections are performed (and subsequently repairs if a defect is detected). The inspections are assumed to be performed with fixed time intervals as in Figure 2.6. Time intervals equal to 2, 3, 4, 5 and 10 years are investigated. Figure 4.13 to Figure 4.15 indicate how Eddy current inspections could be utilized in order to maintain a required reliability level. It is noted that the annual reliability indices obtained by extensive simulations are estimated for each year but have some scatter, and that the vertical lines therefore 'show' that at some years the reliability level is very high (larger than 5) resulting in reliability index curves growing to 'infinity'.

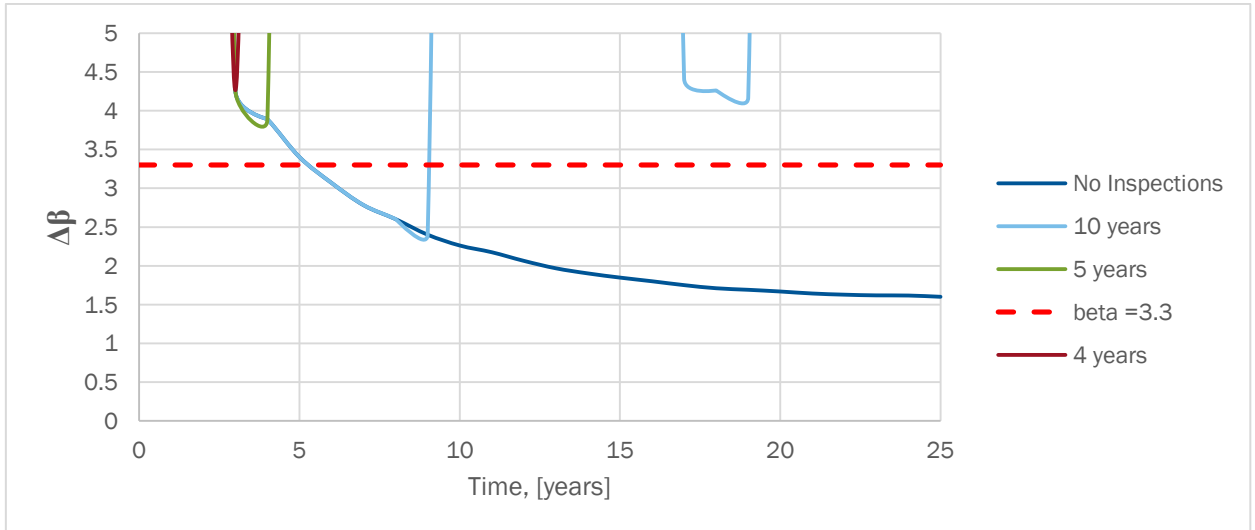


Figure 4.13. Annual reliability with SF=0.85. Joint 52. Eddy current inspection.

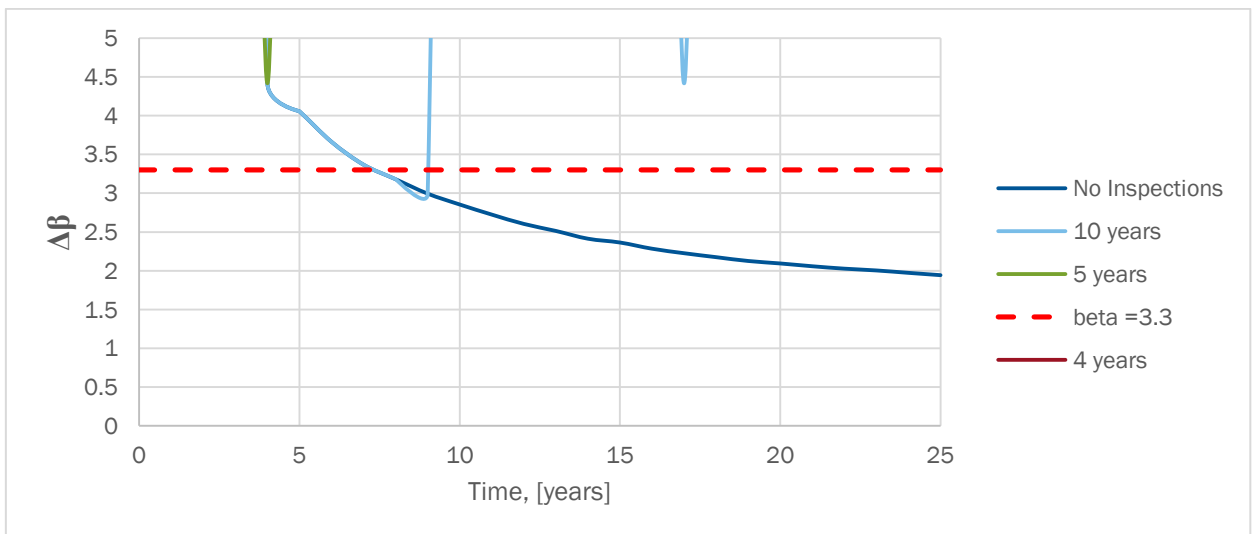


Figure 4.14. Annual reliability with SF=1.0. Joint 52. Eddy current inspection.

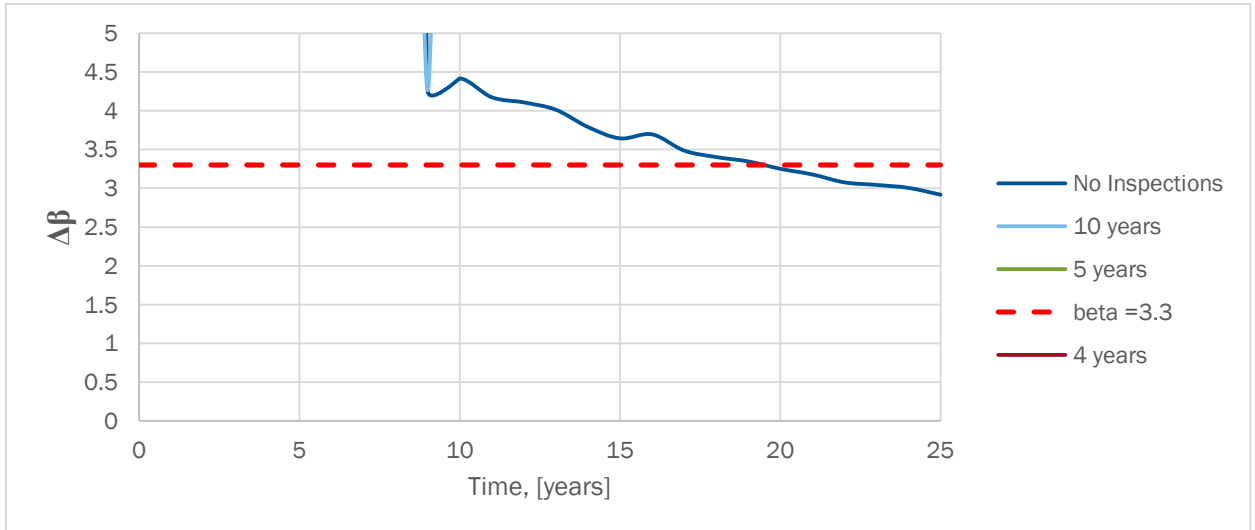


Figure 4.15. Annual reliability with SF=1.15. Joint 52. Eddy current inspection.

It is obvious from the figures that if a higher safety factor is used in design then there is a lower need for inspections throughout the lifetime of the structure. If a safety factor is reduced from 1.25 (1.25 being the standard requirement) to 1.15 the joint still retains a sufficient reliability level (above 3.3) if inspections (and repairs if cracks are detected) are performed every 10 years. If the safety factor is set to 1.0 then inspections become necessary (Figure 4.14) and should be performed at 8-9 year intervals. With further reduction of safety factor to 0.85, inspection interval should be decreased to 5-6 years.

The following figures show how visual inspections impact the reliability level of the selected joint.

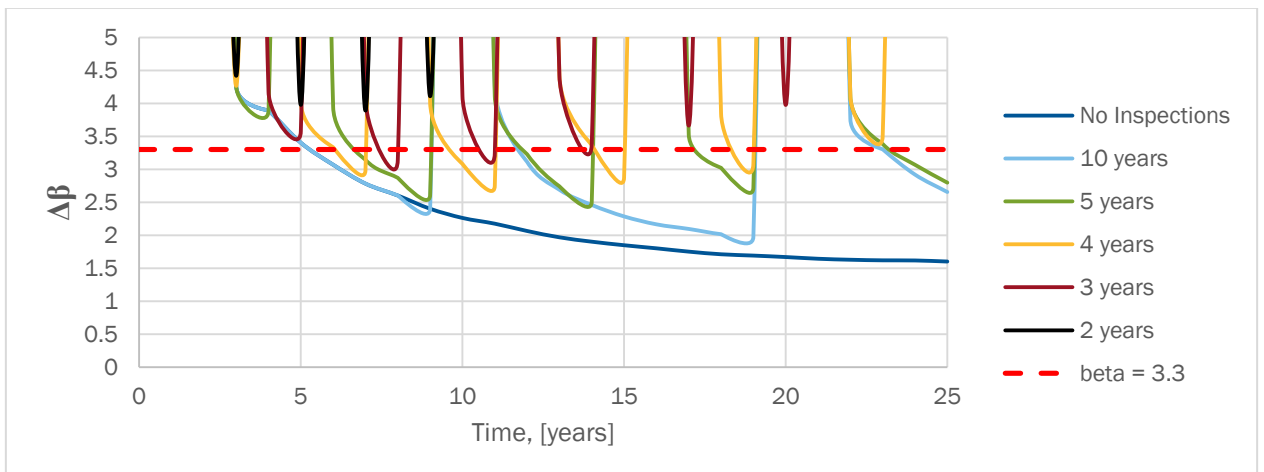


Figure 4.16. Annual reliability with SF=0.85. Joint 52. Visual inspection. Average minimum detectable crack 5mm.

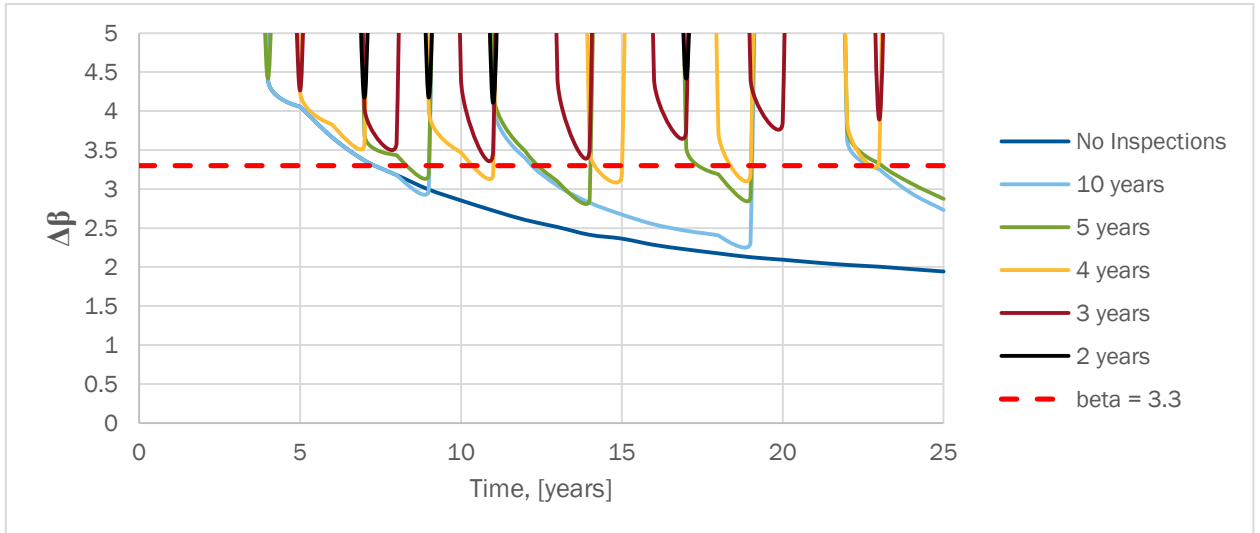


Figure 4.17. Annual reliability with SF=1.0. Joint 52. Visual inspection. Average minimum detectable crack 5mm.

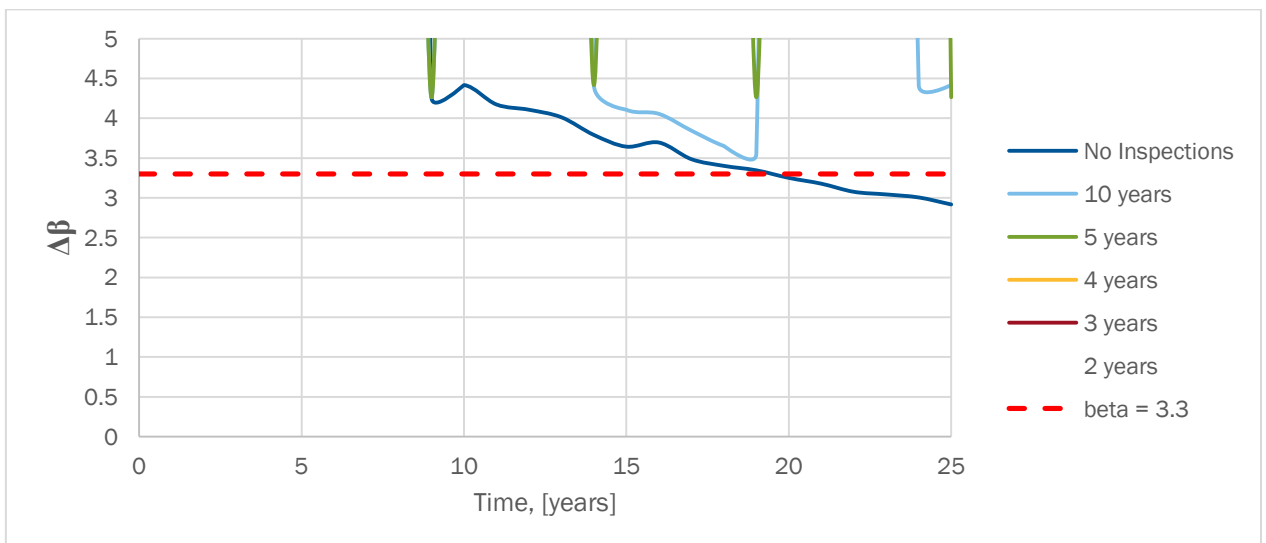


Figure 4.18. Annual reliability with SF=1.15. Joint 52. Visual inspection. Average minimum detectable crack 5mm.

If very close visual inspections with minimum detectable crack size equal to 5 mm are performed the required inspection intervals have to be shortened even more. As was for the case with Eddy current inspections for the case with safety factor of 1.15 inspections with 10 year intervals are sufficient to maintain the required reliability level. If safety factor is reduced to 1.0 then inspections have to be performed every 3-4 years. Further reduction to 0.85 requires an inspection interval of 2-2.5 years.

The following figures show the impact of lower quality *close visual inspections* (minimum detectable crack size equal to 10 mm).

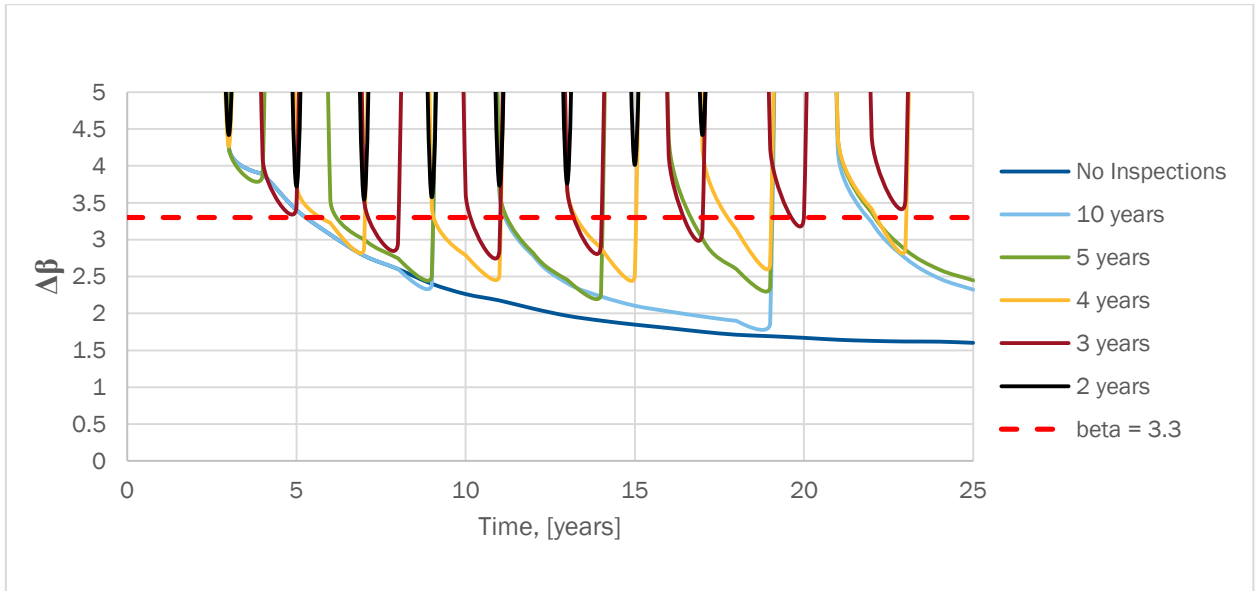


Figure 4.19. Annual reliability with SF=0.85. Joint 52. Visual inspection. Average minimum detectable crack 10mm.

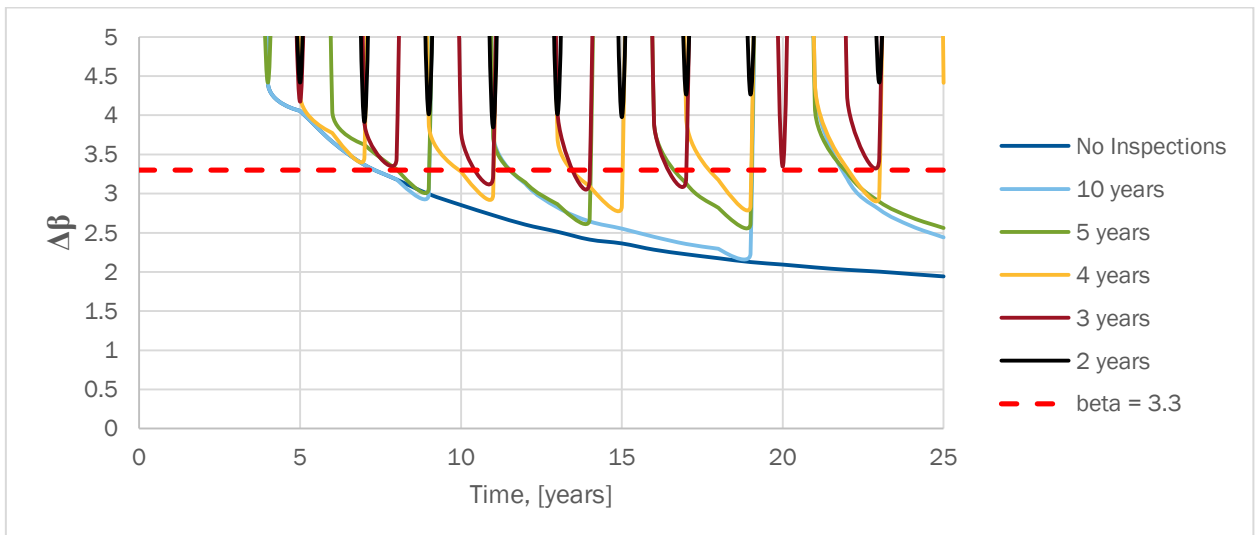
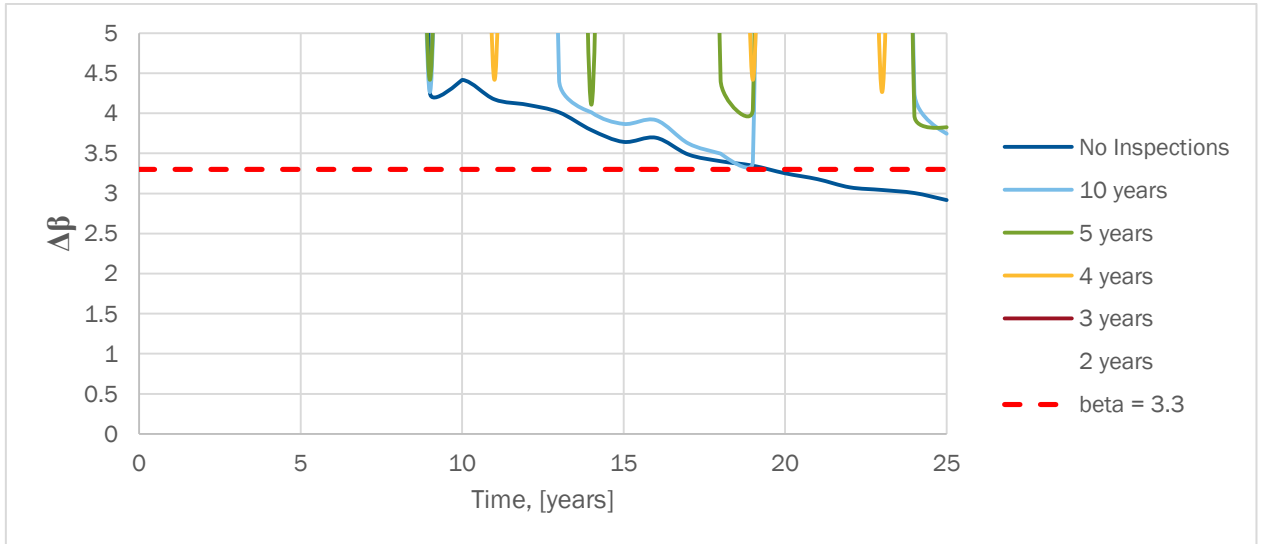


Figure 4.20. Annual reliability with SF=1.0. Joint 52. Visual inspection. Average minimum detectable crack 10mm.



**Figure 4.21. Annual reliability with SF=1.15. Joint 52. Visual inspection. Average minimum detectable crack 10mm.**

When the quality of visual inspections is lower (Figure 4.19 - Figure 4.21) the inspections have to be even more frequent. Whilst a 10 year inspection interval is just sufficient enough to when design safety factor is 1.15 the intervals have to be reduced to 2 years if safety factor is 0.85. This is a clear indication that inspection quality plays a very important role in inspection planning and overall reliability level of the substructure.

All the other joints are analyzed using the same logic and a summary is shown in Table 4.4. For more detail, results of inspection planning for all the joints can be found in Appendix B. In general, the inspection intervals can be interpolated between different safety factors within the same inspection quality category.

Table 4.4. Inspection time intervals for different joints.

	Eddy current			Very close visual inspection			Close visual inspection		
<b>Joint 52 (under water)</b>									
<b>Safety Factor</b>	0.85	1.0	1.15	0.85	1.0	1.15	0.85	1.0	1.15
<b>Inspection interval [years]</b>	5-6	9-10	10	2-3	3-4	10	2	2-3	9-10
<b>Joint 59 (under water)</b>									
<b>Safety Factor</b>	0.85	1.0	1.15	0.85	1.0	1.15	0.85	1.0	1.15
<b>Inspection interval [years]</b>	5-6	9-10	10	2-3	5-6	8-9	4-5	5	5
<b>Joint 42 (under water)</b>									
<b>Safety Factor</b>	0.85	1.0	1.15	0.85	1.0	1.15	0.85	1.0	1.15
<b>Inspection interval [years]</b>	5	9-10	>10	2-3	3-4	5-6	2	2-3	4-5
<b>Joint 57 (above water)</b>									
<b>Safety Factor</b>	0.85	1.0	1.15	0.85	1.0	1.15	0.85	1.0	1.15
<b>Inspection interval [years]</b>	5	10	10	3-4	4-5	5-6	3	4	5-6

Since the simulations were performed with fixed inspection intervals, the values in the table are indicative for every type of joint considered. This analysis could be extended to find the exact inspection intervals for each type of joint/weld, i.e. using time intervals between inspections which are varying with time (general longer time intervals at the end of the design lifetime). However, the general purpose of this analysis is to suggest inspection strategies for the whole wind turbine jacket substructure, which consists of multitude of different types of joints and therefore only one set of inspection interval values per safety factor is suggested. Here it is also important to note that because many joints and many wind turbine substructures have to be inspected, system effects (as discussed in Section 2) become important both from a reliability point of view and from a cost point of view. However, these important system reliability aspects implies much more complex stochastic models to be formulated and computer expensive simulations to be performed. This is outside the scope of this deliverable, but will be considered in a subsequent deliverable.

It is mentioned that the inspection strategy is clearly dependent on the type and way the inspection is performed and also its quality. The following table summarizes the results from Table 4.4. The global inspection strategy is suggested taking inspection type into account, because there is a noticeable difference between inspection types and the associated costs. Minimum values from Table 4.4 are used to produce global inspection strategies for different inspection types because the

jacket structure should be inspected as a whole and at once rather than separate joints at different inspection intervals. When the information in Table 4.4 is coupled Table 4.2 then a first indication of the required inspection plan can be obtained using directly the results in e.g. INNWIND D4.3.1.

Table 4.5. Suggested inspection strategies.

	Eddy current			Very close visual inspection			Close visual inspection		
	0.85	1.0	1.15	0.85	1.0	1.15	0.85	1.0	1.15
Inspection interval [years]	5	9	10	2	3-4	5	2	2-3	5

A sensitivity analysis was performed with respect to the uncertainty related to fatigue load, namely COV was increased from 0.08 to 0.1. This would represent a situation where there is less knowledge about the fatigue loading (the load itself or stress concentration factors) and therefore higher uncertainty is higher. The following two figures show the effect that the change in COV has on the reliability levels of a selected joint.

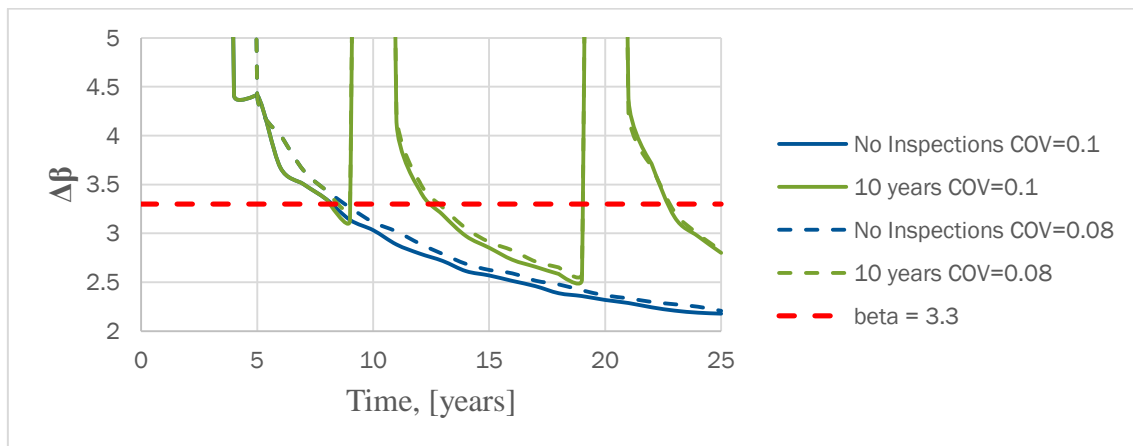
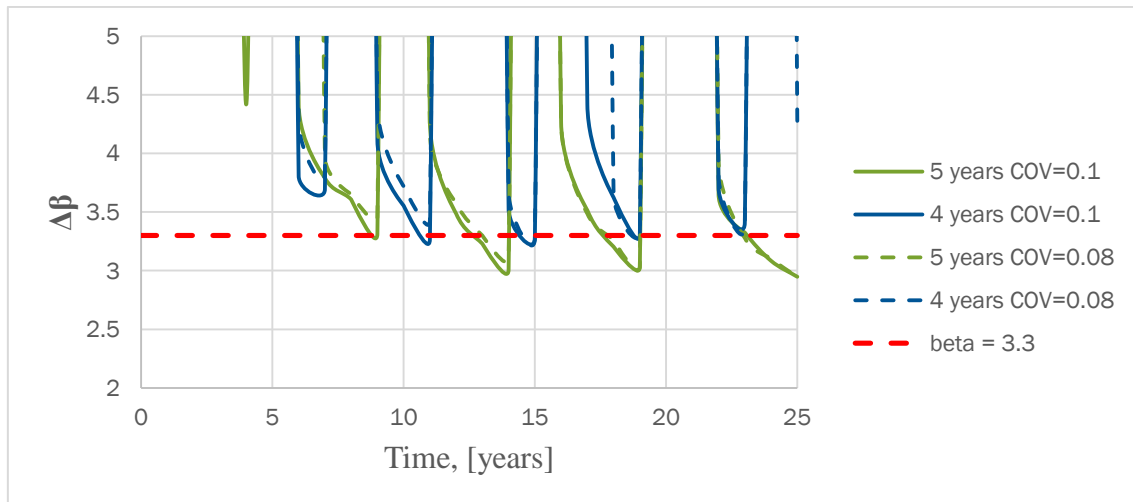


Figure 4.22. Annual reliability with SF=1.1. Joint 42. Visual inspection. Average minimum detectable crack 5mm. Effect of change of COV.



**Figure 4.23. Annual reliability with SF=1.1. Joint 42. Visual inspection. Average minimum detectable crack 5mm. Effect of change of COV.**

Increase in fatigue load uncertainty reduces the annual reliability index to a very limited extent therefore the effect on overall inspection plans can be expected to be small. Change in inspection intervals would be on a scale of a couple of weeks to a month. This change could be considered as negligible knowing the fact that changing sea weather conditions do not allow to plan inspection activities on a weekly basis.

## 5 SUMMARY AND CONCLUSIONS

Different joints of the Reference 10 MW INNWIND jacket substructure are analyzed in terms of reliability and inspection strategies are investigated and suggested. It is evident from the analysis that use of inspections on offshore wind turbine substructures could be used as means of increasing the reliability level of welded tubular steel joints (compared to the situation where no inspections are performed). This can be achieved by using a reduced safety factor when designing the joints by standard methods and compensating for the lower reliability by performing inspections and repairs on the substructure joints during the lifetime.

The results suggest that different techniques of inspection imply different inspection intervals at the same target reliability level. E.g. inspections every 6 years when using Eddy current methods as opposed to 2-4 year inspection intervals when only performing visual inspections at safety factor level of 1.0. The inspection intervals seem to be scalable with respect to the safety factor - increase in safety factor increases inspection intervals. Furthermore, since there is a difference between the two tested visual inspection qualities (5 and 10 mm minimum detectable cracks), more robust inspection methods could be also beneficial; mainly because smaller cracks could be detected earlier in the lifetime and repaired before reaching critical sizes.

## APPENDIX A. ILLUSTRATION OF RELIABILITY-BASED PLANNING OF INSPECTION FOR CALIBRATION OF SAFETY FACTORS FOR FATIGUE

This appendix describes how the methodology for reliability-based inspection planning described in Section 2.5 can be used to assess and calibrate safety factors for fatigue design based on generic fatigue models used in the development of the revision of IEC 61400-1 standard for design of wind turbines. The following illustration is based on (Sørensen & Toft, 2014).

For wind turbine steel substructures fatigue can be a critical failure mode for welded details, especially if joints with high stress concentrations are used. Since design and limit state equations are closely related a detailed model of the fatigue damage is generally not needed for reliability-based assessment of fatigue safety factors. It is 'only' important to model the dependency on the uncertain parameters and the uncertain parameters themselves carefully. In this illustration is considered a case with wind load dominating and no wake effects taken into account, see Section 2.

**Table A. 1. Stochastic model.**

Variable	Distribution	Expected value	Standard deviation / Coefficient Of variation	Comment
$\Delta$	N	1	$COV_{\Delta} = 0.30$	Model uncertainty Miner's rule
$X_{Wind}$	LN	1	$COV_{Wind}$	Model uncertainty wind load
$X_{SCF}$	LN	1	$COV_{SCF}$	Model uncertainty stress concentration factor
$m_1$	D	3		Slope SN curve
$\log K_1$	N	determined from $\Delta\sigma_D$	$\sigma_{\log K_1} = 0.2$	Parameter SN curve
$m_2$	D	5		Slope SN curve
$\log K_2$	N	determined from $\Delta\sigma_D$	$\sigma_{\log K_2} = 0.2$	Parameter SN curve
$\Delta\sigma_F$	D	71 MPa		Fatigue strength
$\log K_1$ and $\log K_2$ are fully correlated				

The stochastic model shown in Table A. 1 is considered as representative for a fatigue sensitive detail using the SN-approach. It is assumed that the design lifetime is  $T_L = 25$  years.

As acceptance criteria are used  $\Delta P_{F,\max} = 5 \cdot 10^{-4}$  (normal/high consequence of failure) and  $5 \cdot 10^{-3}$  (low consequence of failure) as annual maximum probabilities of failure. The corresponding annual reliability indices are 3.3 and 2.6.

The mean wind speed is assumed to be Weibull distributed:

$$F_U(u) = 1 - \exp\left(-\left(\frac{u}{A}\right)^k\right) \quad (\text{A.1})$$

with  $A = 9.0$  m/s and  $k = 2.3$ . It is assumed that the reference turbulence intensity is  $I_{ref} = 0.14$ .

Table A. 2 shows the required product of the partial safety factors  $\gamma_f \gamma_m$  as function of the total coefficient of variation of the fatigue load:  $COV_{load} = \sqrt{COV_{Wind}^2 + COV_{SCF}^2}$  in the case where no inspections are performed during the design life. It is noted that for a linear SN-curve with Wöhler exponent  $m$  the Fatigue Design Factor  $FDF = (\gamma_f \gamma_m)^m$ .

**Table A. 2. Required partial safety factors  $\gamma_f \gamma_m$  given  $\Delta\beta_{min, FAT}$  as function of COV for fatigue load.**

$\Delta\beta_{min, FAT} \setminus COV_{load}$	0,00	0,05	0,10	0,15	0,20	0,25	0,30
2,6 (5 10 <sup>-3</sup> )	0,91	0,92	0,94	0,98	1,01	1,04	1,06
3,3 (5 10 <sup>-4</sup> )	1,04	1,06	1,12	1,21	1,32	1,43	1,56

In the following it is investigated how much the partial safety factor for fatigue can be reduced if inspections are performed during the lifetime of a wind turbine. In order to model the influence of inspections a Fracture Mechanics model (FM) is needed for estimating the crack growth as described in Section 2. The fracture mechanics model is calibrated to give the same reliability as function of time as obtained by the SN-approach.

The Fracture Mechanical (FM) modeling of the crack growth is applied assuming that the crack can be modeled by a 2-dimensional semi-elliptical crack, or simplified models where the ratio between crack width and depth is either a constant or the crack width is a given function of the crack depth, see Section 2. The stochastic model in Table A. 1 is applied.

The reliability of inspections is assumed to be modelled by an exponential model and the fracture mechanics model is used as described in Section 2.

It is assumed that the considered details are very critical for the structural integrity implying that  $RIF = 0$  and  $P_{COL|FAT_j} = 1$ .

Further, the planning is made with the assumption that no cracks are found at the inspections. If a crack is found, then a new inspection plan has to be made based on the observation. It is emphasized that the inspection planning is based on this no-find assumption. This way of inspection planning is the one which is most often used. Often this approach results in increasing time intervals between inspections.

Figure A. 1 - Figure A. 8 show results for both accumulated and annual reliability indices for the following cases:

- Inspection with time intervals 2, 3, 4, 5 and 10 years,  $\lambda = 10$  mm, partial safety factor  $\gamma_m = 1.00$ . Aspect ratio = 0.2.
- Inspection with time intervals 2, 3, 4, 5 and 10 years,  $\lambda = 10$  mm, partial safety factor  $\gamma_m = 1.10$ . Aspect ratio = 0.2.
- Inspection with time intervals 2, 3, 4, 5 and 10 years,  $\lambda = 10$  mm, partial safety factor  $\gamma_m = 1.25$ . Aspect ratio = 0.2.
- Inspection with time intervals 2, 3, 4, 5 and 10 years,  $\lambda = 5$  mm, partial safety factor  $\gamma_m = 1.10$ . Aspect ratio = 0.2.
- Inspection with time intervals 2, 3, 4, 5 and 10 years,  $\lambda = 5$  mm, partial safety factor  $\gamma_m = 1.10$ . Aspect ratio modelled by (4.10)

The results show among others that if the fatigue partial safety factor is chosen to 1.0 then inspection intervals of maximum 5 years should be performed with at least a reliability which corresponds to an expected value of the smallest detectable crack equal to 10 mm. If the fatigue partial safety factor is chosen to 1.1 then inspection intervals of maximum 10 years should be performed with at least a reliability which corresponds to an expected value of the smallest detectable crack equal to 10 mm. If the aspect ratio given by (4.10) is used then slightly larger inspection intervals are needed.

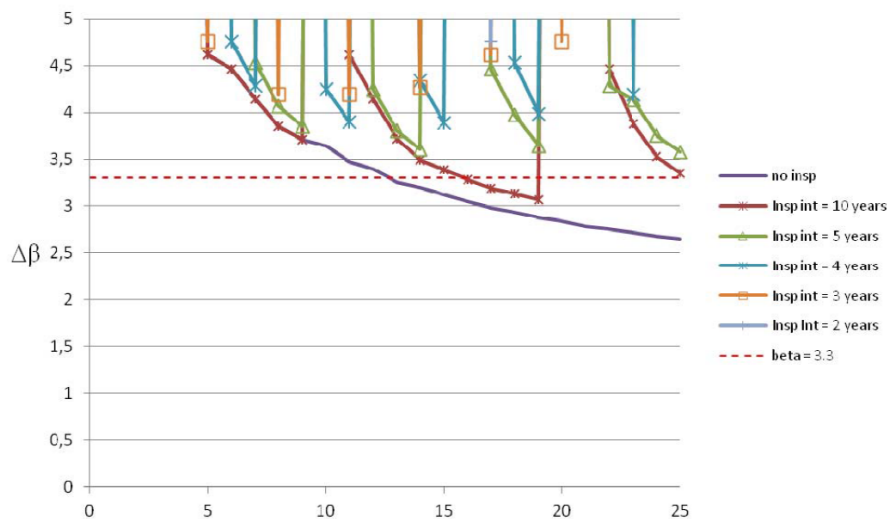


Figure A. 1. Annual reliability index without and with inspections. Inspection time intervals 2, 3, 4, 5 and 10 years and  $\lambda = 10$  mm, partial safety factor  $\gamma_m = 1.00$  and aspect ratio = 0.2.

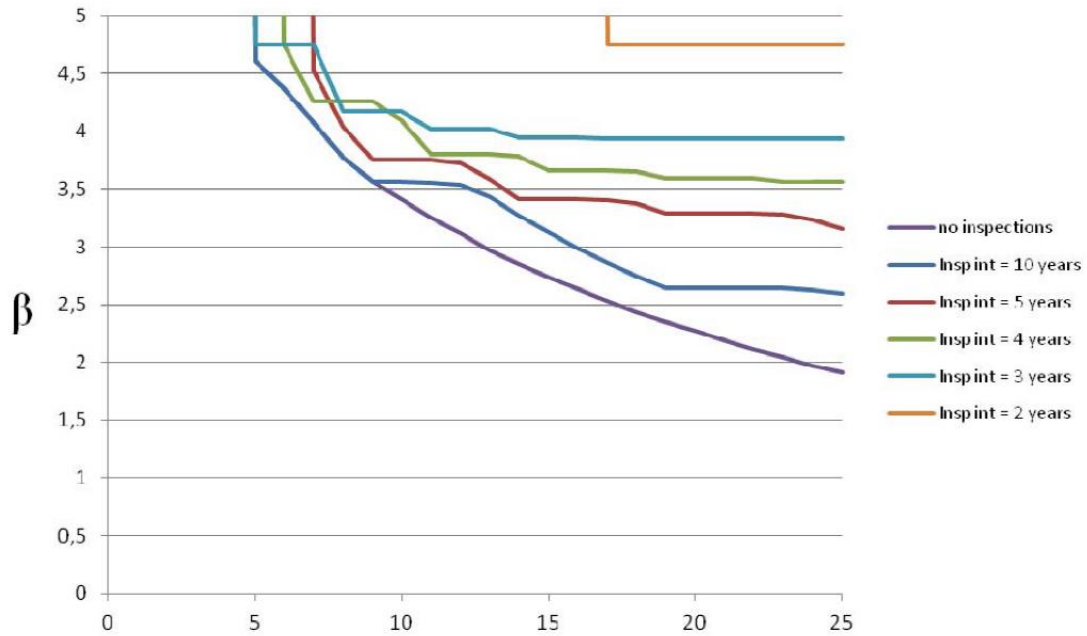


Figure A. 2. Accumulated reliability index without and with inspections. Inspection time intervals 2, 3, 4, 5 and 10 years and  $\lambda=10$  mm, partial safety factor  $\gamma_m = 1.00$  and aspect ratio = 0.2.

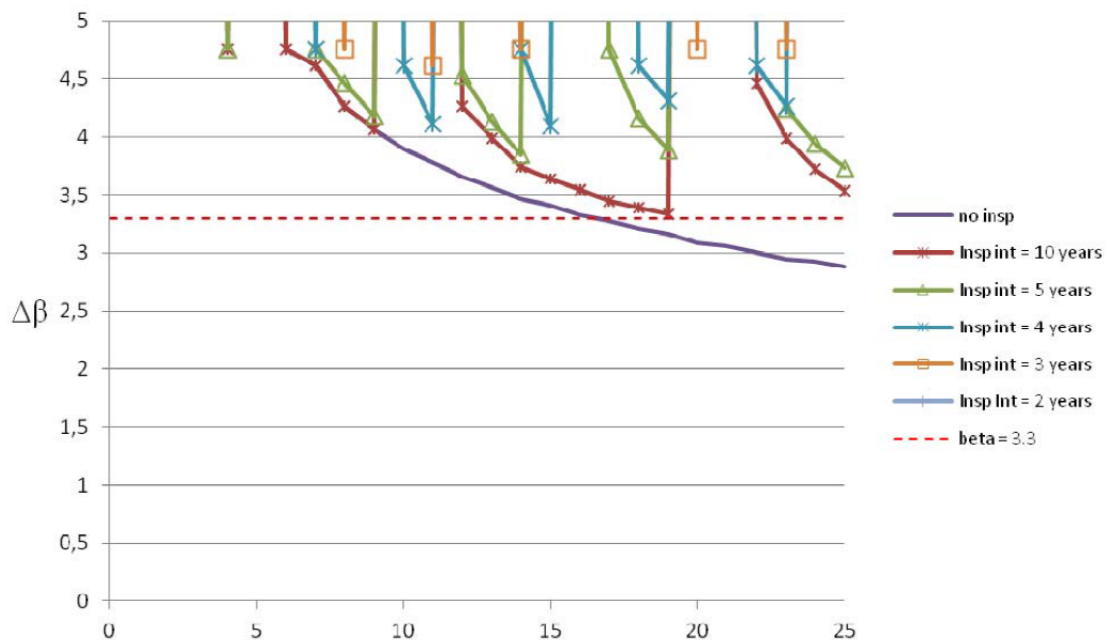


Figure A. 3. Annual reliability index without and with inspections. Inspection time intervals 2, 3, 4, 5 and 10 years and  $\lambda=10$  mm, partial safety factor  $\gamma_m = 1.10$  and aspect ratio = 0.2.

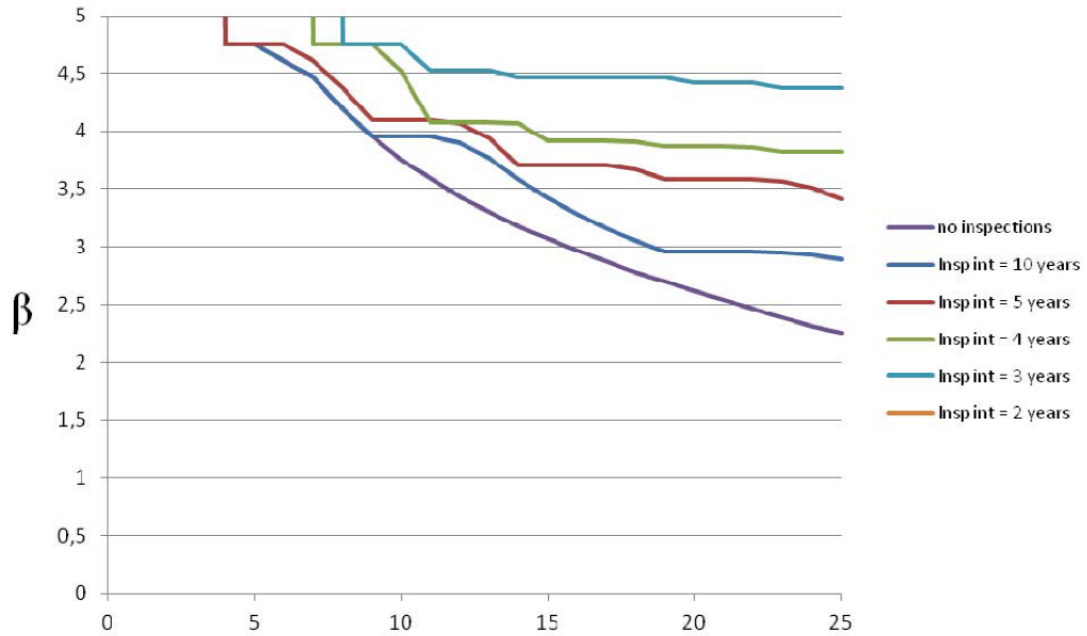


Figure A. 4. Accumulated reliability index without and with inspections. Inspection time intervals 2, 3, 4, 5 and 10 years and  $\lambda = 10$  mm, partial safety factor  $\gamma_m = 1.10$  and aspect ratio = 0.2.

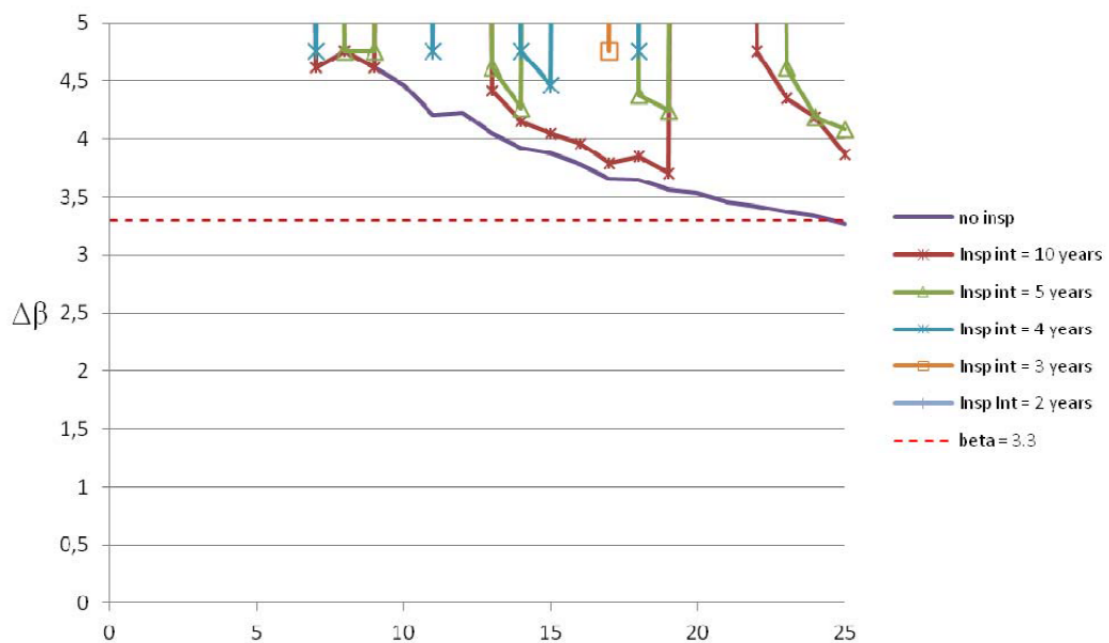


Figure A. 5. Annual reliability index without and with inspections. Inspection time intervals 2, 3, 4, 5 and 10 years and  $\lambda = 10$  mm, partial safety factor  $\gamma_m = 1.25$  and aspect ratio = 0.2.

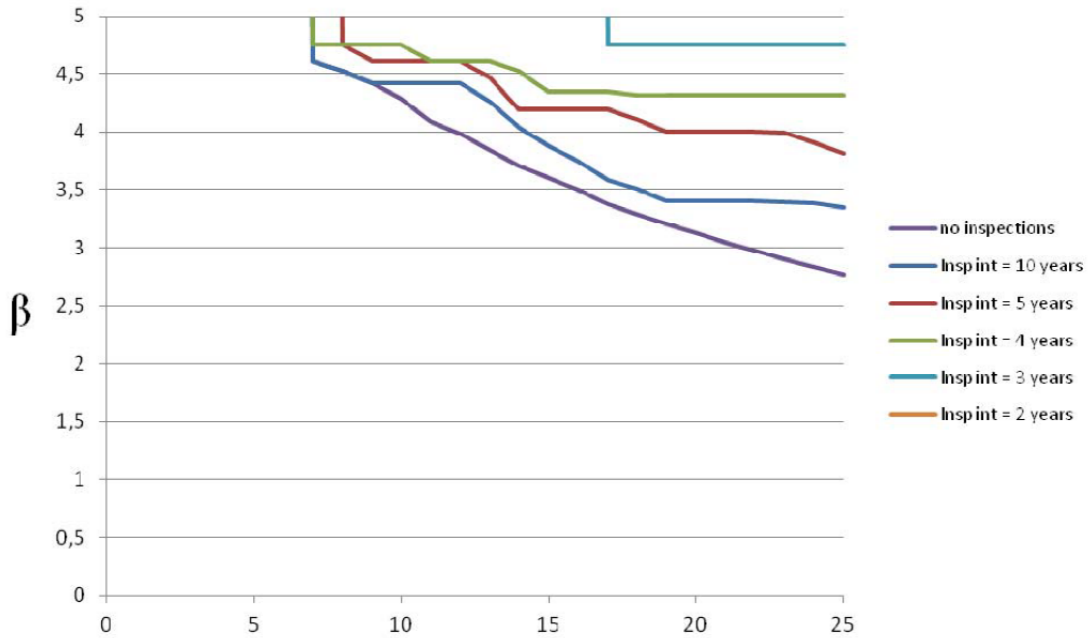


Figure A. 6. Accumulated reliability index without and with inspections. Inspection time intervals 2, 3, 4, 5 and 10 years and  $\lambda = 10$  mm, partial safety factor  $\gamma_m = 1.25$  and aspect ratio = 0.2.

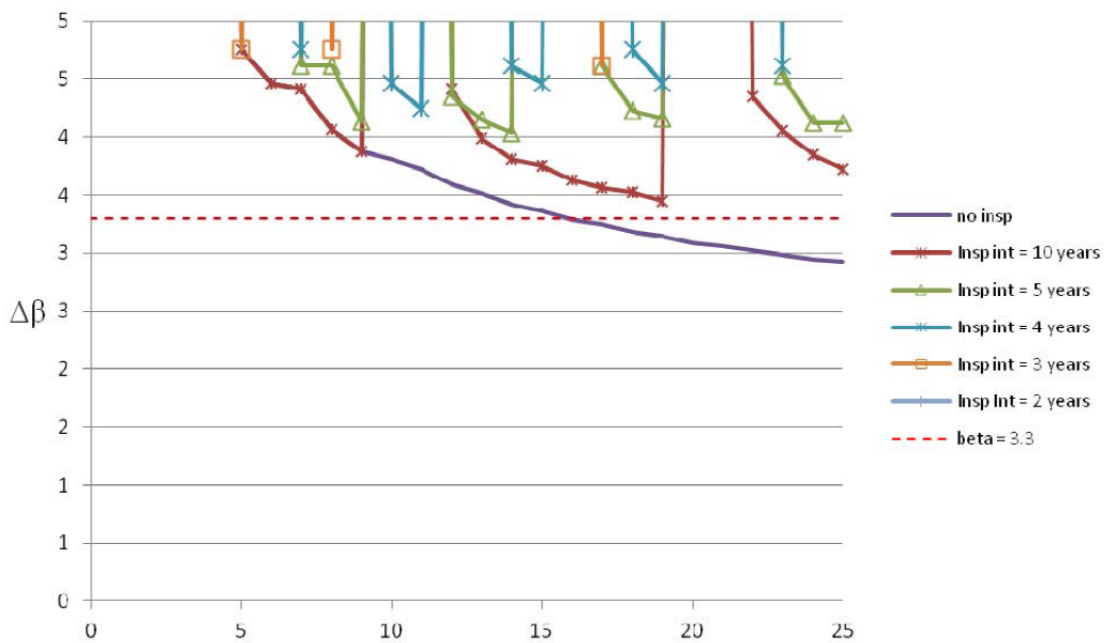


Figure A. 7. Annual reliability index without and with inspections. Inspection time intervals 2, 3, 4, 5 and 10 years and  $\lambda = 5$  mm, partial safety factor  $\gamma_m = 1.10$  and aspect ratio = 0.2.

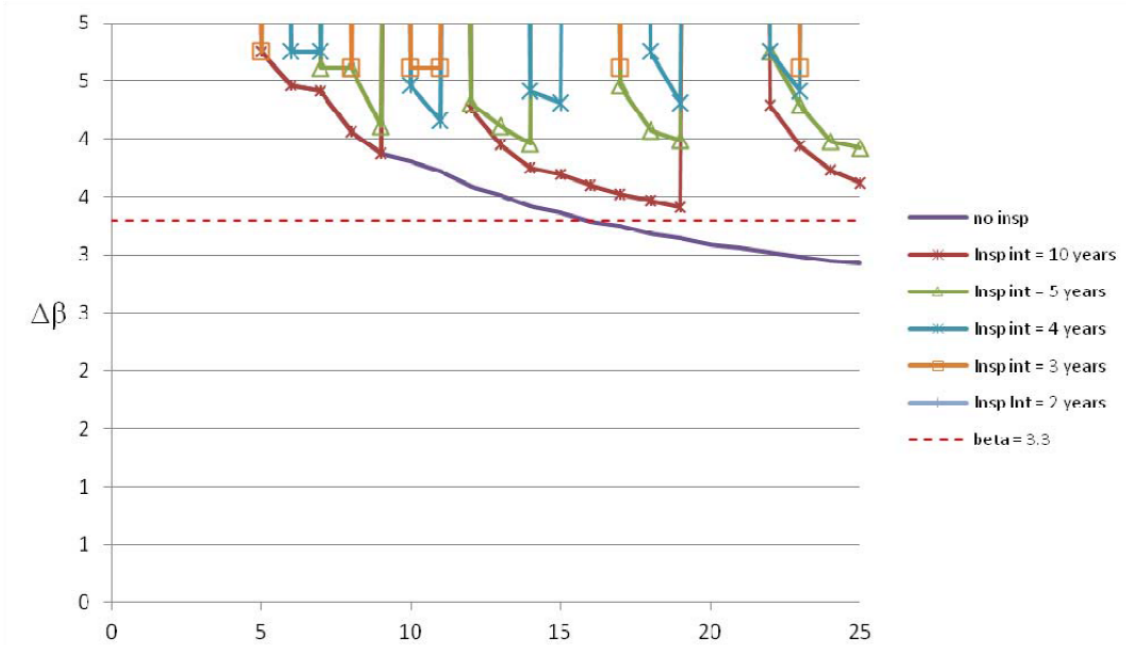
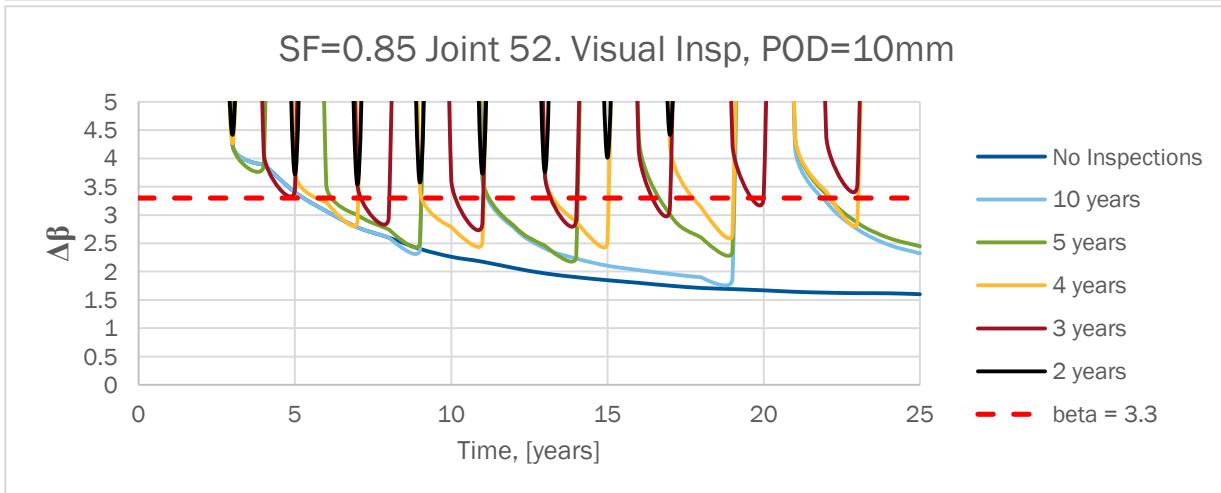
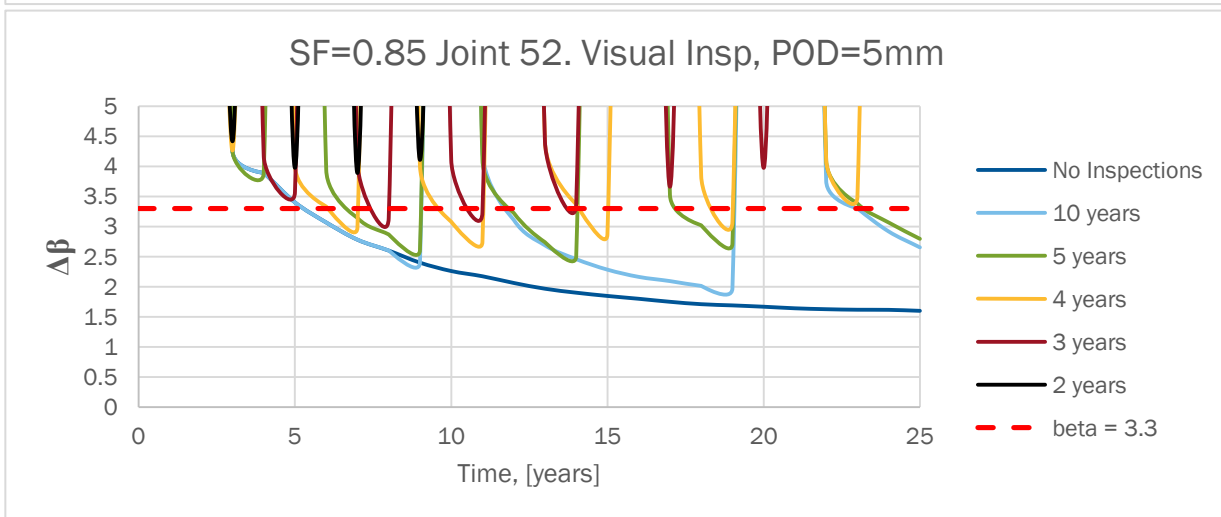
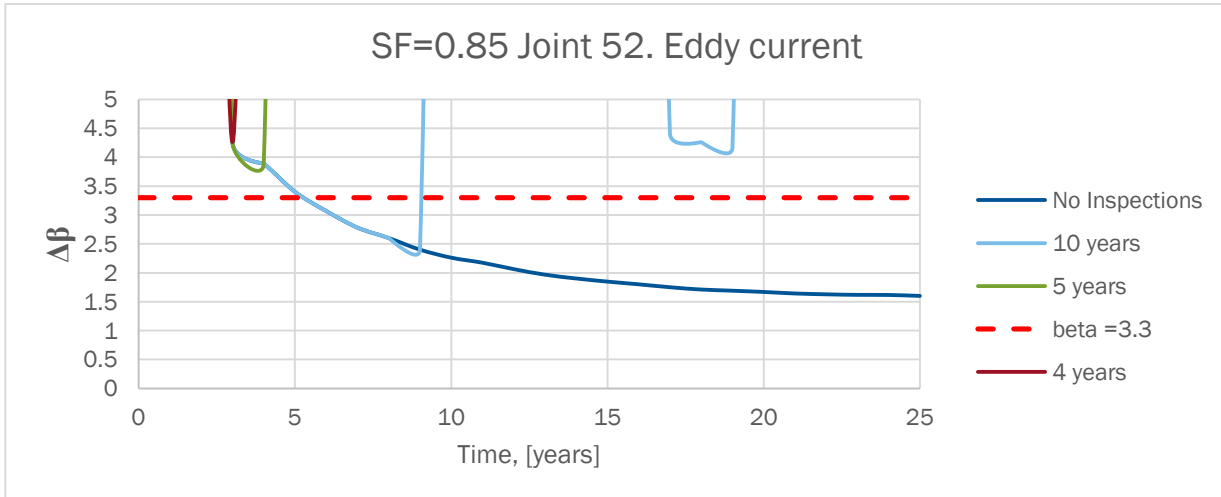
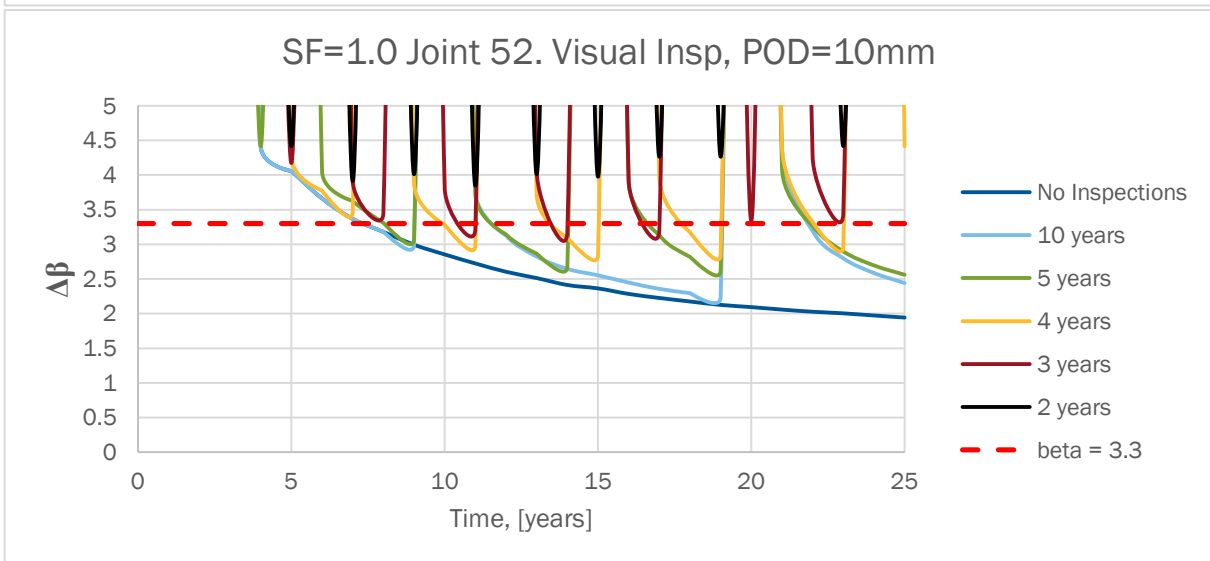
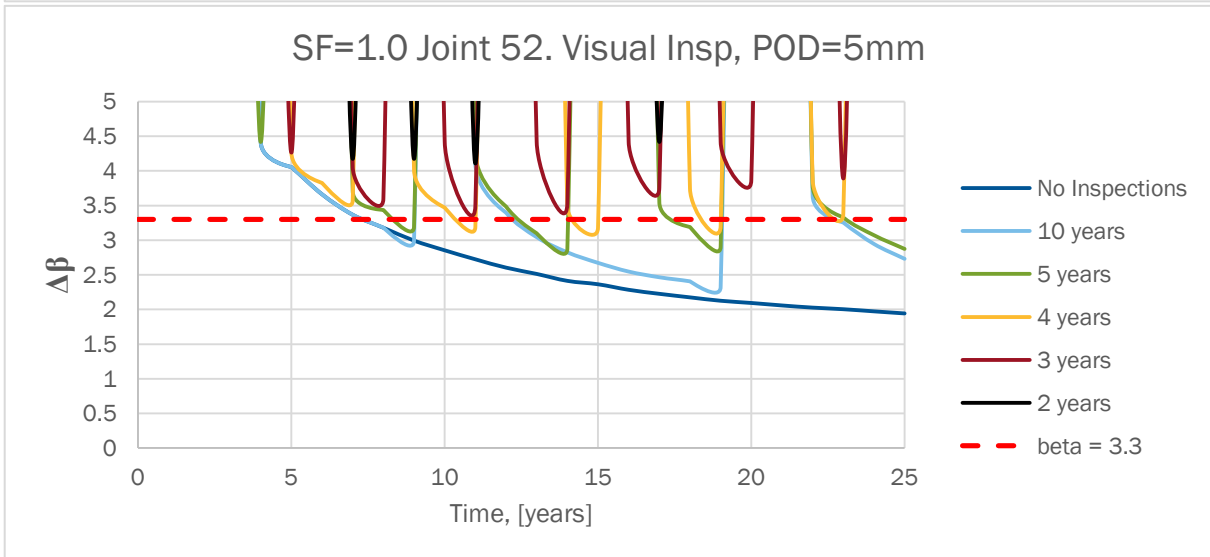
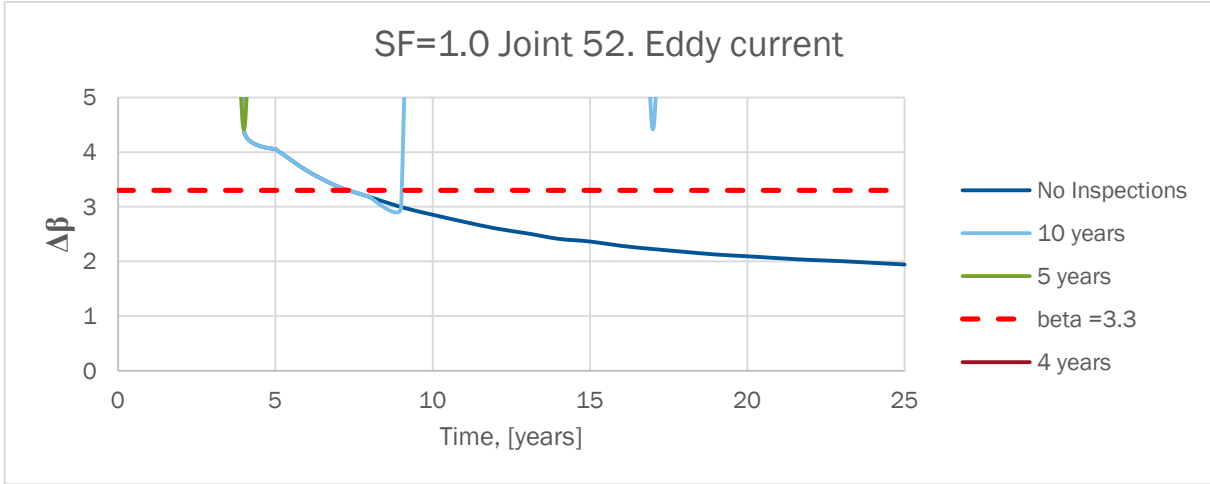


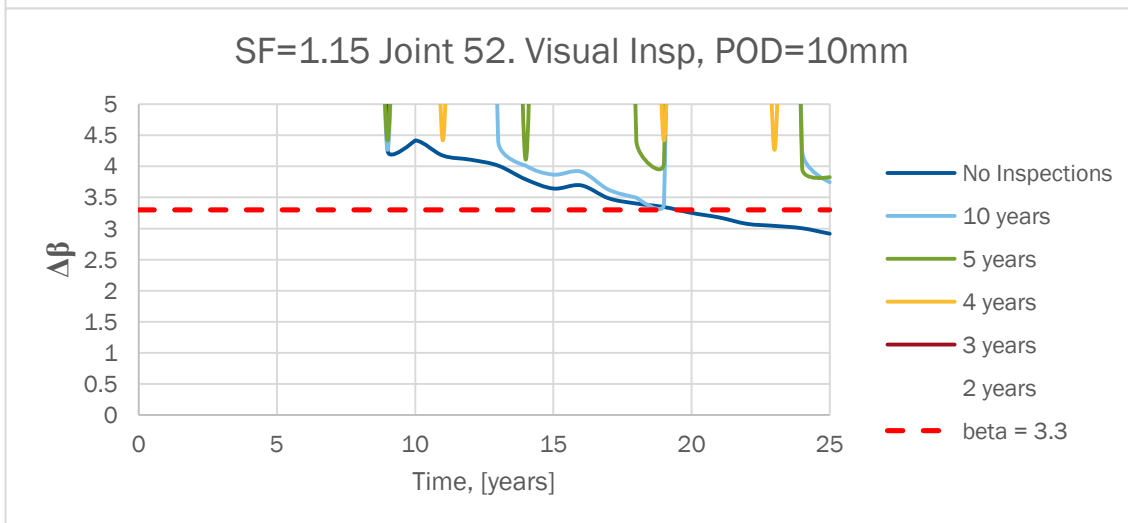
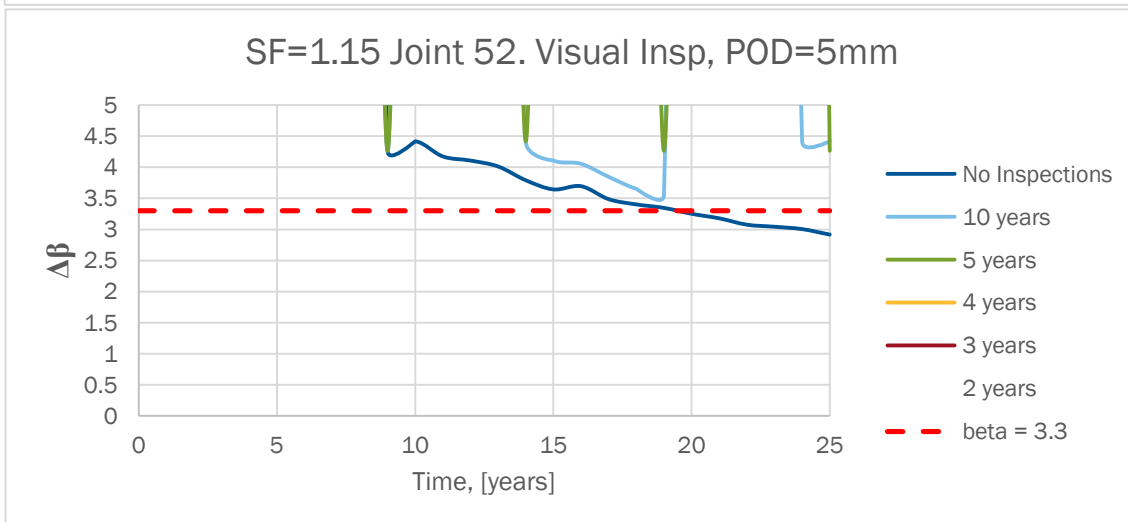
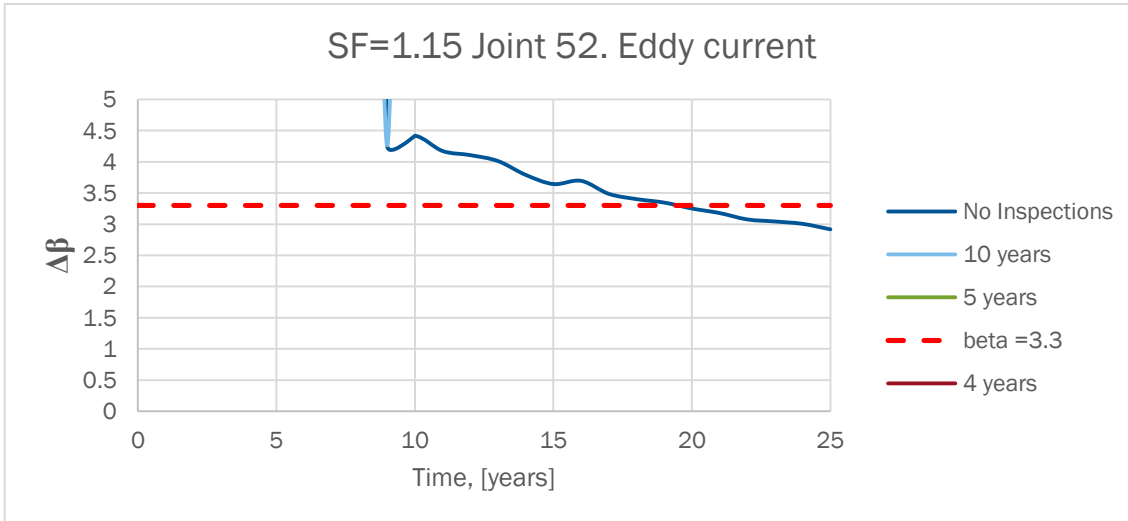
Figure A. 8. Annual reliability index without and with inspections. Inspection time intervals 2, 3, 4, 5 and 10 years and  $\lambda = 5$  mm, partial safety factor  $\gamma_m = 1.10$  and aspect ratio defined by eq. (4.10).

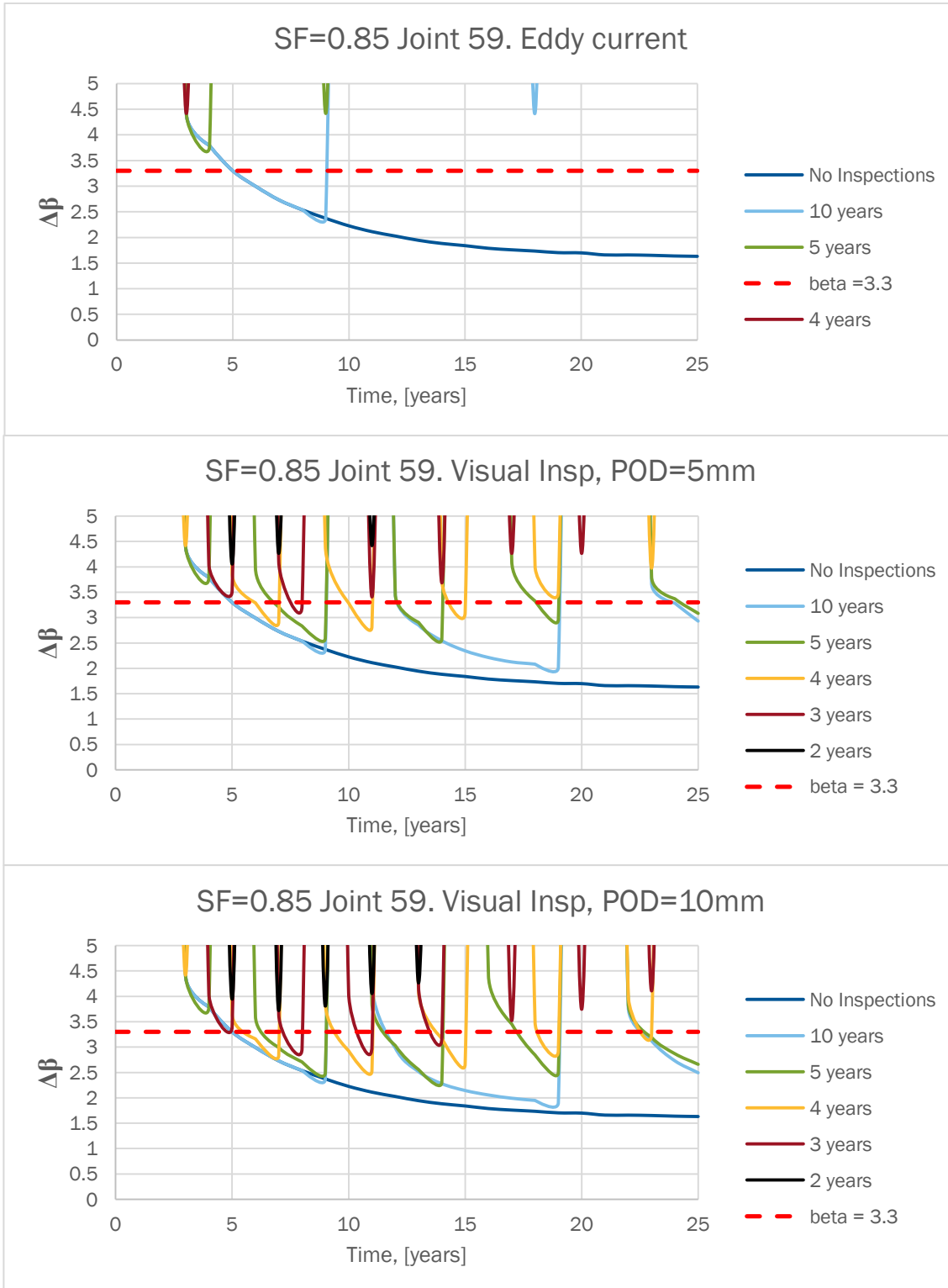


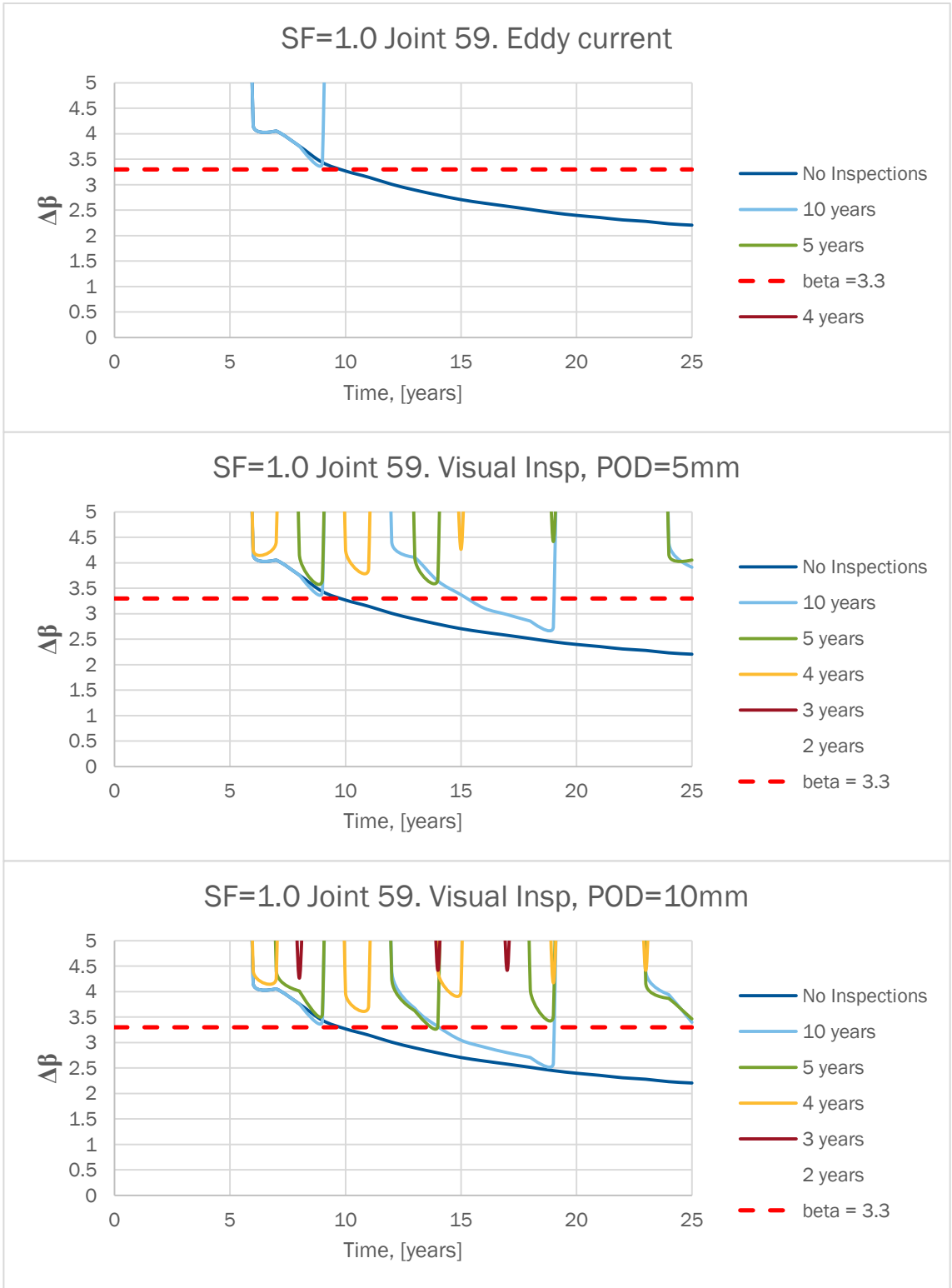
## APPENDIX B. RESULTS OF INSPECTION PLANNING FOR ALL THE ANALYZED JOINTS

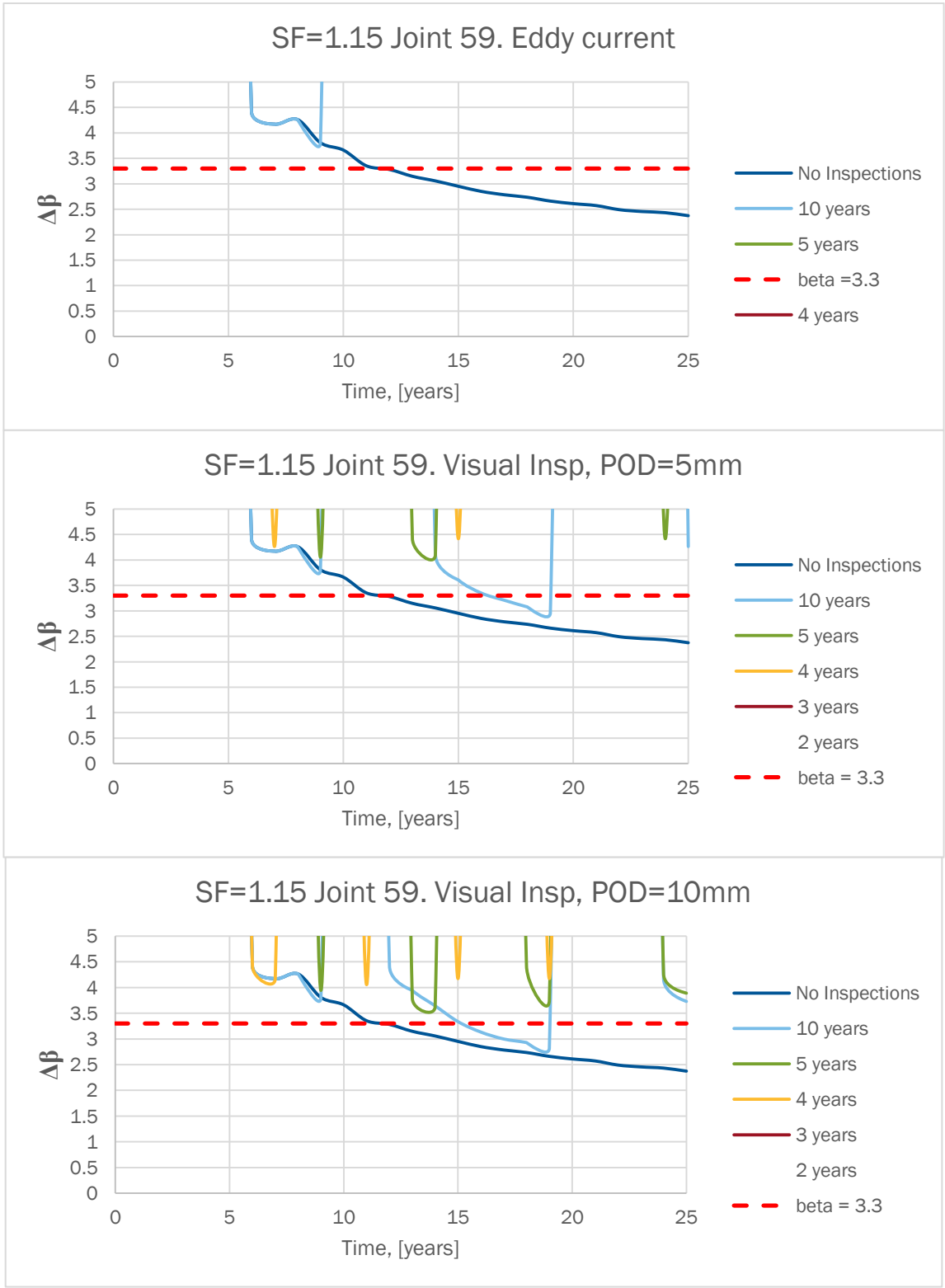


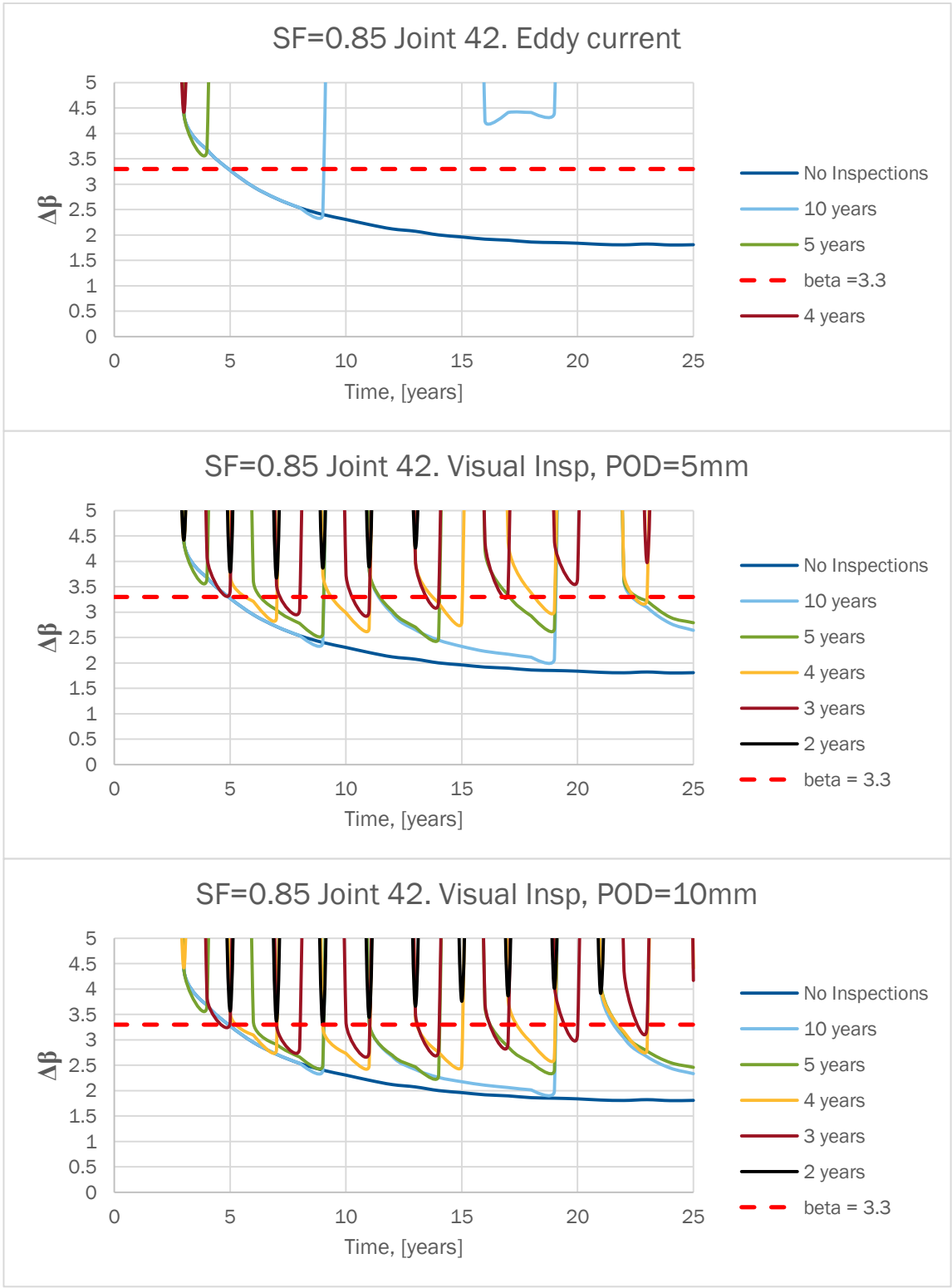


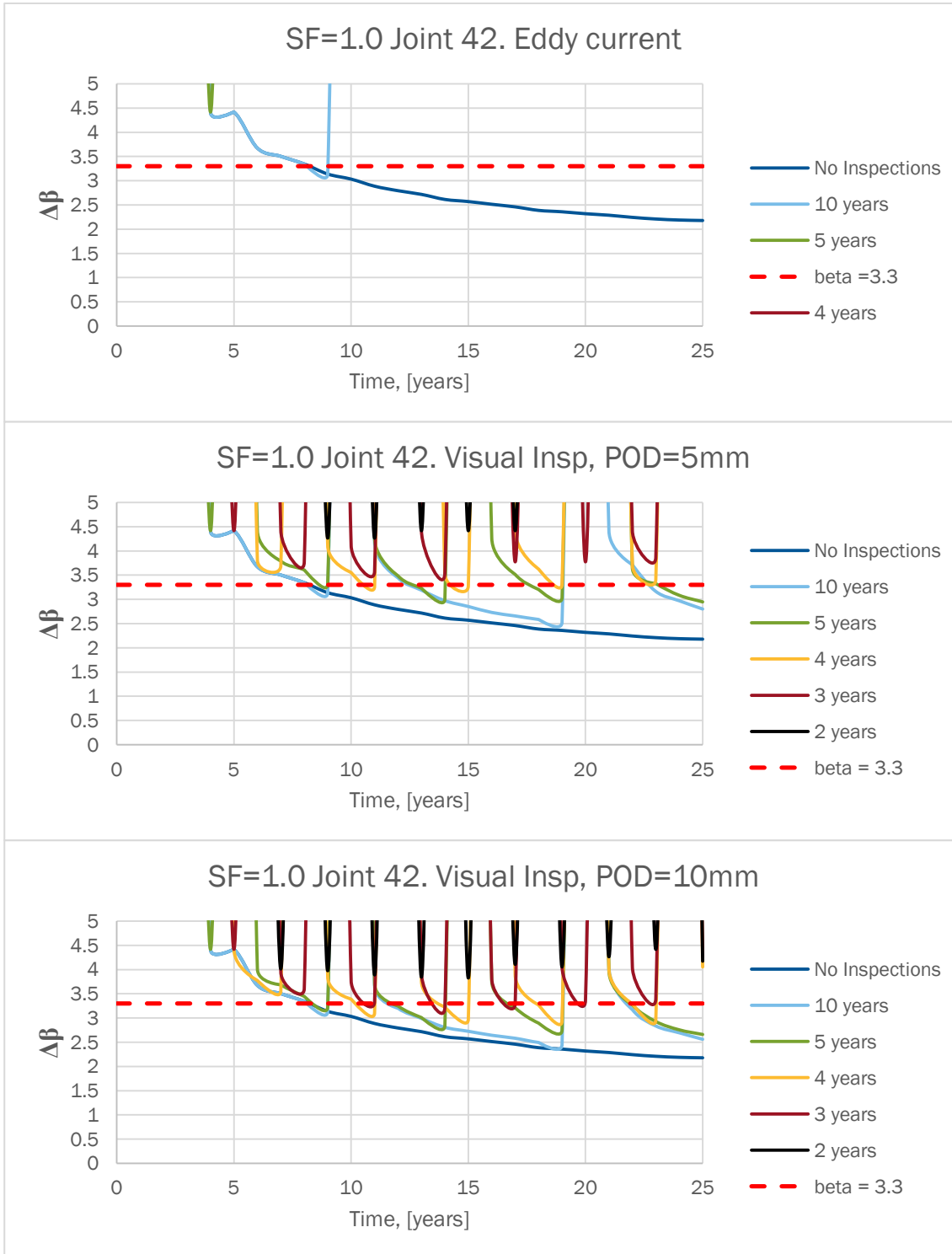


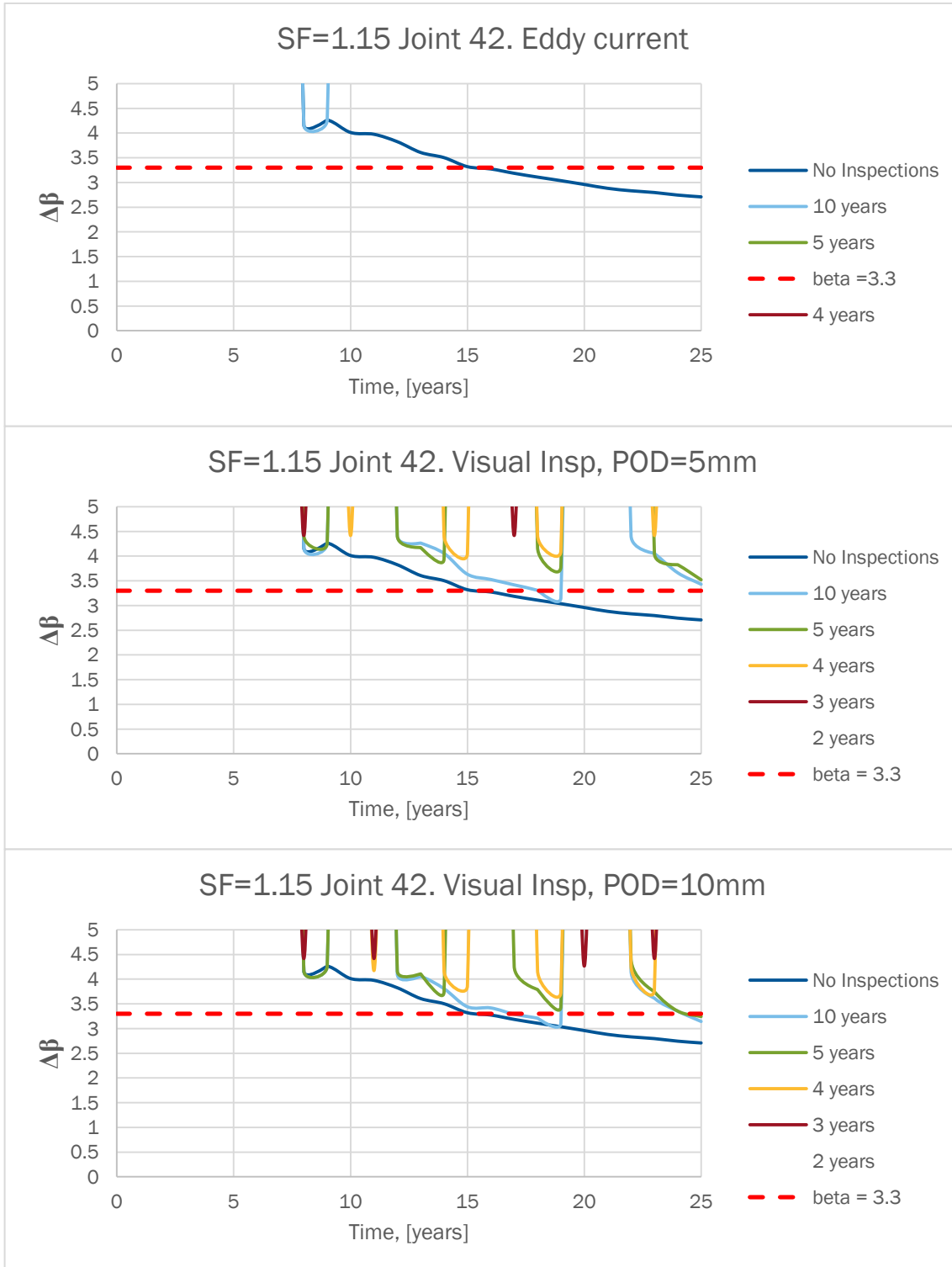


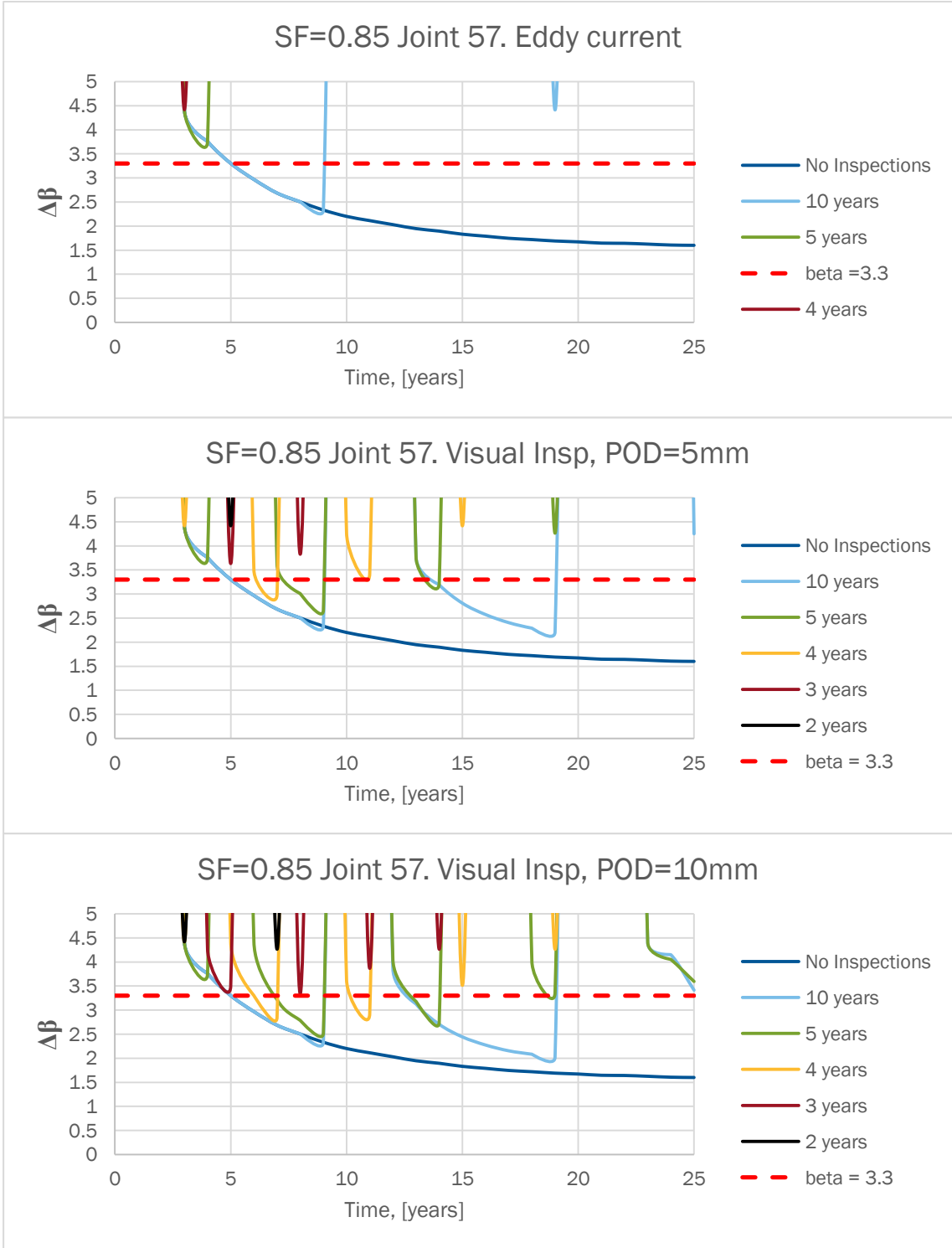


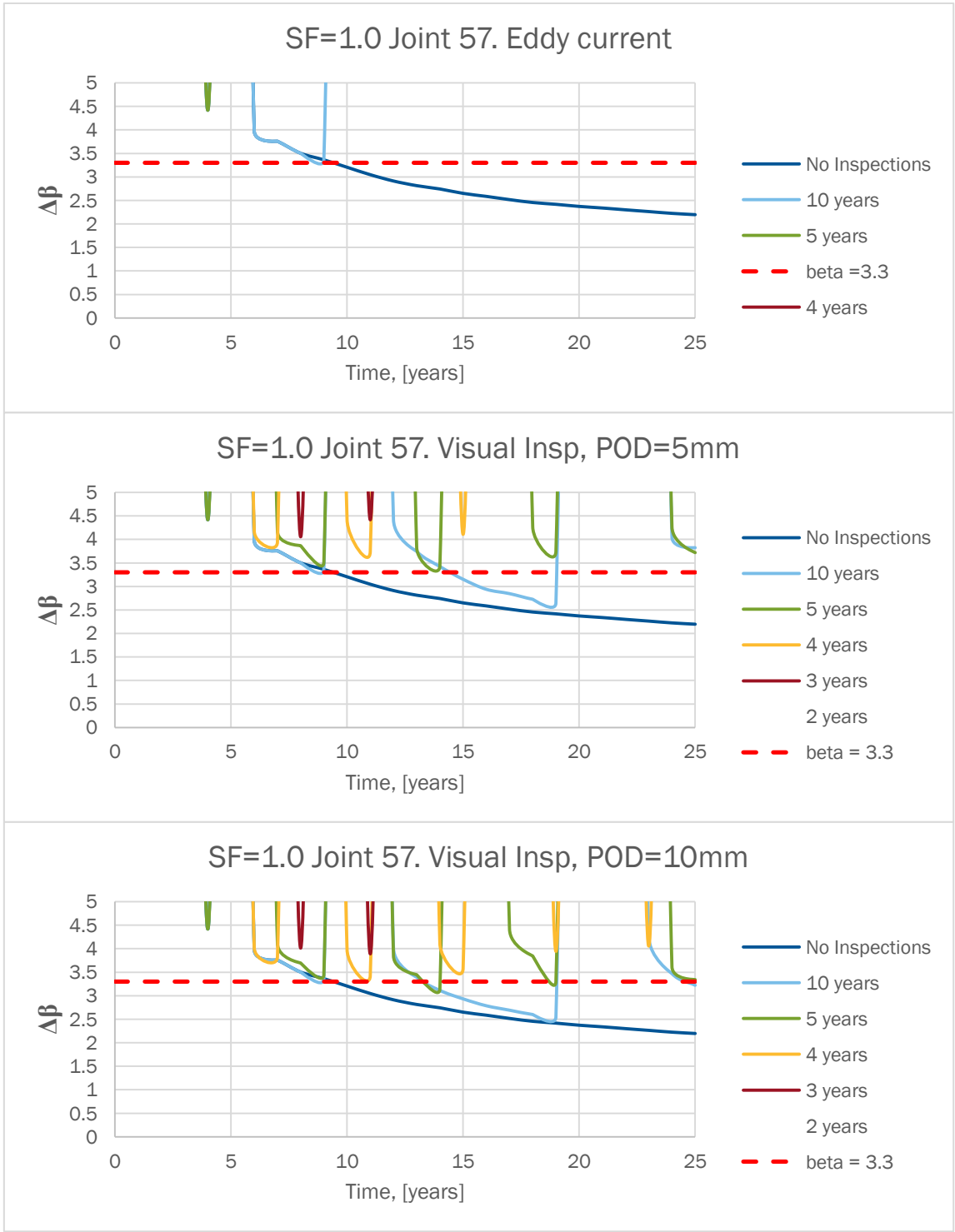


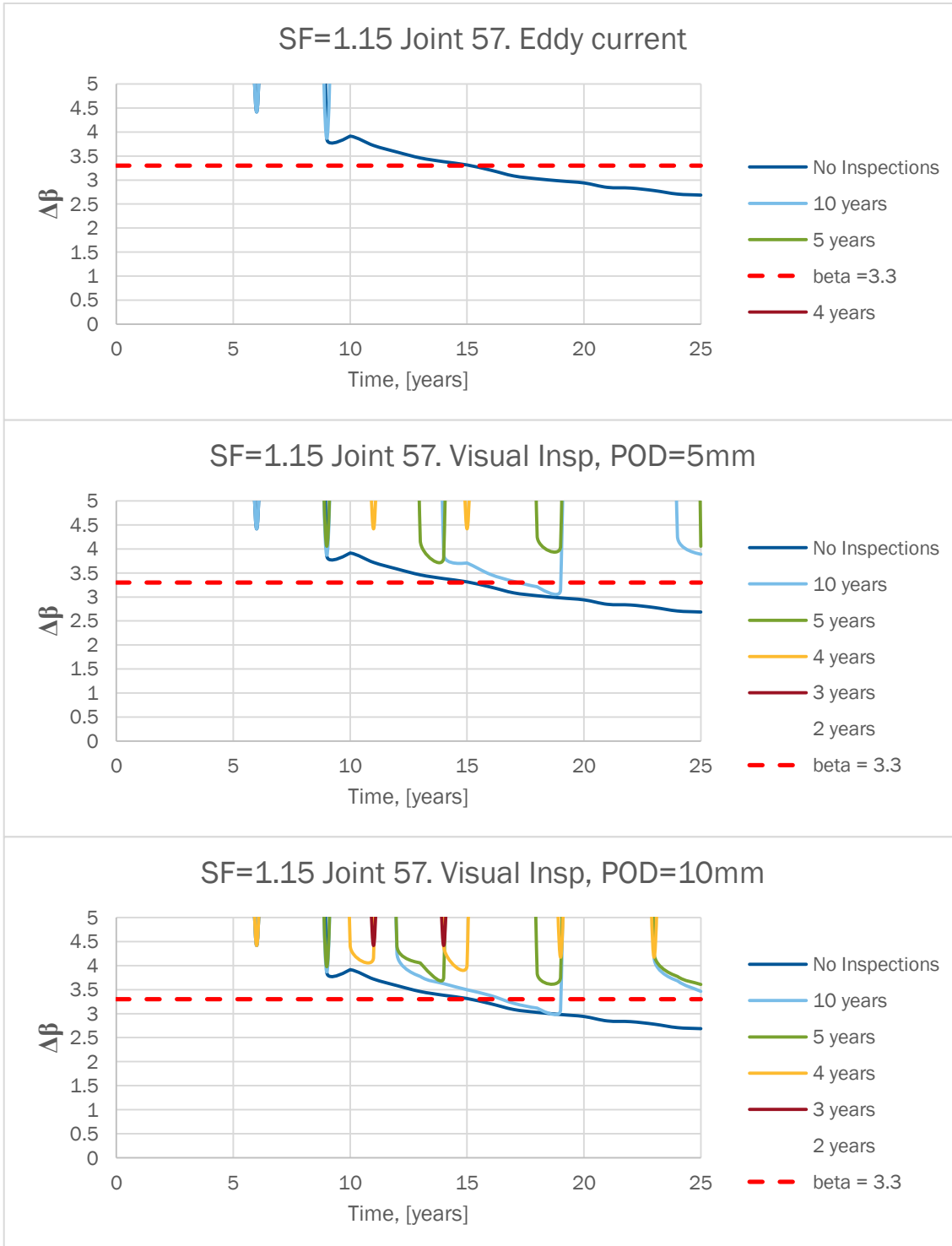


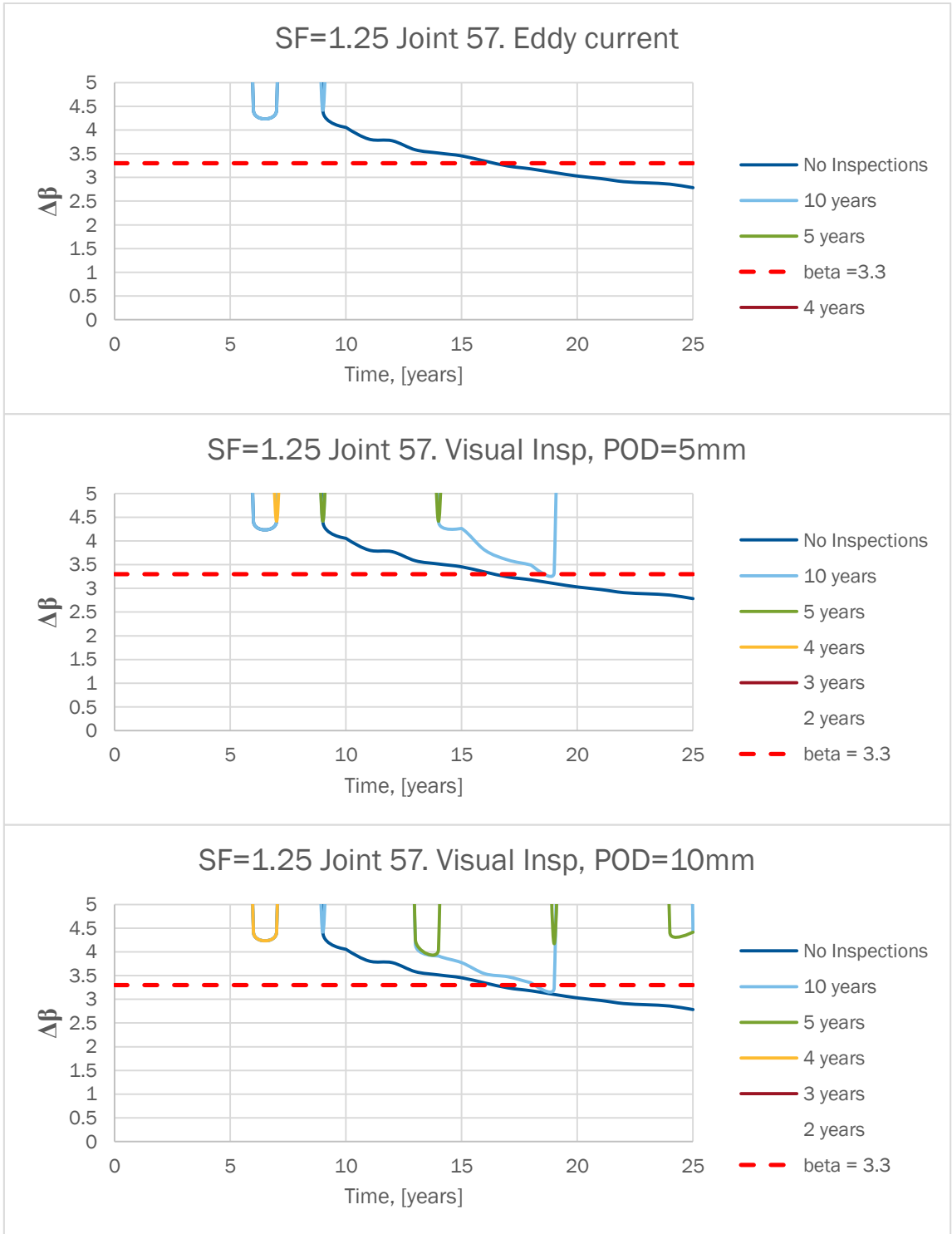












## BIBLIOGRAPHY

- Aker Partner Engineering, 1990. *PIA (Probabilistic Inspection Analysis) Theory Manual*. Oslo, Norway: Aker Partner Engineering AS.
- Benjamin, J. & Cornell, C., 1970. *Probability, Statistics and Decision for Civil Engineers*. New York: McGraw-Hill.
- BS 7910, 2013. *Guide to methods for assessing the acceptability of flaws in metallic structures*. London: British Standards Institution.
- DNV RP-C203, 2014. *Fatigue design of Offshore steel structures*, s.l.: Det Norske Veritas.
- DNV, 2010. *Fatigue design of offshore structures, RP-C203*, s.l.: DNV.
- DNV, 2011. *Design of offshore wind turbine structures, OS-J101*, s.l.: Det Norske Veritas.
- DNV-GL, 2015. *Recommended Practice RP-0001. Probabilistic methods for planning of inspection for fatigue cracks in offshore structures*, s.l.: Det Norske Veritas - GL.
- Dong, W., Gao, Z. & Moan, T., 2010. *Fatigue reliability analysis of jacket-type offshore wind turbine considering inspection and repair*. Brussels, EWEC 2010.
- EN 1993-1-9, 2005. *Eurocode 3: Design of steel structures - Part 1-9: Fatigue*, Eurodoce: s.n.
- Ersdal, G., 2005. *Assessment of existing offshore structures for life extension. PhD thesis*, Stavanger: University of Stavanger.
- Faber, M., Englund, S., Sorensen, J. & Bloch, A., 2000. *Simplified and Generic Risk Based Inspection Planning*. s.l., 19th OMAE.
- Faber, M., Englund, S., Sørensen, J. & Bloch, A., 2000. *Simplified and Generic Risk Based Inspection Planning*. s.l., 19th OMAE Vol. 2.
- Faber, M. & Sørensen, J., 1999. *Aspects of Inspection Planning - Quality and Quantity*. Sidney , ICASP8.
- Faber, M., Sørensen, J., Tychsen, J. & Straub, D., 2005. Field Implementation of RBI for Jacket Structures. *Journal of Offshore Mechanics and Arctic Engineering*, Volume 127, pp. 220-226.
- Fujita, M., Schall, G. & Rackwitz, R., 1989. Adaptive reliability based inspection strategies for structures subjected to fatigue. *ICOSSAR89 Proceedings*, pp. 1619-1626.
- GL, 2005. *Guideline for the certification of offshore wind turbines*, s.l.: GL.
- IEC 61400-1, 2005. *Wind turbine generator systems – Part 1: Safety requirements*. , s.l.: IEC.
- ISO 19902, 2007. *Petroleum and natural gas industries - Fixed steel offshore structures*, s.l.: ISO.

JCSS , 2012. *Probabilistic Model Code - PART 3.12 Fatigue properties for metallic structures. Draft .*, s.l.: Joint Committee for Structural Safety.

JCSS, 2011. *Probabilistic Model Code Part3 : Resistance Models*, s.l.: Joint Committee for Structural Safety.

Kübler, O. & Faber, M., 2004. Optimality and acceptance criteria in offshore design. *Journal of Offshore Mechanics and Arctic Engineering*, Volume 126, p. 258–264.

Lassen, T., 1997. *Experimental investigation and stochastic modelling of the fatigue behaviour of welded steel joints, PhD thesis, Structural reliability theory* , Aalborg : Aalborg University.

Madsen, H., Krenk, S. & Lind, N., 1986. *Methods of Structural Safety*. New Jersey: Prentice-Hall.

Madsen, H. & Sørensen, J., 1990. *Probability Based Optimization of Fatigue Desing Inspection and Maintenance*. Glasgow, International Symposium of Offshore Structures.

Madsen, H., Sørensen, J. & R., O., 1989. *Optimal Inspection Planning For Fatigue Damage of Offshore Structures*. San Francisco, ICOSAR 89.

Maljaars, J., Steenbergen, H. & Vrouwenvelder, A., 2012. Probabilistic model for fatigue crack growth and fracture of welded joints in civil engineering structures.. *Int. Journal Fatigue*, Volume 38, pp. 108-117.

Moan, T., 2005. Reliability-based management of inspection, maintenance and repair of offshore structures. *Journal Structure and Infrastructure Engineering*, pp. 33-62..

NORSOK, 1998. *Design of Steel Structures N-004, Rev. 1.*, s.l.: NORSOK .

Raiffa, H. & Schlaifer, R., 1961. *Applied Statistical Decision Theory*. Cambridge, Mass.: MIT Press.

Rangel-Ramírez, J. & Sørensen, J., 2010. RBI optimization of offshore wind turbines. *Journal of Structure and Infrastructure Engineering*.

Rouhan, A. & Schoefs, F., 2003. Probabilistic modelling of inspection results for offshore structures. *Structural Safety*, Volume 25, pp. 379-399.

Schuman, B. & Kaufer, D. (., 2015. *Design Report - Reference Jacket*, Copnehamen: Ramboll.

Skjong, R., 1985. Reliability based optimization of inspection strategies. *ICOSAR85 Proceedings*, Volume 3, pp. 614-618.

Sørensen, J., 2009. Framework for risk-based planning of operation and maintenance for offshore wind turbines. *Wind Energy*, Volume 12, pp. 493-506.

Sørensen, J., D., S. & Faber, M., 2005. *Generic Reliability-Based Inspection Planning for Fatigue Sensitive Details – with Modifications of Fatigue Load*. Rome, ICOSAR 2005.

Sørensen, J., Faber, M., Rackwitz, R. & Thoft-Christensen, P., 1991. *Modeling in optimal inspection and repair*. Norway, OMAE91, pp. 281-288.

Sørensen, J., Frandsen, S. & Tarp-Johansen, N., 2008. Effective Turbulence Models and Fatigue Reliability in Wind Farms. *Probabilistic Engineering Mechanics*, Volume 23, pp. 531-538.

Sørensen, J. & Toft, H., 2014. *Safety Factors – IEC 61400-1 ed. 4 - background document.-0066 (EN)*., Copenhagen: DTU Wind Energy-E-Report.

Straub, D., 2004. *Generic Approaches to Risk Based Inspection Planning of Steel Structures. PhD thesis*., Zurich.: Swiss Federal Institute of Technology, ETH.

Straub, D. & Faber, M., 2005. Risk based acceptance criteria for joints subject to fatigue deterioration. *Journal of Offshore Mechanics and Arctic Engineering*, Volume 127, pp. 150-157.

Tarp-Johansen, N. J., Madsen, P. H. & Frandsen, S. T., 2003. *Calibration of Partial Safety Factors for Extreme Loads on Wind Turbines*.. Madrid, European wind energy conference and exhibition, EWEC.

Thoft-Christensen, P. & Sørensen, J., 1987. Optimal Strategies for Inspection and Repair of Structural Systems. *Civil Engineering Systems*, Volume 4, pp. 94-100.